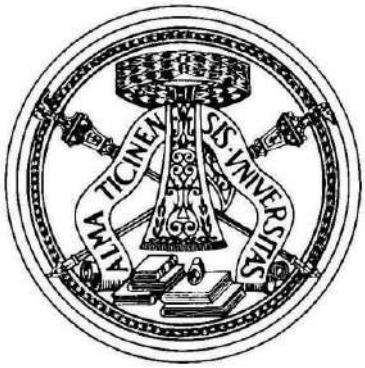

UNIVERSITÀ DEGLI STUDI DI PAVIA

FACOLTÀ DI INGEGNERIA

DIPARTIMENTO DI INGEGNERIA INDUSTRIALE E DELL'INFORMAZIONE

CORSO DI LAUREA MAGISTRALE IN BIOINGEGNERIA

TESI DI LAUREA

PARAMETRIC 3D MODEL OF THE MITRAL VALVE

MODELLO PARAMETRICO 3D DELLA VALVOLA MITRALE

Supervisor:

Chiar.mo Prof. Simone Morganti

Author:

Laura Mazzocchi

Academic Year 2015/2016

Alla Gerry…

“Anyone who has never made a mistake
has never tried anything new”

Albert Einstein

Contents

Abstract

Morphology of the mitral *apparatus* is very complex and wide variation exists in mitral valve (MV) geometry, both in physiological and pathological conditions. It is difficult to understand its *in vivo* mechanics also because CT and cMR can provide accurate images and volume data sets, but they have some constraints, including radiation exposure and high costs, respectively, while echocardiographic methods remain the gold standard even if their quality is highly operator-dependent. For these reasons, there is lack of standardized models that realistically take into account all aspects characterizing mitral valve functioning.

We have developed a parametric 3D modeling algorithm which generates a real-time patient-specific model of the MV, using only echographic measures.

The long-term goal of this work is not only to offer an improved 3D visualization to both medical operators and patients, but also to provide analysis-suitable models which may be used for predictive simulations of valve performance.

Abstract

La morfologia dell'apparato mitralico è molto complessa ed esiste un'ampia variabilità nella geometria della valvola mitrale (VM), in condizioni sia fisiologiche sia patologiche. È difficile comprendere i meccanismi del suo funzionamento *in vivo* anche perché TC e RM cardiaca possono fornire immagini accurate e dati volumetrici, ma hanno dei limiti, legati, rispettivamente, all'esposizione a radiazioni e agli alti costi, mentre i metodi echocardiografici rimangono il gold standard anche se la loro qualità è fortemente operatore-dipendente. Per questi motivi mancano modelli standardizzati che prendano realisticamente in considerazione tutti gli aspetti caratteristici del funzionamento della valvola mitrale.

Abbiamo sviluppato un algoritmo parametrico di modellazione 3D che genera in tempo reale un modello preliminare patient-specific della valvola, utilizzando solo misure ecografiche.

L'obiettivo a lungo termine di questo lavoro è, non solo offrire una migliore visualizzazione 3D sia ai medici sia ai pazienti, ma anche fornire modelli adatti all'analisi, che possano essere utilizzati per simulazioni predittive del funzionamento della valvola mitrale.

Introduction

The Mitral Valve (MV) is located between the left *atrium* and left ventricle: whole valvular complex, consisting of different substructures, works in a coordinated manner in order to ensure the atrioventricular orifice opening during diastole and closing during systolic phase to prevent regurgitation of blood back from left ventricle into the *atrium*. Knowledge of the mitral valve anatomy still represents a challenging task owing to its high complexity and because data reported in literature are poor and discordant. A detailed study of valvular structures is of great importance especially for the treatment of mitral diseases, which are increasing in world population and can lead to severe heart dysfunctions. Surgical treatment is the only approach with defined clinical success and nowadays, if it is possible, valve repair is preferred over replacement. Therefore, diagnostic tools are necessary to obtain detailed morphological and functional data to monitor cardiac performance, understand physiology of MV pathologies, and provide important information for selecting candidates for specific therapies.

Given these premises, the present work represents a first step for the development of a predictive tool encouraged by Heart Surgery Division of University-Hospital of Padua (Dr. Gerosa G. and Dr. Colli A.), looking for a computational tool to support the *Neochord* intervention. In particular, they needed a predictive tool that would provide an overview of the mitral valvular pathology, allowing the investigation of different surgical scenarios and possible outcomes.

During the last decades, advances in imaging techniques such as echocardiography (particularly 3DE), multi-slice computed tomography (MS-CT) and cardiac magnetic resonance (cMR) have allowed to provide higher accuracy of measurements. Even if echocardiography has also some possible limits due to patients' acoustic windows and medical operators capabilities, it remains the imaging approach of choice because of its ease of use, low costs and no (transthoracic echography) or limited (transesophageal echography) invasiveness. It is the first and most widely used tool for diagnosis and surgical planning.

For these reasons, predicting or, in general, supporting tools in clinical decision-making are increasingly demanded.

In this work we aim to generate a user-friendly software that would allow to realize a patient-specific parametric model of the mitral valve geometry starting from echocardiographic imaging.

To my knowledge, none of the currently available geometrical models realistically takes into account all morphological and functional aspects of the mitral valve. Existing three-dimensional models are not parametric, or they are based on data available from not-routine exams (e.g. Magnetic Resonance) or derived by very complex processes which could not be included in everyday clinical practice.

In fact, our supra-mentioned goal results in the development of 3D parametric model of the mitral valve, which allows detailed morphological visualization of geometry of this structure to the clinicians (when echocardiographic image is not clear) and qualitative validation. Moreover, our purpose could be to use the valve model to perform suitable analyses and predictive simulations (e.g. FEM).

1. THE HUMAN HEART

1.1. Basic Concepts of Anatomy and Physiology

The human heart is a hollow muscular organ, of a conical form, located at the center of the chest cavity, behind the sternum, between the lungs and in the middle *mediastinum*, enclosed in the *pericardium* (Fig.1.1).

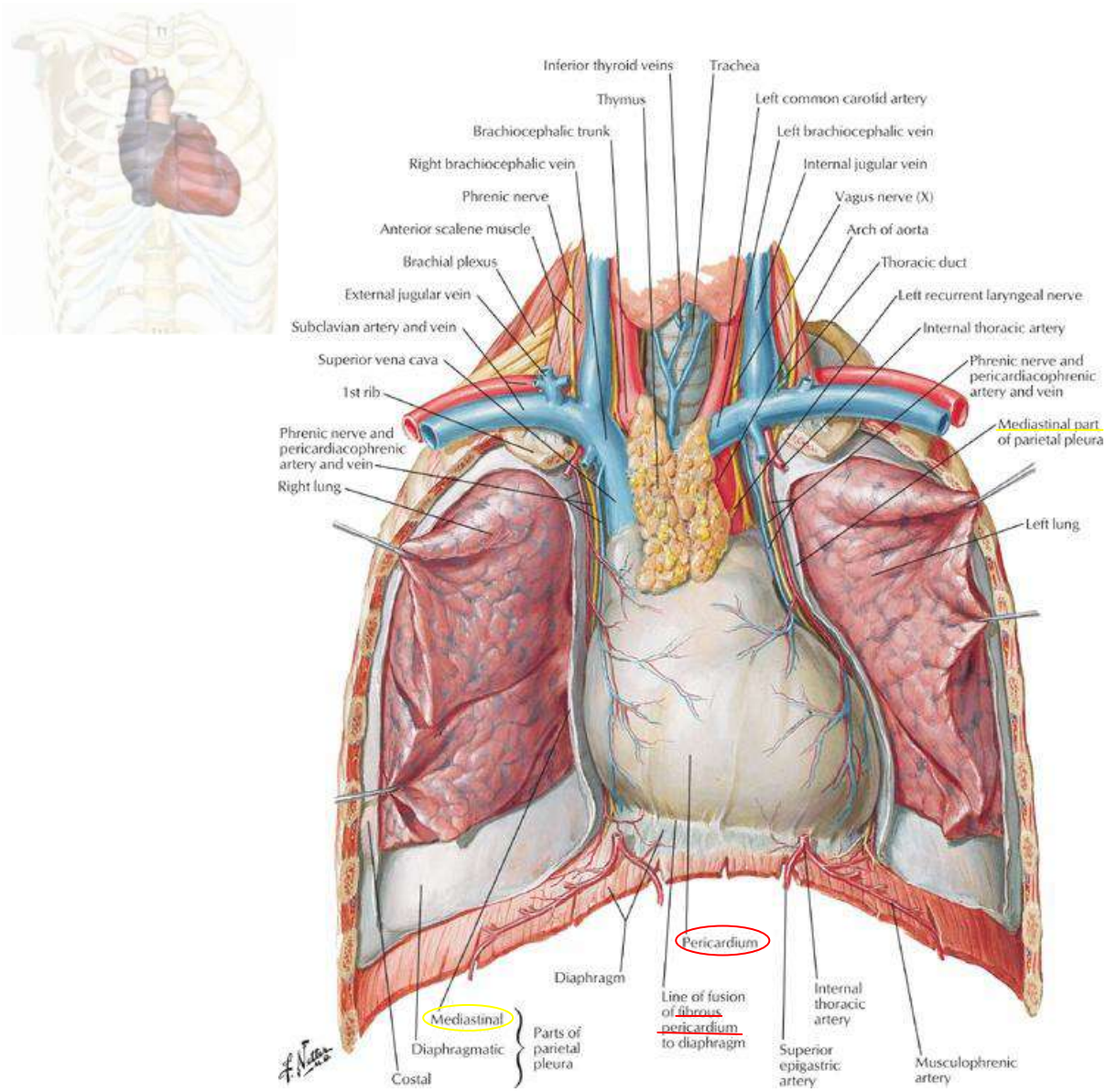

Fig.1.1: Heart *in situ* [140,78]

Pericardium is a thin membrane which externally covers the heart, fixes it in *mediastinum* and limits its motion, gives protection against infections, provides the lubrication for the

heart and prevents its excessive dilation in case of acute volume overload. It is a double-walled sac, in fact it is composed of two layers, called *fibrous* and *serous pericardium*. The first one is the most superficial layer and it is made up of dense and loose connective tissue [119]; the second one is the inner part and it prevents friction during heart activity. The serous membrane is also divided into *parietal* and *visceral* layers. In the cavity delimited by these two membranes, the presence of the pericardial (serous) fluid allows the heart to disperse the heat generated by the sliding of the membranes during heart movement and protects it from any kind of external shock.

The cardiac organ is composed of three layers of tissue (Fig.1.2):

- *Epicardium*: also called *visceral pericardium*, immediately outside of the proper heart muscle [46], in contact with it, it adheres to the heart and externally covers it. Largely made of connective tissue, it functions as a protective layer. Coronary arteries branches from here: they start directly from the Aorta and supply the heart with necessary oxygen and nutrition;
- *Myocardium*: thicker in the ventricles, it represents the greatest part of the contractile cardiac mass, consisting of several different oriented layers of striated and smooth muscles;
- *Endocardium*: a thin membrane that covers all the inner cavities of the heart and valves surfaces, in direct contact with the blood, it consists of endothelial cells, which avoid blood coagulation.

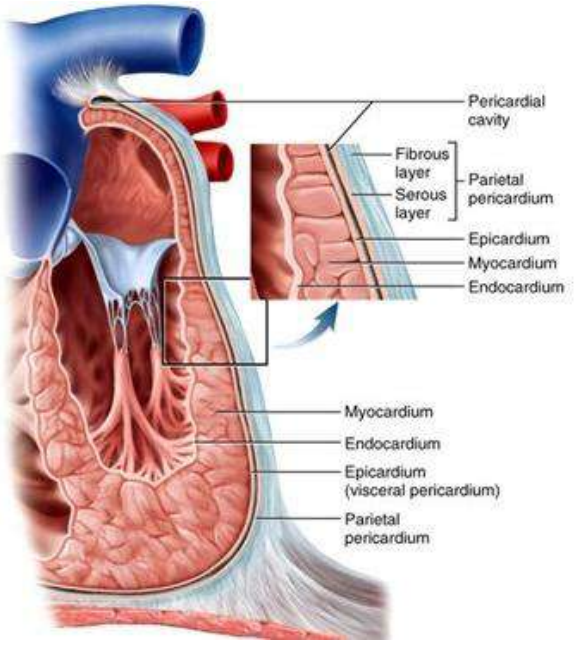

Fig.1.2: Pericardium and heart wall pericardial cavity [101]

The heart has independent contractile activity which allows the blood circulation throughout the body. The *myocardium* is composed by contractile muscular cells and the *sinoatrial node* is the natural pacemaker of the heart, responsible of the initiation of the heartbeat: it spontaneously generates an electrical impulse which spreads throughout the heart, via gap-junctions, causing the heart contraction. It is located in the myocardial wall, near where the S*uperior Vena Cava* joins the right *atrium* [79].

From a mechanical point of view, the human heart is a double pump, that periodically contracts and expands while pumping blood into the circulatory system.
It is divided into two cavities by a strong muscular septum: each one of them is also divided into two chambers, called *atrium* and *ventricle*. Hence the heart is overall composed of four cavities: the two thin-walled *atria*, positioned in the upper part of the heart, separated by an *intra-atrial septum*, and the two *ventricles*, located in the lower part, separated by an *intra-ventricular septum* and having thicker walls. Particularly, the *left* ventricle is the thickest one because it has to cope with the high impedances of the *systemic* circulation, so it works at the same flow rates as the other chambers, but at higher pressure regimes [22,83].
The human heart governs two pathways: pulmonary and systemic circuit: the former concerns the right heart (right *atrium* and the underlying ventricle, with venous blood), which has the purpose of saturating blood with the oxygen, and pumping it towards the lungs; the latter, called left heart (left *atrium* and ventricle), concerns the oxygen and nutrients distribution to supply tissues and organs. This side of the heart accepts oxygenated blood at a low pressure from the lungs into the *left atrium* (LA); then, the arterial blood moves, through the *Mitral Valve*, to the *left ventricle* (LV), which pumps it forward to the Aorta to circulate the body, through the *Aortic Valve* [127].
Each *atrium* is in direct communication with the corresponding ventricle through endothelial valves devoid of muscles; the right and the left side should not have any exchange of blood, but they contract synchronously because of an electrical stimulation spreading of neighboring cells. More precisely, *right ventricle* (RV) pumps blood, through the *Pulmonary Valve* in the pulmonary trunk, which branches into two pulmonary arteries (the right one and the one on the left) and carries deoxygenated blood to the lungs, where it can release CO_2 and get oxygen. Oxygenated blood goes now back to the left heart through four pulmonary veins, across the LA and LV, to the Aorta, in order to be pumped in the systemic circulation and supply peripheral tissues; then it returns to the *right atrium* (RA) through the Superior and the Inferior *Vena Cava* (see Fig.1.3).

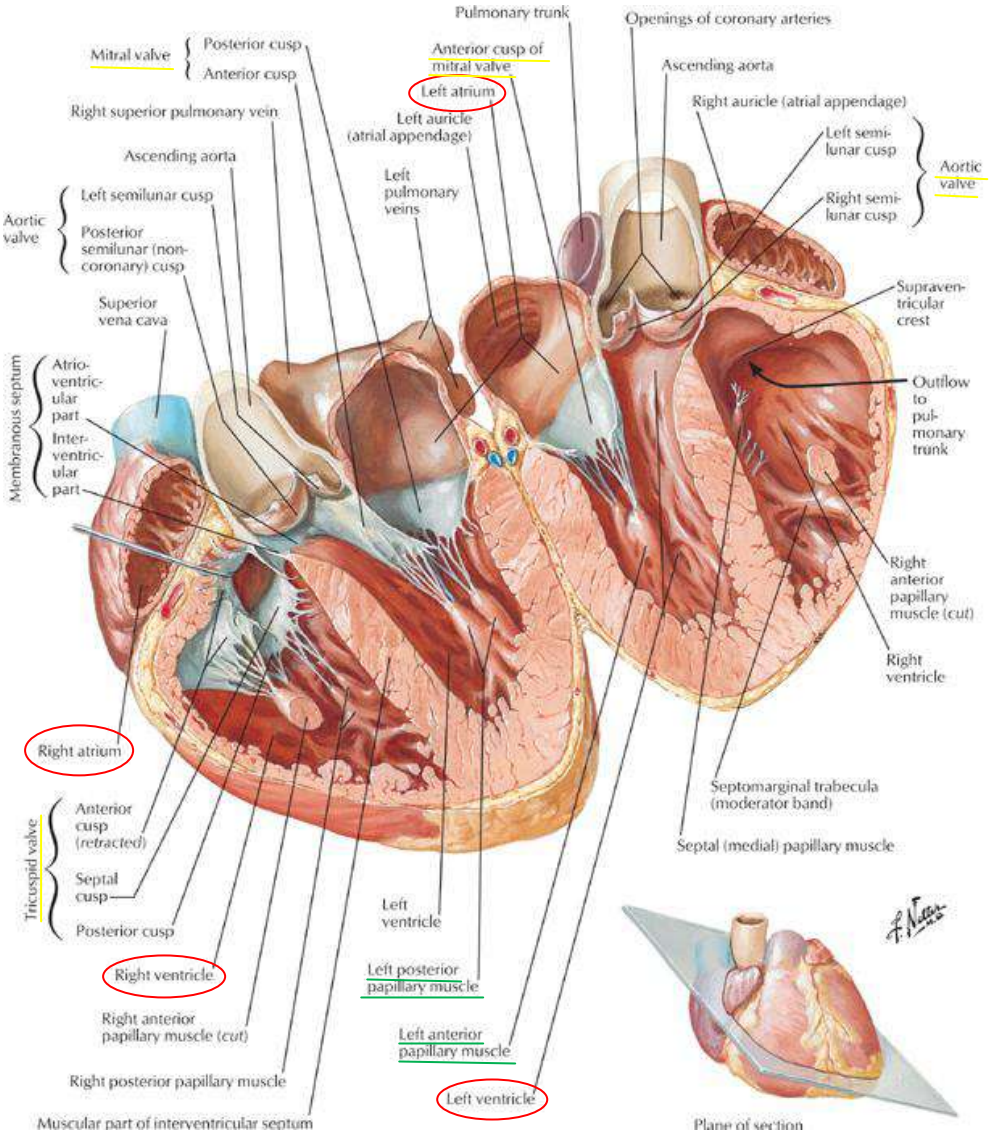

Fig.1.3: The anatomy of the four-chambered heart [78]

The presence of four valves maintains the unidirectional flow of the blood through the heart [22,83], preventing a retrograde flow. A couple of atrio-ventricular valves controls blood flow from the *atria* to the ventricles, whereas two semilunar valves control the flow from the ventricles to the arteries. They approximately stay on the same plane (*valvular plane*) [3], connected by a fibrous skeleton (Fig.1.4) that consists of high density connective tissue, which provides the point of insertion for the bundles of heart muscles and forms the *Annulus* of the valves. This element anchors the heart valves among them, connects valvular orifices and transmits the forces exerted through the valves, moreover it prevents their over dilation and gives mechanical strength to the structure [47]. This

skeleton is stronger on the left side of the heart rather than on the right one, due to higher pressures to which the LV is subjected.

The *Tricuspid* and *Mitral Valve* (MV) are the atrio-ventricular valves: as this name implies, they are located between *atrium* and ventricle, respectively, right and left. The *Pulmonary* and *Aortic Valve* (AV) are called, instead, semilunar valves because of their particular shape, similar to a pocket, and they are placed near the junction between the outflow tract of each ventricle and the origin of respective arteries [143]: the Pulmonary Artery (on the right side) and the *Aorta* (on the left).

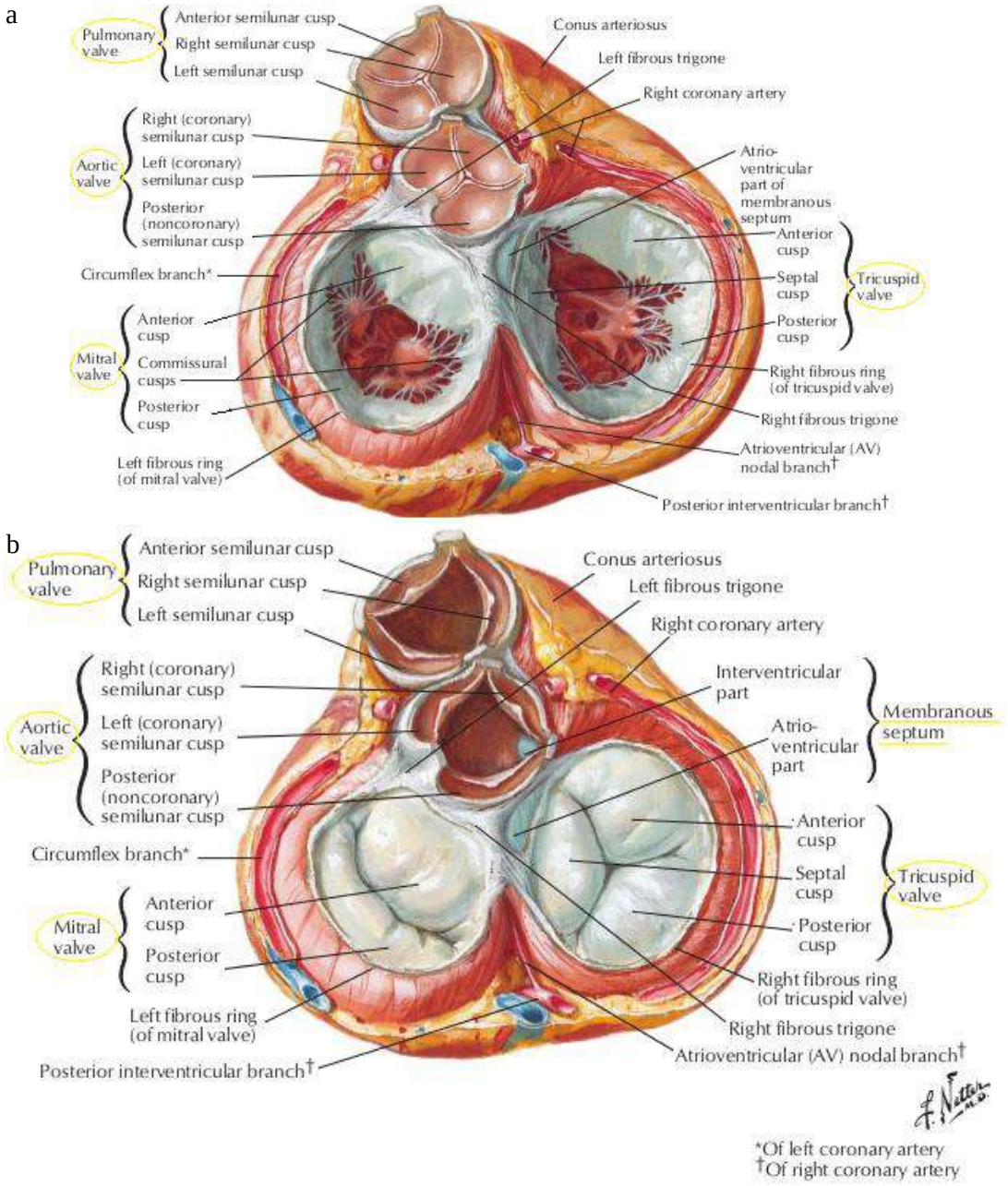

Fig.1.4: View from base with atria removed: heart in diastole (*a*) and systole (*b*) [78]

The atrio-ventricular valves are open in diastolic phase (see Fig.1.4,a) and closed during systole; vice versa the semilunar valves are closed in diastole, while they passively are opening during systolic phase (see Fig.1.4,b) because of the blood flow [8,105].

Considering now the cardiac cycle, for example, in the left part of the human heart, taking into account that the same mechanics can be associated also to the right half (except for few differences in the anatomy), two main phases can be distinguished: *systole* (heart contraction) and *diastole* (tissues relaxation). The opening and closing of the valves are controlled by the difference of blood pressure between upstream and downstream of each valve: when the upstream pressure exceeds the downstream one, the valve opens, and vice versa [105]. So the *Mitral Valve* prevents regurgitation from the LV to the LA during ventricle systole and the Aortic Valve prevents blood flowing back from the *Aorta* into the ventricle during diastole [127]. The set of contractions and relaxations produces a sequence of periodically repeated events called *cardiac cycle* (see Fig.1.6). More precisely, a single heartbeat can be divided into the following periods:

- Atrial diastolic phase: left *atrium* and ventricle are relaxed. In late diastole, the *atrium* receives blood from the incoming veins, but the *Mitral Valve* isn't open yet, so the chamber internal pressure increases; this time correspond to the early ventricular diastole.
- Ventricular diastolic and atrial systolic phases: the late diastolic phase begins with the LV *iso-volumic relaxation* of the wall (without any enlargement of the cavity volume; see violet line in Fig.1.5,a), with consequent and sudden ventricular reduction of pressure. When the pressure in the LA rises and overcomes the LV pressure, the *Mitral Valve* opens and the *Aortic Valve* roughly closes. Left ventricular chamber rapidly and passively fills with the greatest part of the blood (about 80%), from the corresponding *atrium*, because of gravity force: herein the pressure gradually increases until it reaches the same one in the *atrium* [73].

  The end of the ventricular diastole overlaps the atrial systolic phase, characterized by the LA contraction (small contribute of the remaining 20% of blood to the LV, but with negligible *filling* (see Fig.1.5,b, orange line)) and only depending on the flow from the pulmonary veins, through the LA, which acts as a passive conduit [39].

  Then the electrical signal reaches the *atrioventricular node* and propagates in the ventricle [73].

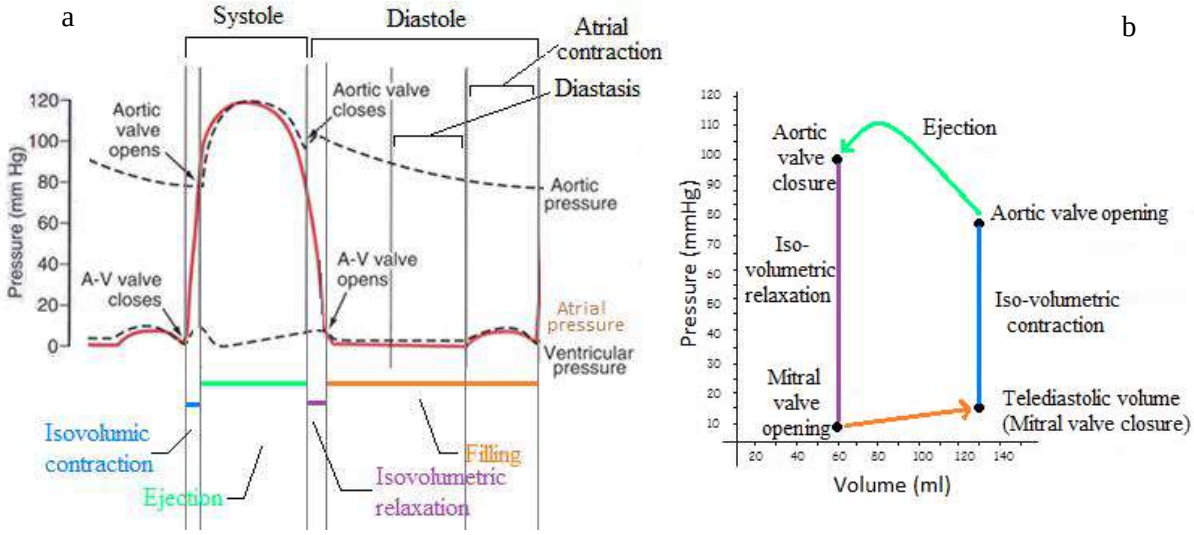

Fig.1.5: (*a*) Wiggers diagram: in red is shown LV pressure during one entire cardiac cycle; the maximum reached is about 120mmHg, while the minimum is about 5mmHg. The different phases of the cycle are color coded as follows: blue iso-volumic contraction, green ejection, violet iso-volumic relaxation, orange filling. (*b*) Volume-Pressure diagram of the LV during an entire cardiac cycle. [10]

- Early ventricular systolic phase induces the rapid *Mitral Valve* closure because the ventricular pressure overcomes the pressure in the LA, while the Aortic Valve is still closed. During the *iso-volumic contraction* (see Fig.1.5,a, blue line), the myocardium contracts increasing the pressure in the ventricular cavity without changing its volume but also causing the contraction of the *papillary muscles* attached to the *chordæ tendineæ* of the *Mitral Valve*, which ensure a proper valvular closure. When muscular cells contract, they push the blood toward the inferior part of the atrio-ventricular valve, which is forced to close, preventing a backward flow to the *atrium*.

  When the pressure in the LV exceeds that one in the Aorta, the Aortic Valve opens and the ventricle pumps high pressure blood into the artery, through the valve, during the so-called *ejection* phase (see Fig.1.5,a, green line). At each systolic cycle, LV pressure reaches about 120 mmHg (Fig.1.5,b); at the beginning of the ejection period, the ventricle *rapid*ly empties by 70%, while the remaining 30% of blood drains out during the *slow* ejection phase.

  At the same time the muscular fibers of the *atrium* relax: in this chamber the pressure is going to decrease and become lower than the pressure in the veins, therefore the blood will fill the *atrium* again.

Finally also the LV relaxes and the pressure decreases: when it becomes lower than that one in the Aorta, the blood flows back and fills the cusps of semilunar valve; as consequence the Aortic Valve is forced to close and the systolic period ends.

The pressure in the ventricle further decreases: the *iso-volumic relaxation* starts again and it goes on until the ventricular pressure does not become lower than the atrial one. At this point, the atrio-ventricular valve can open again and the blood stored in the *atria* flows down again to the ventricles: so a new cardiac cycle begins.

Electrical and mechanical events are shown in the so-called Wiggers diagram (Fig.1.5,a).

The duration of the entire cardiac cycle is about 0.8 seconds and systole has a period of time of about 1/3 of the cycle.

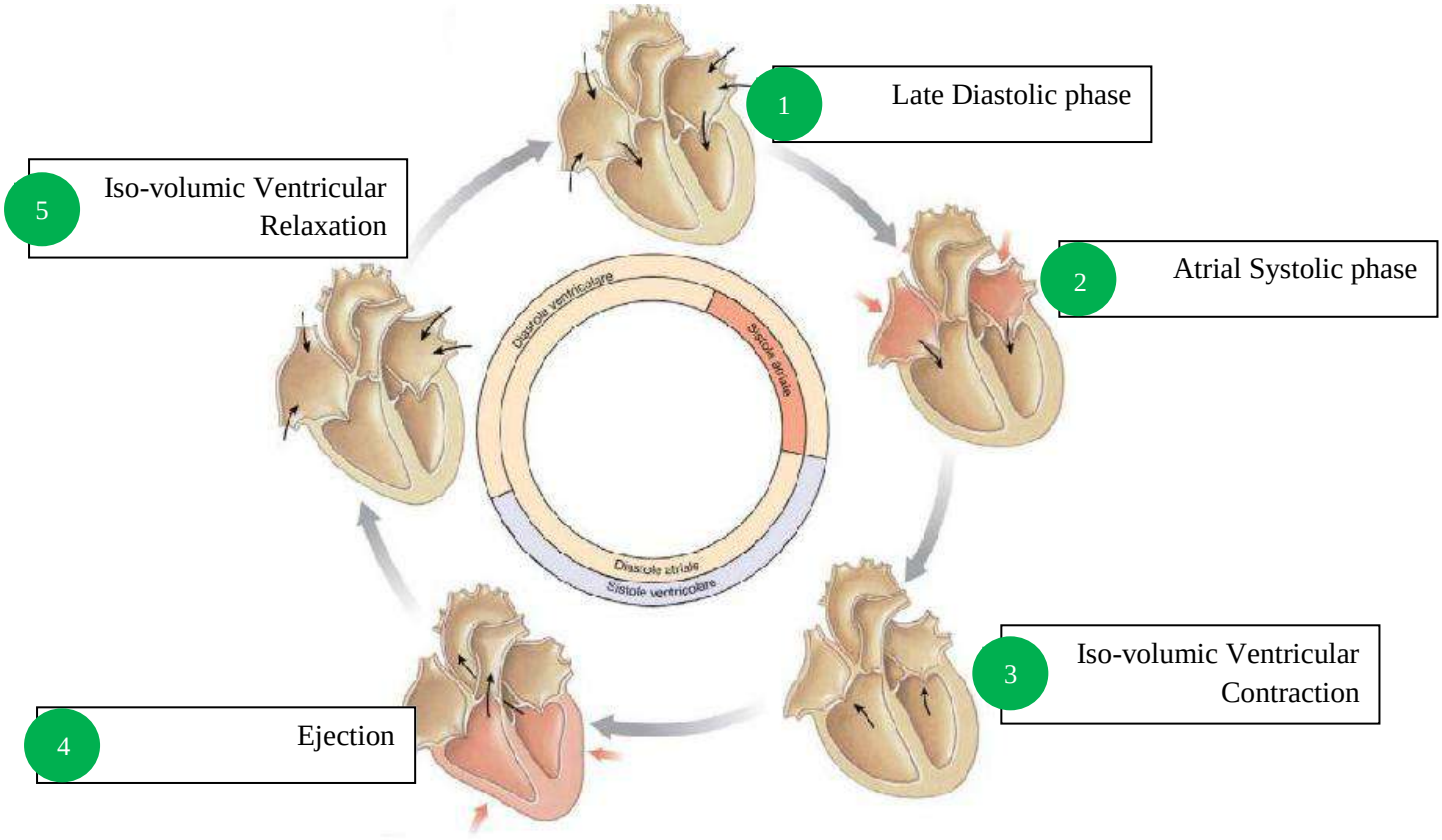

Fig.1.6: Cardiac Cycle [145]

1.2. Anatomy and Function of Heart Valves

The tri-leaflets Aortic and Pulmonary Valves separate the ventricles from the Aorta and the Pulmonary Artery, respectively. They have no tensor apparatus (*chordæ tendineæ* and *papillary muscles*), in fact they exhibit a passive mechanism of opening and closure, controlled by the pressure differences between LV and Aorta (in the case of the Aortic Valve), or between the RV and the Pulmonary Artery (regarding the pulmonary valve). They are circular openings, presenting three cusps, similar in structure and in their mode of attachment to the walls of respective arteries, where slight dilatations (*sinuses*) originate. The aortic leaflets are larger, thicker and stronger than the pulmonary ones, but both present attached margins and free borders (directed upward into the lumen of vessel) strengthened by tendinous fibers.

The Aortic Valve belongs to the *aortic valve complex* (Fig.1.7) and its anatomy is closely connected with its functioning. As shown below, it is composed, from the top, by one *Sino-Tubular Junction* (*STJ*), three *Sinuses of Valsalva* and their *valvular leaflets* originating from the supporting ventricular structure [89,113], three *commissures* and *interleaflet triangles* and, at last, one *Ventriculo-Arterial Junction* (*VAJ*, i.e. the *Annulus*).

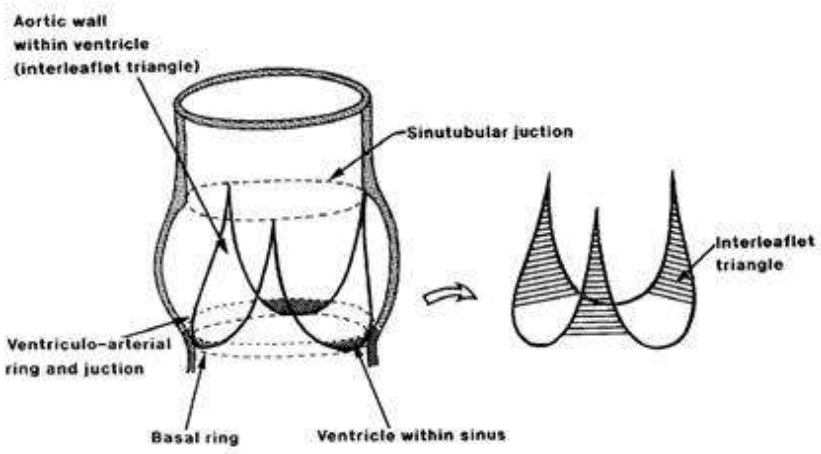

Fig.1.7: Scheme of the Aortic Root [113]

The *Sino-Tubular Junction* (initial tract of the aortic root) supports the peripheral part of the attachment of the aortic *leaflets* and it is mainly composed of elastic tissue.

The *Sinuses of Valsalva* (Fig.1.8) are hemispherical cavities behind the respective *leaflets*: three dilatations at the base of the *Aorta*, which separate this artery from the left ventricle and fill the aortic root for the most part.

The *leaflets* are the most mobile part of the Aortic Valve (Fig.1.9): they are three semilunar cusps attached to the walls of the aortic root, that converge at the centre of the valve to close it. When they are closed, they support the pressure load in the artery and move it to the center of the *commissures*. Only fibrous portions of valvular leaflets that can move are called free edges.

The *Annulus* (*VAJ*) is a no fixed structure, rich in collagen fibers, *in continuum* with the parietal lamina, similar to a three-pointed crown (see Fig.1.7); it dilates when the ventricle is filling and shrinks if the ventricle is contracting, so the distance that the leaflets have to cover in order to close the aortic orifice decreases [113].

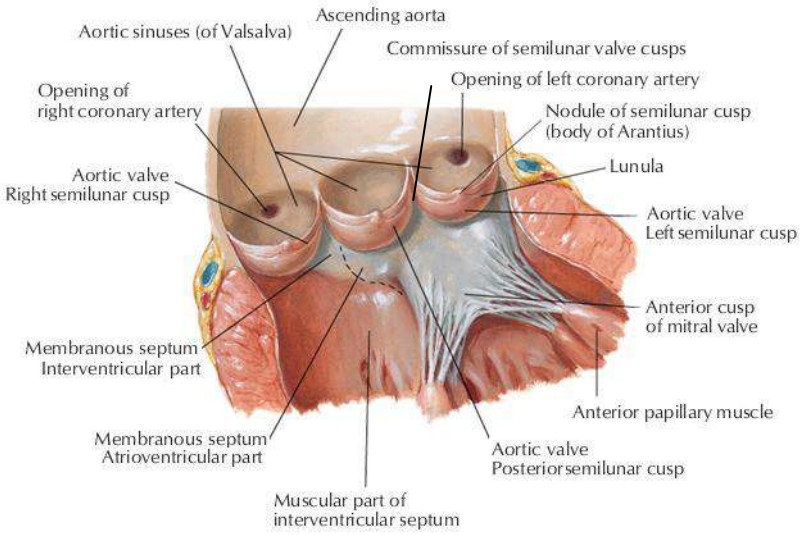

Fig.1.8: Aortic Sinuses of Valsalva [78]

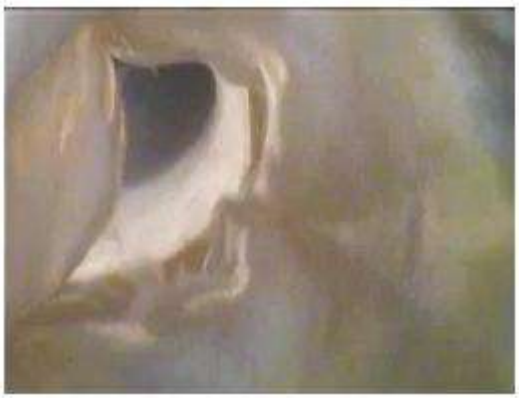

Fig.1.9: Aortic leaflets [140]

Inter-leaflets (*subcommissural*) *triangles* are supporting structures, part of ventricular wall, detectable between every couple of *Sinuses of Valsalva* (Fig.1.10). They are subjected to the ventricular hemodynamic and allow the *sinuses* to move independently of each other.

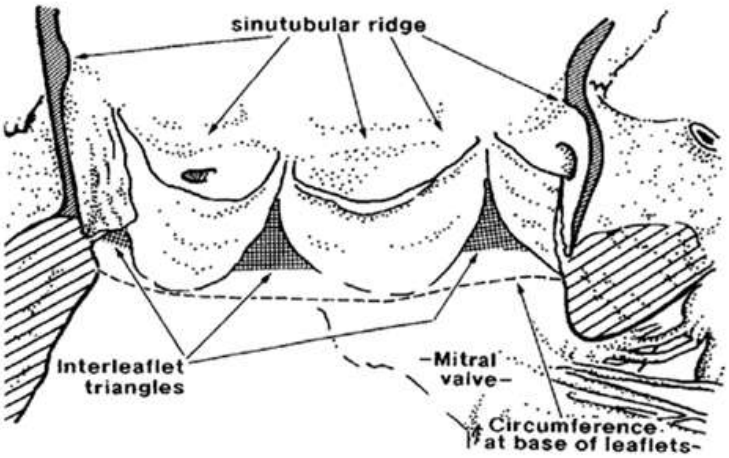

Fig.1.10: Aortic Root cut off longitudinally through the coronary sinus [113]

The aortic insufficiency can result from anatomic and functional abnormalities of valvular leaflets or root (such as, for example, STJ or annular dilations, deformation of sinuses,…), or both [114].

The *Pulmonary Valve* (Fig.1.11) shows a similar anatomy to the Aortic one and, also in this case, there is no presence of an anatomically well-defined *annulus* since the attachment points of the leaflets and the pulmonary root form a *continuum* [16].

Fig.1.11: Left view of the pulmonary valve depicting its three leaflets

The Tricuspid Valve (Fig.1.12) is located on the right side of the heart, between the *atrium* and ventricle. It is so called because of its three leaflets, which are approximately three triangular cusps originating from the edge of the valvular orifice and projecting towards the ventricular cavity [145].

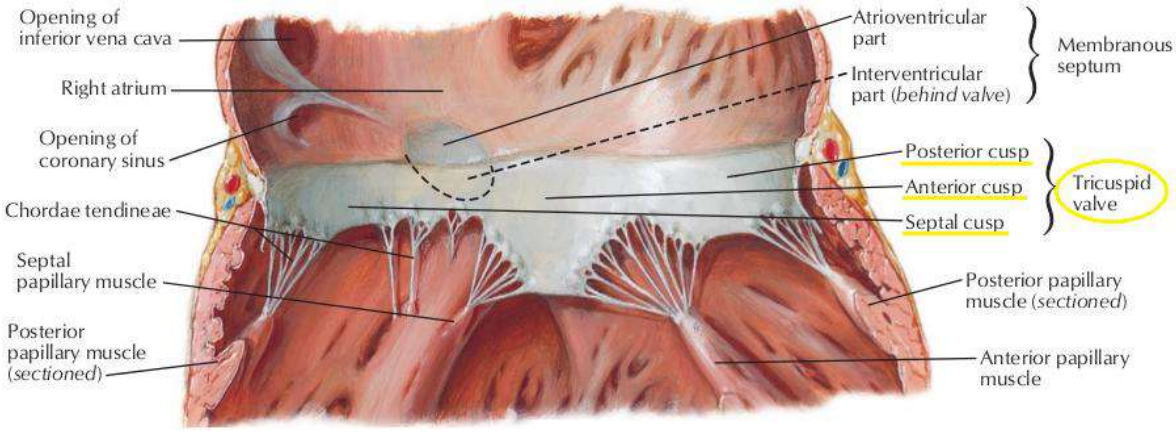

Fig.1.12: Tricuspid valve [78]

This valvular complex is composed by *papillary muscles* and *chordæ tendineæ*, apart from a *tricuspid annulus* and *leaflet tissue*. The annulus is a non-planar structure with a saddle-shaped pattern [118], while *chordæ tendineæ* are attached to the papillary muscles at one end, and to the *free margin* of ventricular leaflet surface on the other side (Figs.1.13). These structures are composed of fibrous connective tissue and ensure proper leaflets coaptation at end-systolic phase [10].

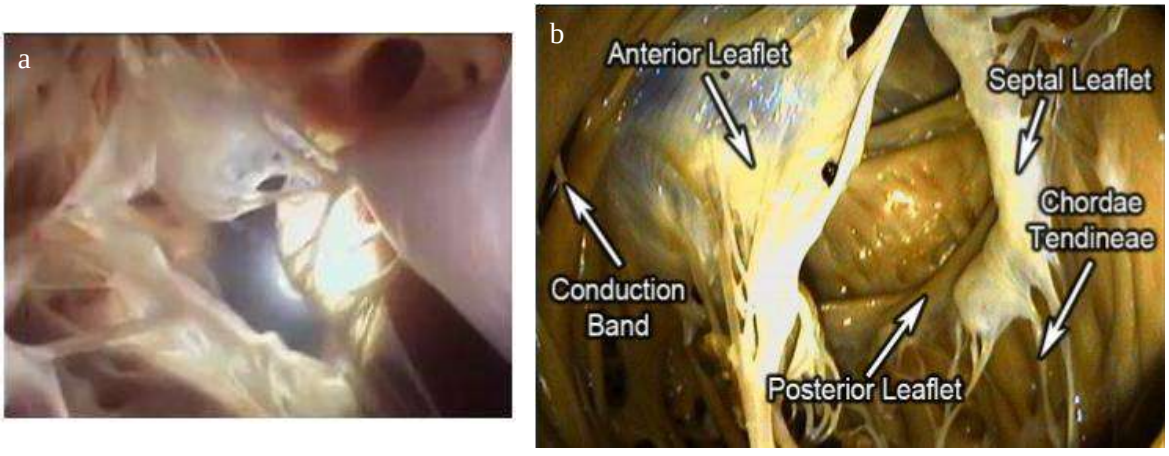

Fig.1.13: Ventricular view of tricuspid valve: leaflets, chordæ tendineæ and papillary muscles [140]

1.2.1. The Mitral Valve

The left *atrium* communicates with the left ventricle through the Mitral Valve (also named bi-leaflet valve): it lies in the floor of the *atrium*, separating the inflow from the outflow tract of the ventricle, by shifting its position, as shown in Fig.1.14.

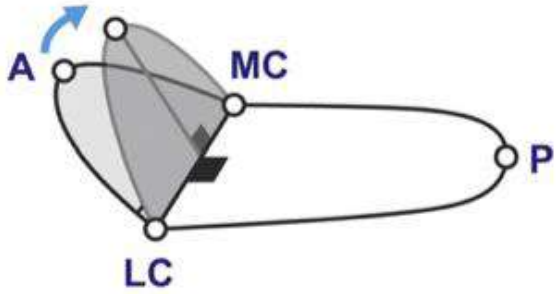

Fig.1.14: Annulus folding along the intercommissural axis (LC-MC) [104]

This valvular complex is composed of several structures, shown in Figs.1.15: Mitral *Annulus* (MA), Mitral *Leaflets* (ML), *chordæ tendineæ* and *papillary muscles* work in synchrony for the atrioventricular orifice opening during diastole and its tight closure in systole, within the high-pressure systemic environment. Morphological features and finely-tuned system of elements acting in a coordinated manner should also ensure a normal leaflets closure to prevent regurgitation of blood back from the LV into the *atrium* [26].

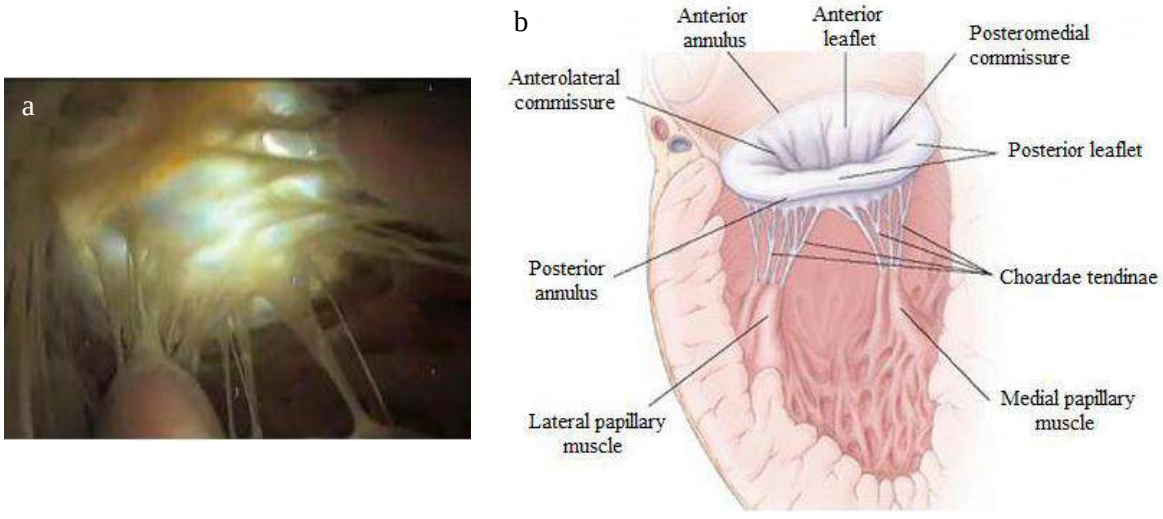

Fig.1.15: (*a*) Ventricular view of the components of the Mitral Valve; (*b*) Axial section of the LV where the MV can be observed [140,10]

1.2.1.1. Mitral Complex and Subvalvular Structures

The Mitral Valve (MV) is an active valve and not a mere passive flap bordering the atrioventricular junction; it has a structure similar to the tricuspid valve but, differently from that, this is part of the left ventricular outflow tract because it can facilitate the accommodation of blood, followed by its rapid, efficient and forceful ejection.

The *leaflets* represent an uninterrupted structure (Fig.1.16,a and 1.16,c) with regional differences that reflect particular functional characteristics [77]. Traditionally, the mitral valve has two leaflets usually identified as anterior and posterior leaflets, even if it would be more correct to define them, respectively, Antero-Superior and Infero-Posterior, according to a more appropriate description of their real orientation [26].

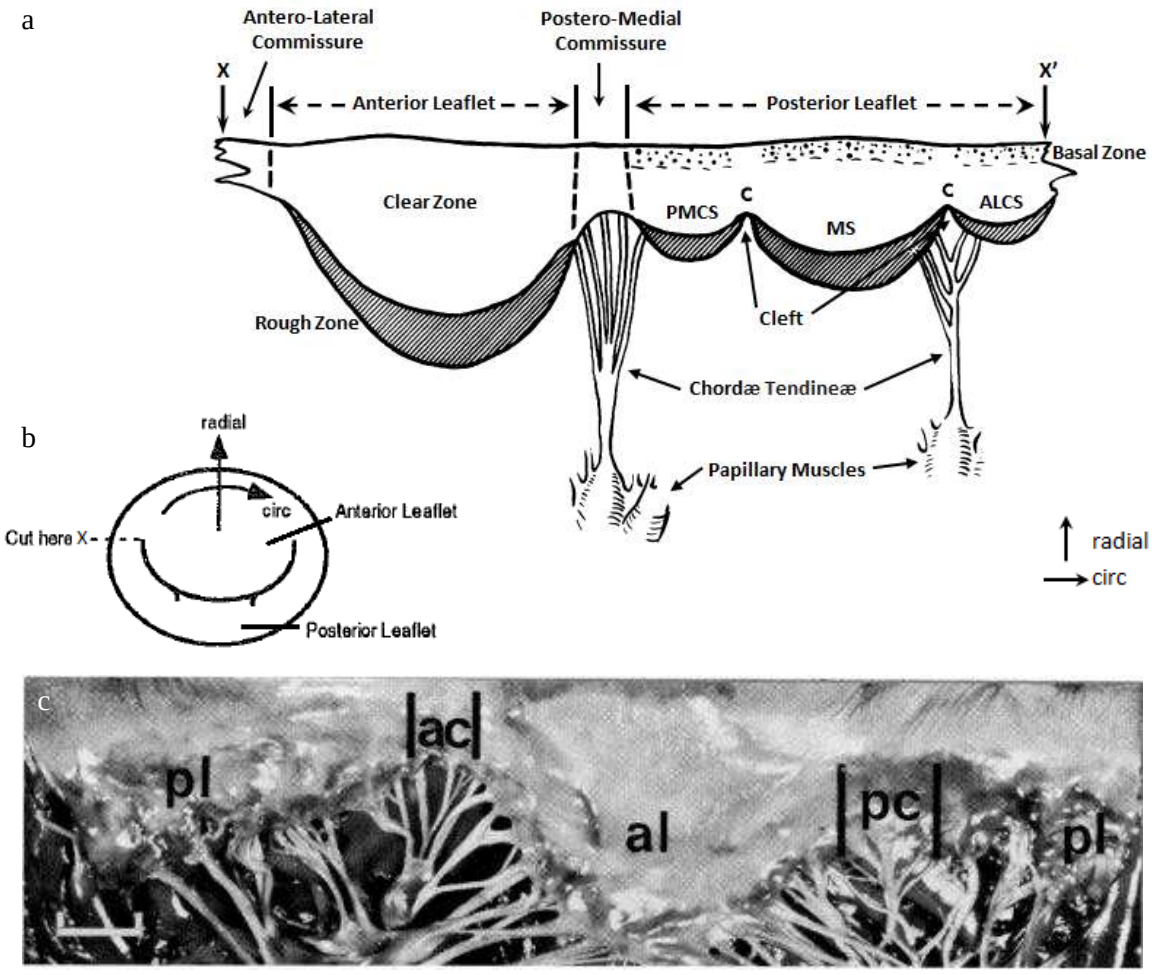

Fig.1.16: (*a*) Diagrammatic representation of the MV, excited 23mm outside the muscle-leaflet border, leaving intact chordæ tendineæ (commissural and cleft, with their typical attachment) and papillary muscles; PMCS=PosteroMedial Commissural Scallop; MS=Middle Scallop; ALCS=AnteroLateral Commissural Scallop. (*b*) Schematic showing of the intact valve where it was cut open. (*c*) MV tissue portioned into anterior leaflet (al), posterior leaflet (pl), anterolateral commissure (ac) and posteromedial commissure (pc); scale indicates 1cm. [95,72]

The *anterior* leaflet has a semi-circular shape and is attached to approximately two-fifths of the annular circumference, while the *posterior* one has a quadrangular shape and is attached to the rest of the circumference [82]. Although very different in shape, they share an almost equal area: the anterior leaflet has a reduced circumferential length but it is wider than the posterior one. The total area of the two leaflets is approximately twice the annular one: this redundancy enables the valve a correct coaptation (Fig.1.17) in different hemodynamic conditions [75]. The measure of the Antero-Posterior Diameter can be identified as the maximum width, between the two extreme points of the leaflets, passing through the center of the valve and lying on the annular plane.

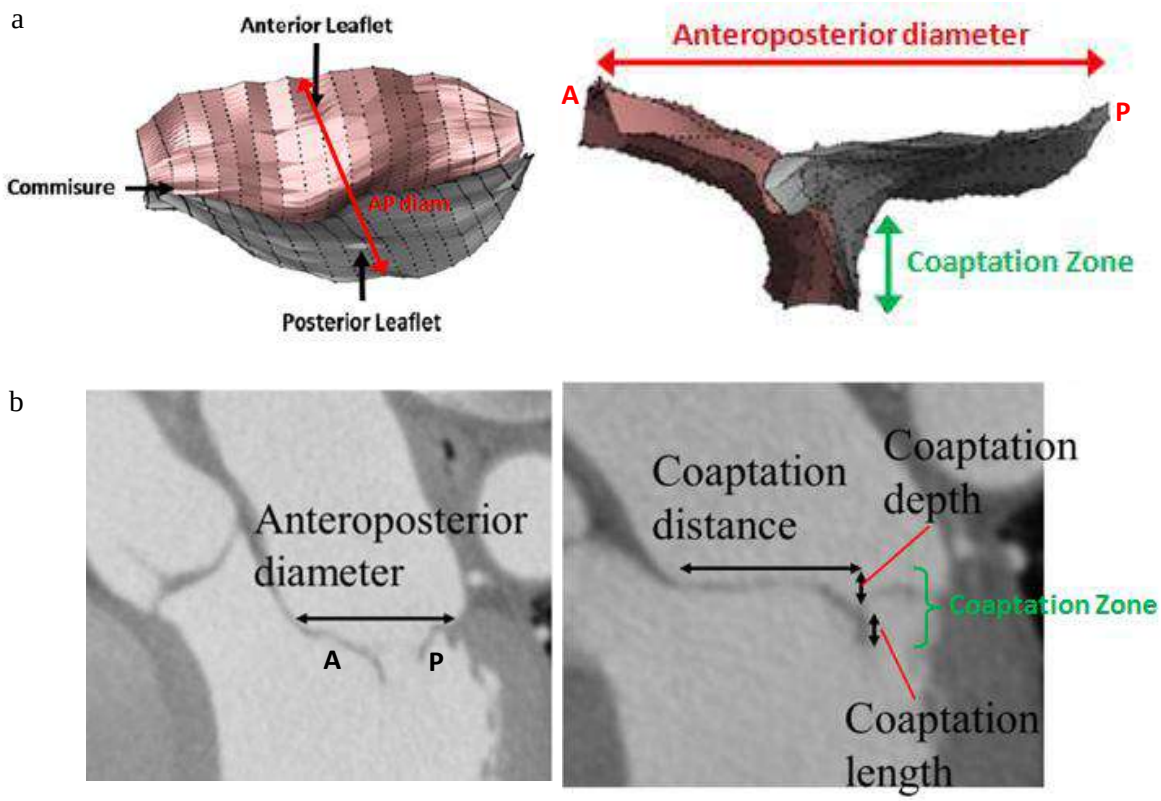

Fig.1.17: (*a*) Views of a segmented Mitral Leaflets derived from 3D echocardiography: 18 long-axis slices (dotted lines) used for semi-automated segmentation of the anterior (red) and posterior (grey) leaflets. (*b*) MV at middle diastole (left) and systole (right); the Coaptation distance is measured form the anterior leaflet attachment to the point of coaptation, along the annular plane [41], while the Coaptation depth is calculated as the perpendicular distance from the annular plane down to the coaptation point [42]. The instantaneous maximal vertical distance between the highest (anterior or posterior) and the lowest (AL or PM) points is named Annular Hight. [93,126]

Because of the relationships with the septal structures and the Aortic Valve (fibrous continuity with its left and non-coronary leaflets), the anterior leaflet is also called *aortic leaflet*, while, on account of its position and function, for the traditionally-labeled posterior

leaflet, the preferred term is *mural leaflet* [77]. However, during this work, we will label the leaflets as *anterior* and *posterior*, to greater clarity.

The *aortic* leaflet is a compact structure, without any indentation, positioned antero-superiorly in the left ventricle. Unlike the tricuspid valve, which is separated by muscle from its counterpart (i.e. the Pulmonary Valve), the mitral valve is immediately adjacent to the aortic one. As seen in a previous figure (Fig.1.16,a), it is largely made by a *clear* (*smooth*), central and thin zone which is devoid by tendinous chords; their layered attachments represent the so called *rough* zone [95]. It includes the *coaptation* zone and it is present in both leaflets, but it is broadest in the lowest portion of each one and tapers toward the periphery of the closure line (*commissures*) [26]. Each leaflet has also a *basal* zone that joins annulus, nervous structures, blood vessels and smooth muscular cells, which make leaflets active and adaptive tissues.

The *mural* leaflet has more variability than the anterior one and shows greater extensibility in both directions, possibly due to the more abundant chordal sustain [77]. It is narrow and extends three-fifths around the left atrioventricular junction within the inlet portion of the ventricle. Made mainly by three scallops, there is still debate if it represents a single unit or a whole of independent leaflets [26]. Starting from the superior (anterior) commissure and proceeding in a counter clockwise direction, towards the opposite inferior (posterior) one, the scallops of the mural leaflet can be labeled P1, P2 and P3 as initially proposed by Carpentier et al. in 1976 [14] (see Figs.1.18). In spite of the fact that the aortic leaflet is an undivided structure, as clearly shown in Fig.1.18,a, its corresponding portions can be analogously labeled A1 (*anterior*), A2 (*middle*), and A3 (*posterior*) [77].

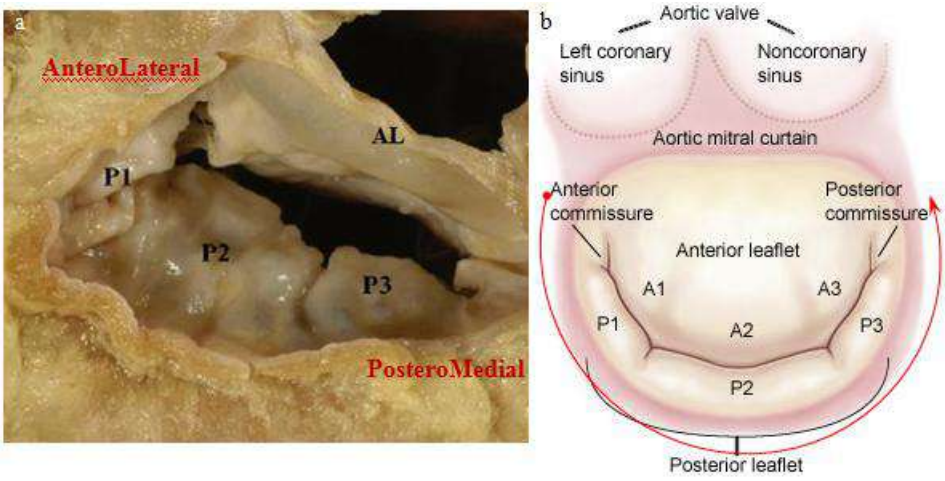

Fig.1.18: (*a*) Posterior valvular leaflet: three scallops named, from the AL to the PM zone, P1, P2 and P3. (*b*) Illustration of the atrial surgical view of the MV with standard nomenclature for each segment/scallop in the Mitral Leaflets. [94,137]

The *aortic* leaflet is a monolithic structure (see Fig.1.18,a), which participates passively in the mechanism of closure of the valve: its insertion includes fibrous tissue of the annulus, but it doesn't participate to the change of the mitral area during the cardiac cycle [116]. On the contrary, the *posterior* leaflet is the key structure in the closure of the valve: when the posterior annulus contracts, first the scallops coapt together then this leaflet, moving towards the anterior one, coordinates the valve closure process. This mechanism determines the complete closure (coaptation) and correct apposition (symmetrical overlap) of both leaflets, that are essential in preventing regurgitation.

Other two zones can be identified (see Fig.1.19): basing on a description of isolated organ, the *commissures* (and the underlying papillary muscles) are traditionally labeled as Antero-Lateral (*left*, *superior* and *parietal* position) and Postero-Medial (*right*, *inferior* and *septal*). Instead, if considering heart in the body, they respectively correspond to the posterior (with larger perimeter) and anterior portion (fibrous region in continuity with the aortic root, near the aortic valve) [26,77].

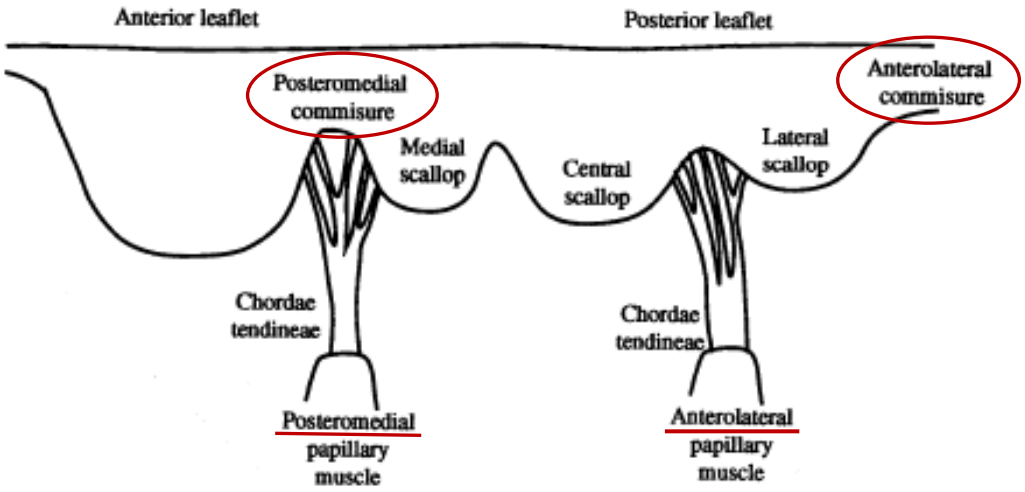

Fig.1.19: Representation of the MV leaflets [132]

The mitral *annulus* (MA) is a concept rather than an anatomical well defined structure; it can be described as a fibroelastic ring, a junctional zone which separates LA and LV, at the hinge point of the leaflets, and gives attachment to the muscles [88].

In a bi-dimensional view, the MA appears D-shaped (Figs.1.20) with Intercommissural (CC) diameter longer than the septo-lateral (AP) one (Fig.1.20,a) [26]. But, far from being a planar structure and a rigid circumferential ring, it is pliable and, also in 3D view, it has a

distinct saddle-shaped configuration (Figs.1.21), with the highest point along the anterior annulus towards the left atrium and the lowest point at the level of the commissures as shown in Fig.1.21,b (hyperbolic paraboloid) [102]. This is a dynamic three-dimensional structure, therefore it requires 3D deformation during the cardiac cycle [60,77].

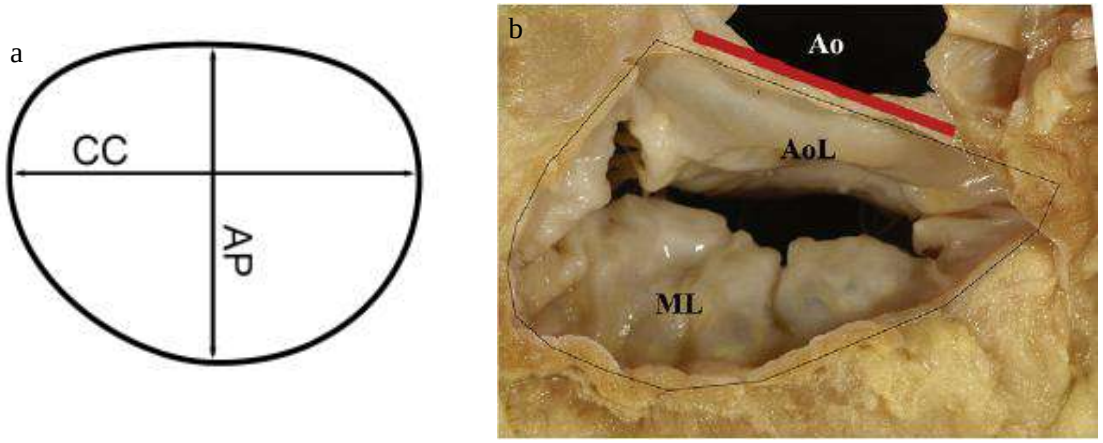

Fig.1.20: (*a*) Atrial planar view of the MA: almost elliptical, it can be described by its two main diameters (variable geometrical characteristics): AP=AnteroPosterior and CC=Commissure-Commissure diameter. (*b*) The D-shape of MA: anatomical view; the flattened portion of the "D" incorporates the mitro-aortic continuity (red line). Ao=Aortic valve; AoL=Aortic Leaflet; ML=Mural Leaflet. [61,26]

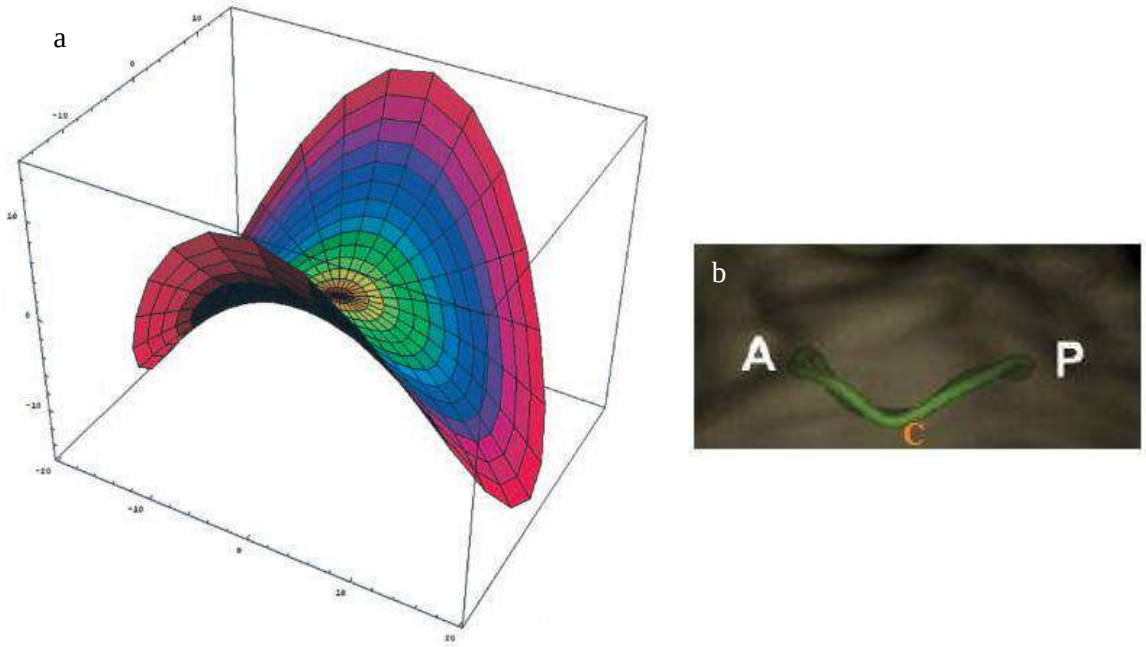

Fig.1.21: (*a*) Nonplanar annulus model: hyperbolic paraboloid as fundamental shape, not leaflets; this configuration represents the minimal surface area (38.75mm across the major axis, 30mm on the minor). (*b*) Echocardiographic view: the 3D silhouette of MV is saddle-shape with the highest point indicated as A, along the anterior annulus towards the LA, and the lowest point indicated as P (a part from the commissures, C) at the middle of the posterior annulus, deep into the LV. [102, 26]

The region of the mural leaflet insertion is dynamic, being mainly formed by muscular components [4], and coincides with the atrio-ventricular junction; instead, the flattened portion of the "D" extends away from the junction.

Fibrous support can be differently present along the ring in normal population but, commonly, dense fibrous aggregations are detectable just at the site of the two *trigones* – left and right, the major collagenous structures, which represent the anchorage of the overall valvular complex to the wall of the LV (Fig.1.22). The *right trigone* (also *central fibrous body*) lies in the midline of the heart and represents the confluence of fibrous tissue from the Mitral Valve, Tricuspid Valve, membranous septum and posterior aspect of the Aortic Root, while the *left* one lies at the confluence of the left margin of the aortic and mitral valves [117] (see Figs.1.24).

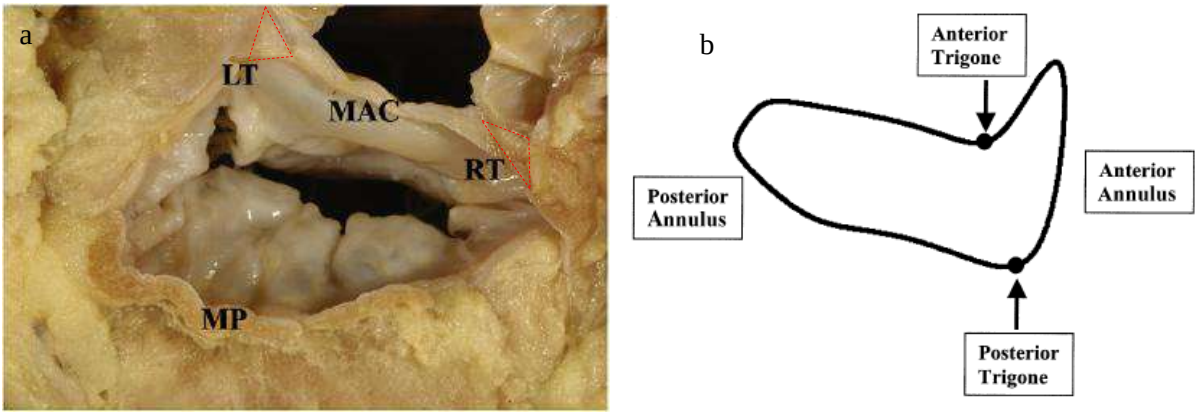

Fig.1.22: (*a*) Fibrous portion of anterior leaflet represented by mitro-aortic continuity (MAC) up to the trigones (left (LT) and right (RT)) and remaining muscular portion (MP); (*b*) Normal Mitral Annulus after computer reconstruction. [26,1]

The mitro-aortic continuity (Fig.1.23,a) plays an important role, forcing both the mitral and the aortic valves to work in synchrony: in systole, the posterior annulus moves toward the apex, while the anterior horn of the saddle moves toward the LA (Fig.1.23,b), contributing to the late systolic increase of the aortic orifice while, during diastole, the anterior horn moves toward the aortic annulus, contributing to the diastolic increase of the mitral area, and upwards, accompanying the Aorta movement [26].

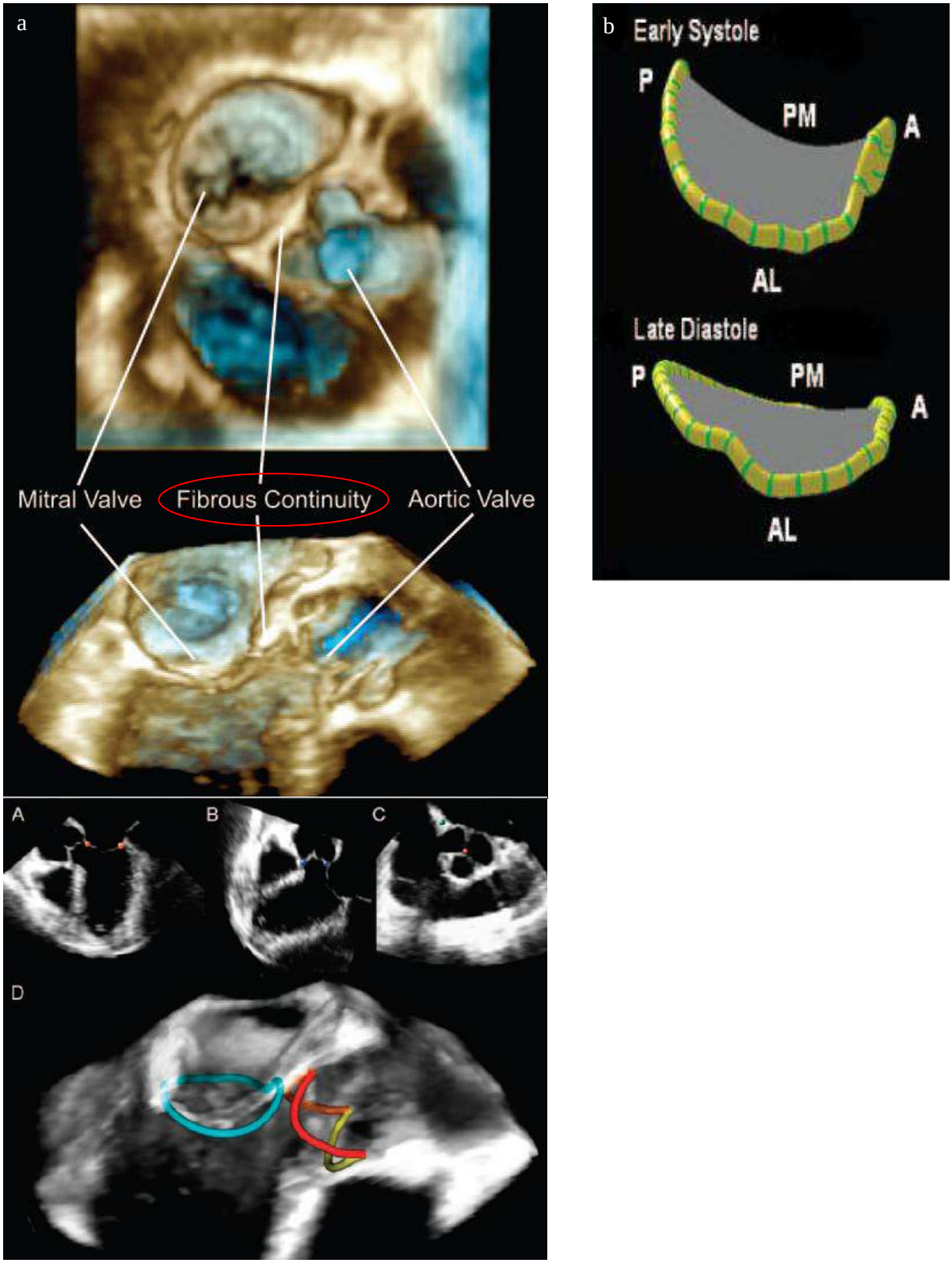

Fig.1.23: (*a*) Volume rendering of RT3DE data visualized from atrium (top) and in a long axis view (bottom); A-anterior and posterior MA points on a cut plane. B-Aortic annulus (AoA) points. C-Automatically displayed aortic valve short axis cut plane; coaptation point (red dot) manually identified. D-Computed MA (cyan) and AoA (red noncoronary cusp, orange left cusp, yellow right cusp) splines on RT3DE volume rendering. (*b*) Schematic profile view of a normal MV annulus in late diastole and early systole: the saddle shape is accentuated from late diastole to early systole. [120,42]

The normal MA not only moves, but also changes shape during cardiac cycle, as shown in Figs.1.23, and under different hemodynamic conditions: it undergoes area changes of roughly 23-40%, reaching a maximum in late diastole, determined by the annular relaxation, and a minimum in mid systole, with substantial pre-systolic area narrowing, due to the atrial contraction. Annular expansion and motion maximize fluid transport into the left ventricle facilitating its filling, while annular size reduction aids leaflets coaptation and competent valve closure [26,115,88,120].

However, the sphincteric action of the annulus can be affected by lack of atrial contraction, ischemia, atrial fibrillation or heart failure; this mechanism and the MA size may have important effects on valve performance, both in health and disease states (Fig.1.25), but the non-planar shape of the annulus is maintained throughout the cardiac cycle [115]. This out–of–plane motion is not uniform across the annulus, as the anterior portion adjacent to the Aorta exhibits larger displacements than the centre of the posterior one (Fig.1.26) [99].

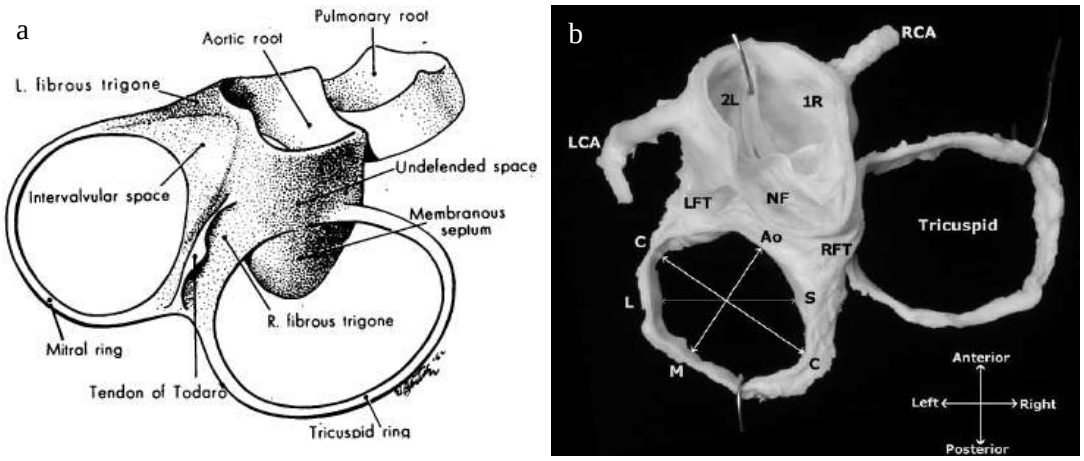

Fig.1.24: (a) Diagram of the fibrous skeleton of the heart. (*b*) Superior view. Tricuspid annulus left in place in order to reveal the original position and general orientation of the orifices. NF=aortic nonfacing sinus; LCA and RCA indicate the origin of the two coronary arteries (left and right, respectively). The intercommissural diameter of the mitral annulus is marked with C-C; the so-called septo-lateral diameter is actually the aorto-mural diameter (Ao-M). (*Note*:the literally-speaking and anatomically-positioned septo-lateral diameter (S-L) skirts closer to the intercommissural one.) [28,77]

The area enclosed by the annulus is a clinical measured parameter as it is used in the classification of dysfunctions, but its estimation is strongly dependent upon the definition of the annular border and the conversion of the non–planar geometry into a planar area (Fig.1.27) [57].

This measurement in human studies shows that significant variations exist between different imaging methods: discordant findings regarding annular dimensions and

dynamics appear to be the result of varying patient characteristics, species differences, as well as various and different methods of measurement used in experimental studies [99].

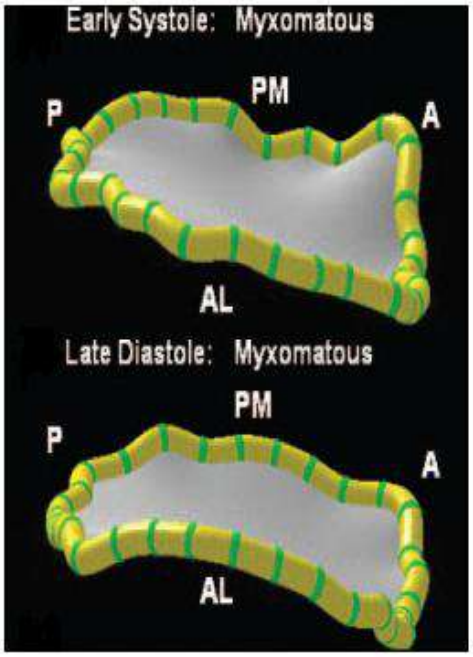

Fig.1.25: Schematic profile view of a myxomatous mitral valve annulus; the saddle shape changes from early systole to late diastole is blunted in MV diseased compared to the normal one. [42]

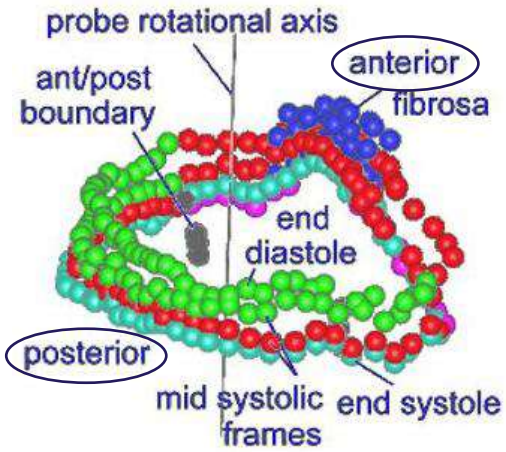

Fig.1.26: Annular profile reconstruction at different times during cardiac cycle; data obtained by 3D echocardiography. [53]

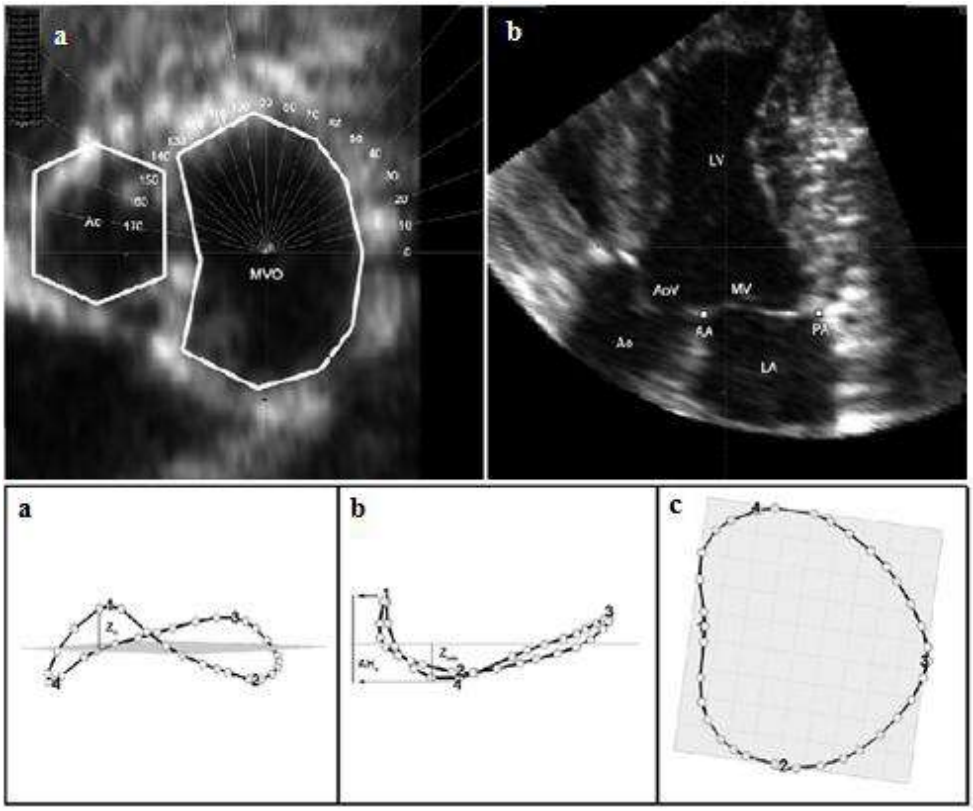

Fig.1.27 Top: *A*) Selected short-axis plane corresponds to the plane of the MV. *Ao* indicates tha Aorta and *MVO* the mitral valve orifice. Rotational template consists of 18 long-axis planes evenly spaced at 10° increments and centered at geometric center of mitral valve. *B*) Single long-axis view (0° on rotational template of panel *A*) of heart. Anterior and posterior annular points are labeled *AA* and *PA*, respectively. *Bottom*: Oblique (*A*), intercommissural (*B*) and transatrial (*C*) views of single human mitral annulus, including 36 data points (white spheres). Label: (*1*) Aorta, (*2*) anterior commissure, (*3*) midsegment of posterior annulus and (*4*) posterior commissure. Lowest point coincides with posterior commissure. [99]

The competence of the valve cannot be afforded by leaflets without the support of subvalvular apparatus [26], formed by *papillary muscles* and *chordæ tendinæ*.

The *papillary muscles* (generally two) lie directly beneath the two ends of the zone of apposition between the leaflets: the quantification of this coaptation zone resulting during the MV closure is of diagnostic importance for the assessment of valve's morphology and dynamics [16].

They originate from the left ventricular wall in the apical region and represent the connection between valvular leaflets and annulus, on one hand, and the ventricular wall, on the other side (Fig.1.28). Like the mitral commissures, the papillary muscles are more commonly defined as Antero-Lateral (AL or Inferior) and Postero-Medial (PM or Superior), considering the heart as an isolated organ (or as lying in the body, respectively) (Fig.1.29) [26,77].

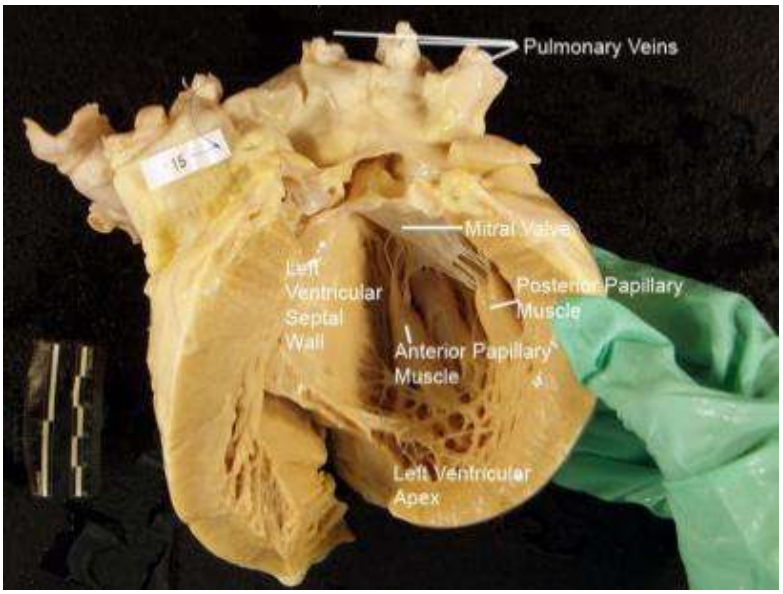

Fig.1.28: Section of left ventricle: orientation of papillary muscles. [140]

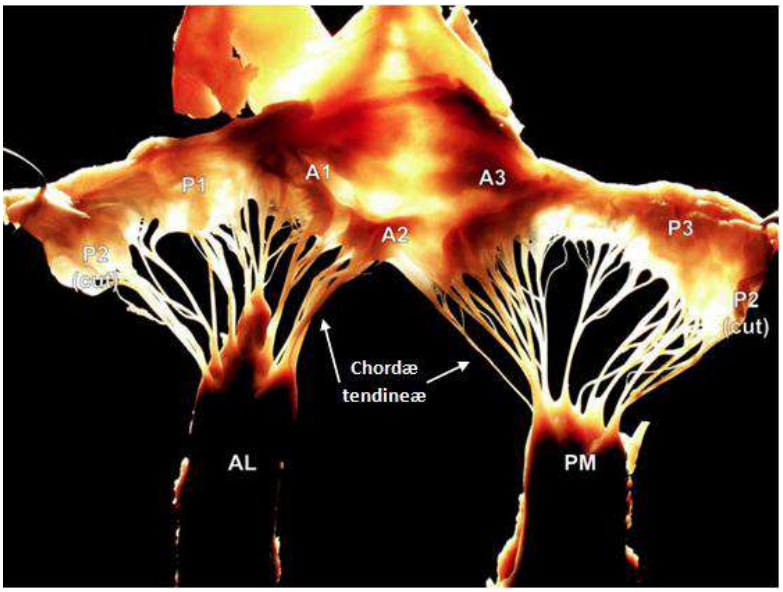

Fig.1.29: Components of the MV apparatus: fascicles of papillary muscles and intra-leaflet disposition of the cordal support. Normal asymmetry of the valve (backlit), opened in the middle of the P2 scallop; the cords of the PM muscle appear longer and more slender. [76]

The two muscles represent the ends of a more or less continuous column of papillary structures (Fig.1.30), with usually one "head" (but could be also two or multiple). Their fascicles position three-dimensional orientation has an important role in the distribution of forces and in assisting the proper closure of the mitral valve leaflets [17,51,103]. Their number and spatial relationships have a determinant impact on ventricular geometry and function both in physiologic definition of mitral components as well as in diseases [77].

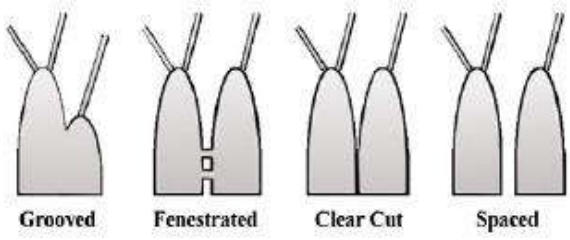

Fig.1.30: Different arrangements of papillary muscles [26]

The *chordæ tendinæ* are attached, on one end, to the ventricular surface of the anterior and posterior mitral leaflets and, on the other side, to the papillary muscles: together they determine also position and stress of each leaflet at the end-systole [82].

The papillary muscles function as shock absorbers maintains constant the papillary-annulus distance during the cardiac cycle, compensating geometric changes; this stability is probably due to the presence of the *second-order* cords, directly in contact with the trigones (see red arrow in Figs1.31,b) through the collagen fibers [26]. On the contrary, the distance between the papillary muscles and the ventricle apex varies significantly.

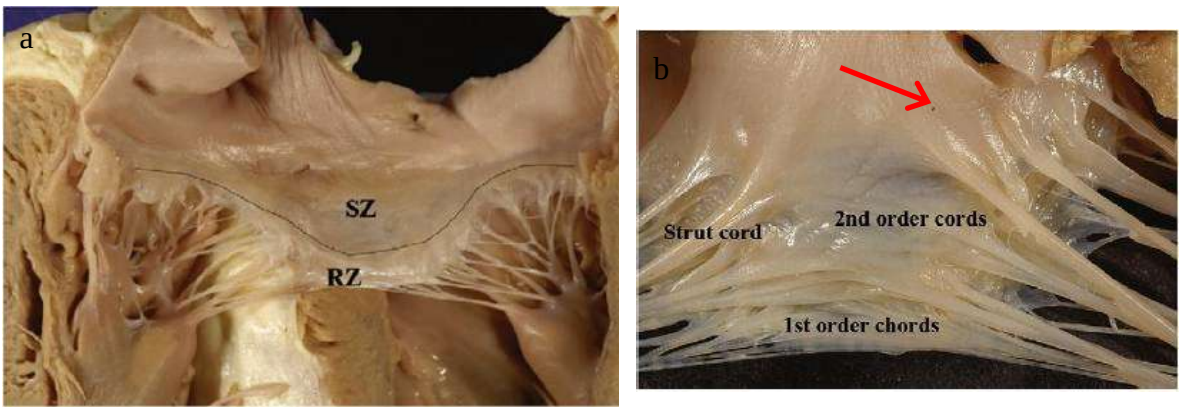

Fig.1.31: (*a*) Rough zone (RZ) is the border area where tendinous cords attach, while the larger remaining portion of the leaflet is called smooth zone (SZ). (*b*) Primary chords insert into the free edge, on the rough zone; The second order chords ensure coaptation; The thickened cords (Strut) are the strongest ones [94,26]

In the 70's, Lam et al. studied human *chordæ tendineæ* form 50 normal mitral valves: the hearts obtained at autopsy were selected from patients who did not have any clinical indication of MV disease. They were 27 males and 23 females, all Caucasian; ages varied from 15 to 85 years. On average, 25 *chordæ* inserted into the MV, without any significant difference in the total number between the two sexes. Some main types of *chordæ* were

distinguished by their mode of insertion, as shown in the diagram below (Fig.1.32): 9 of them pass to the anterior leaflet (7 *rough zone chordæ* and 2 *strut chordæ*), 14 to the posterior one (10 *rough zone chordæ*, 2 *cleft chordæ* and 2 *basal chordæ*) and 2 are inserted directly *into the commissures* [58].

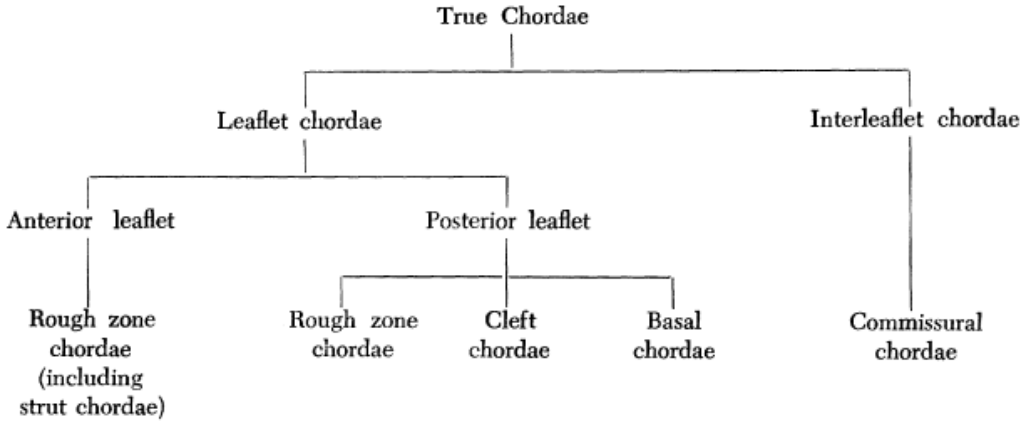

Fig.1.32: Classification of True *Chordæ Tendineæ* of MV (False chords are not included: from papillary muscle to papillary muscle, from PM to ventricular wall, from ventricular wall to ventricular wall) [58]

Other different classifications were based on functions of chordæ tendineæ or their biochemical composition, mechanical and histological characteristics, because some studies demonstrated that the amounts of their different components were related to their function and location [96]. Fenoglio [36] used scanning electron microscopy to observe the appearance of the normal features of human *chordæ* from young subjects: in his study, the cross-sectioned *chordæ* showed layers of endothelial cells on a basal lamina and the underlying layer consisting of collagen with occasional elastic fibers. Lim & Boughner [65] investigated morphology and mechanical properties while, in late 90's, Hall & Julian [43] outlined the functional aspects of the combined papillary muscles, *chordæ* and valve system in the LV, concluding that stretching of the *chordæ* were maximised when the blood were expelled from the ventricle. Millington-Sanders et al. [43] used inclined light illumination in a reflecting mode, besides conventional light and scanning electron microscopy, to observe and compare disposition of the structural components of the human *chordæ* under tension and when relaxed: a permanent and regular planar wave arrangement of collagen fibrils surrounded by two distinct layers of elastic fibers and endothelium are present.

Chordæ tendineæ resulted to be fibrous structures composed by connective tissue which join papillary muscles to the mitral valve leaflets, ensuring their coaptation during systolic phase; they could originate from tiny nipples on the apical portion of the two left ventricular papillary muscles or directly from the ventricular wall [58]. These *chordæ* intermingle within the very substance of the leaflets, contributing to their fibrous framework, specially at the level of the leaflets rough zone; some of the cordal intraleaflet extensions reach the annulus and the two fibrous trigones (see red arrows in Fig.1.33). They transmit contractions of muscles to the leaflets and secure them to maintain the valve closure and prevent its prolapse; at last, the *chordæ* must withstand the large repetitive forces that are encountered in the LV during every cardiac cycle. In order to perform these functions, the chords must contain a high degree of elasticity, as well as considerable strength and endurance [96]. Observing them in scanning electron microscope, they are composed of an inner collagen core (undulating fibrils) and multiple layers of elastin fibers, longitudinally arranged in parallel, aside from an outer layer of individual endothelial cells, as summarized in Fig.1.34 [43].

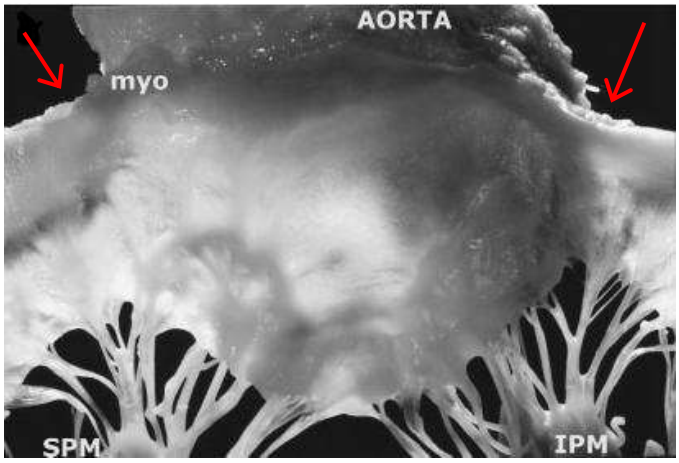

Fig.1.33: Aortic leaflet and adjacent commissural areas: intra-leaflet disposition of the cordal support, which proceeds very deep in the leaflet, sometimes reaching the level of the annulus. The commissural areas depict less and thinner leaflet material, with diminished cordal support. The atrial myocardium (myo) also contributes to the reinforcement of the basal portion of the leaflet [77]

Chordæ tendineæ are living tissues that act to support and feed mitral apparatus, more than simple collagenous structures: the arrangement of wavy collagen is well adapted to the cyclic stresses to which the *chordæ* are continuously subjected and also provides a mechanism for smooth transfer of forces to the leaflets, protecting the structural

components of the valve. The complex three-dimensional arrangement of the collagen fibers offers a built-in elasticity to the cords, mitigating the peak stress developed during ventricular and papillary muscles contraction [43].

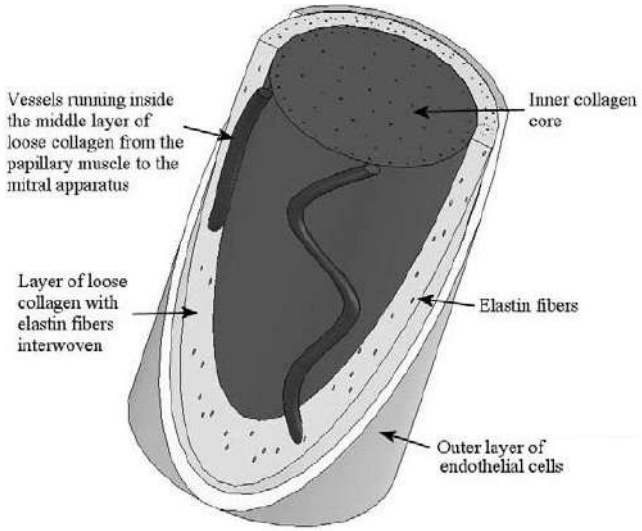

Fig.1.34: Three-dimensional models of the mitral valve *chordæ tendineæ* describing histologic composition [96]

Some studies demonstrated that the extensibility of the cords increases with their size and decreases with age [63,65]. Presence in the *chordæ* of young subjects of a regular periodicity suggests that it is likely to be a wave pattern, which gradually changes and elongates with age, becoming eventually randomized showing an irregular broad striped pattern. In fact, *chordæ* from elderly subjects (70-92y) show characteristic enlargements of the subendocardial connective tissue and a noticeable disorganized nature of the elastic fibers.

As shown in Fig.1.35, the aortic leaflet, and each scallop of the mural leaflet, have a convex free margin and receive cordal support from the two distinct papillary muscles or papillary muscle fascicles (‘‘heads’’), in such a manner that cords from different papillary muscles *converge* towards every leaflet. On the other hand, the clefts and commissural areas have a concave free margin (see red circles in the following figure) and receive from papillary muscle, or fascicles situated immediately underneath them, a cordal support that *diverges* (dichotomously or in a fan-like manner) while approaching the leaflet [77].

Chordæ tendineæ depict different microstructures according to their type (see Table1 and Fig.1.36); also tensions in tendinous cords vary with their type and with left ventricular pressure, reaching their maximum in early systole [67].

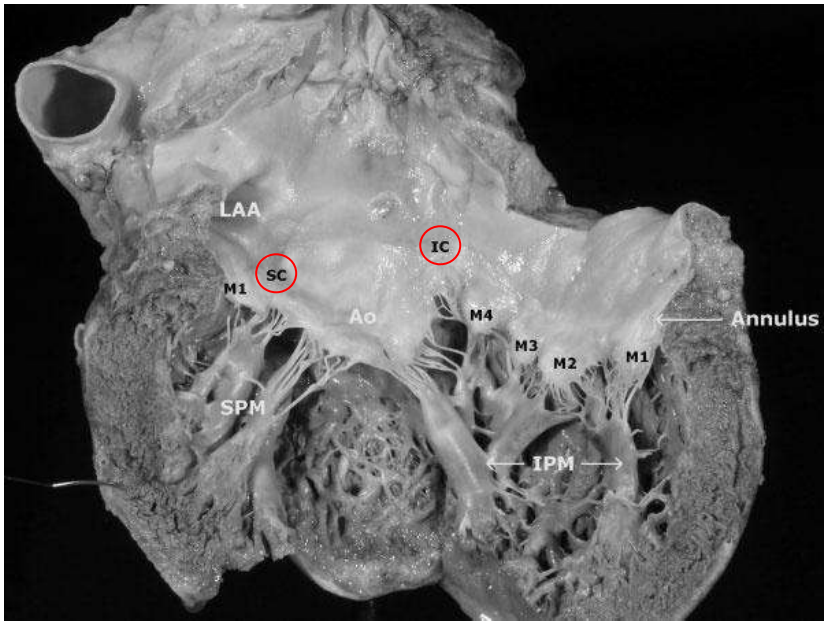

Fig.1.35: Mitral valvular complex exposed by cutting the heart specimen at the level of the left aspect, through the posterior scallop of the mural leaflet (M1). The inferior papillary muscle (IPM=AL, AnteroLateral) depicts more fascicles, while the superior one (SPM=PM, PosteroMedial) consists of two heads, one of which lies directly under the superior commissure (SC). The approximate position of the annulus is also evident. [77]

Old terminology	**Lam et al. (1970)**	**Ritchie et al. (2005)**
First order[a]	Commissural Rough zone cords of AoL and ML that insert into the free margin Branches of the cleft cords of the ML	Commissural Posterior marginal cord Anterior marginal cord
Second order[b]	Rough zone cords of AoL and ML that insert beyond the free margin Strut cords of the AoL Main stem of cleft cords of the ML	Posterior intermediate cord Anterior strut cord
Third order[c]	Basal cords of ML	Basal posterior cord
Type of cord	**Major role**	**Equivalent traditional terms**
Proposed simplified classification		
Marginal cords	Essential for coaptation	"First order"
Rough zone cords	Essential for leaflet geometry	"Second order"
Strut (sustain) cords Basal cords	Essential for ventricular geometry Annular reinforcement	"Third order"

Tab.1: Comparison of the old terminology of *chordæ tendineæ* with the new one.
AOL, aortic leaflet; ML, mural leaflet.
a) Inserting on the free edge of the leaflet.
b) Inserting on the ventricular aspect of the leaflet and contributing to the rough zone.
c) Origin from the posterior left ventricular wall. [77]

The ability to define the commissures with certainty comes from the recognition of unique commissural *chordæ*, that inserted into these areas [95]: they arise from tips of papillary muscles as a main stem, branch radially and insert into the free margin of the commissural regions, defining interleaflet areas; some fibers continue within the leaflet toward the base of the cusp. Usually, of the two commissural *chordæ*, one passes to the anterolateral (AL) commissural area, while the second one to the posteromedial (PM) commissure.

The fan-like arrangement would aid the hinge-like movement that brings anterior and posterior leaflets into contact with the commissural region (Fig.1.37).

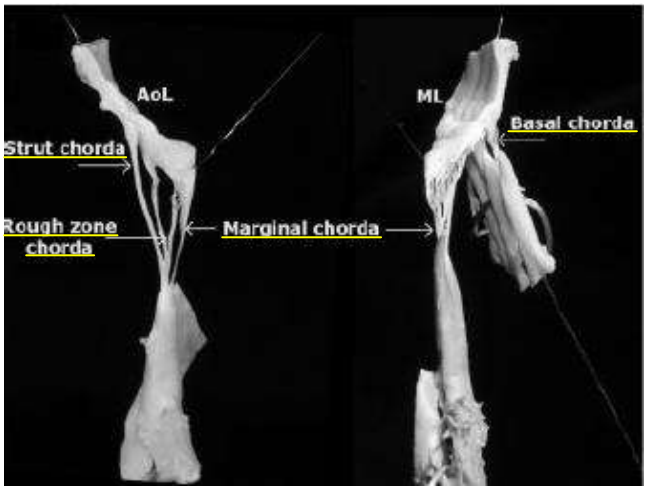

Fig.1.36: Tendinous cords of the mitral valve: anatomical distribution of the cordal support at the level of the leaflets. The wider aortic leaflet (AoL) allows to identify *marginal* (free edge) cord, *rough zone* and *strut* cord. *Rough zone* (intermediate) cords divide in two or more branches, some of which intermingle with the *marginal* cords: it is difficult to make a separation between the two types, both anatomically and functionally. The mural leaflet (ML) depicts the characteristic basal cords, which origin from the ventricular wall. [77]

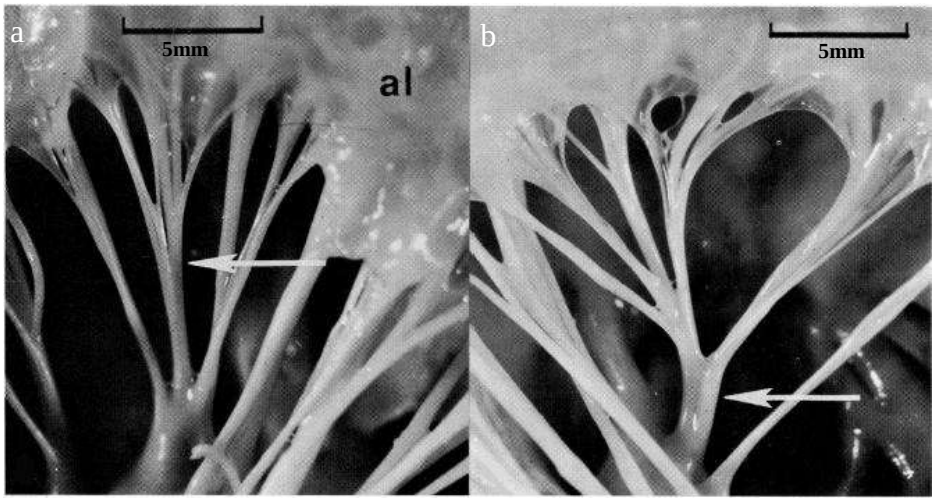

Fig.1.37: *Commissural chordæ*: (*a*) Insertion into the anterolateral commissural area(al = anterior leaflet); (*b*) Wide insertion into the posteromedial commissural area. [58]

The central stem of the PM commissural chorda points toward the center of its respective commissural area; this is also true of the AL one but, sometimes, it is slightly eccentric and points toward the anterior cusp. The branches of the PM *chordæ* are longer, thicker, and have a wider spread than their AL counterpart [58].

The anterior leaflet, whose thickness is related, in part, to the abundant chordal insertions in its ventricular surface, is membranous between the rough zone and the valve annulus, while the clear zone is devoid of chordal insertions but may show prolongations of chordal fibers [95]; here the *chordæ tendineæ* insert exclusively into the distal part of the leaflet. Typically, each one splits into three cords immediately after its origin from the papillary muscle: one inserts into the free margin of the leaflet, one beyond its free margin, at the line of closure, and an intermediate cord inserts between them (Fig.1.38). Among these *chordæ*, there are two thickest and largest tendinous *chordæ*, called "strut" *chordæ* (see white arrows in Fig.1.39); occasionally, each one branches further, giving rise to secondary branches which insert in the same area as the parent cords [58]. They are more extensible and less stiff than the marginal chords [63]; they function to prevent the leaflets from prolapsing during valve closure and withstand the highest mechanical load during the cardiac cycle (they bear the greatest tension, together with the basal cords) [50].

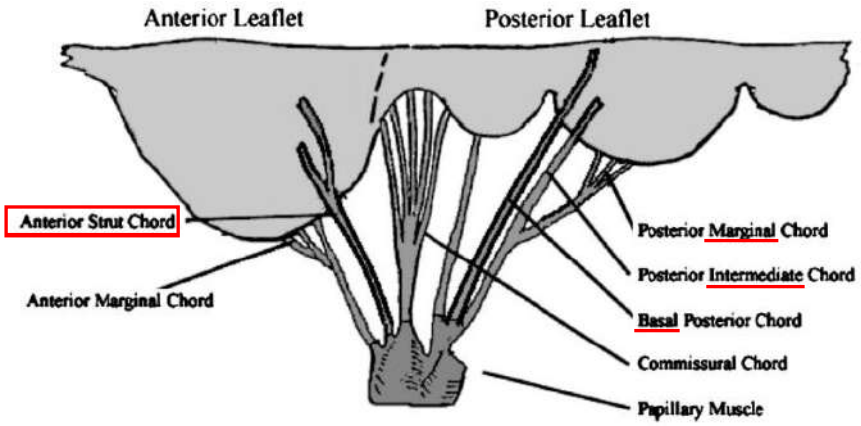

Fig.1.38: Diagram of extended mitral valve identifying *chordæ tendineæ* [50]

During valve closure the posterior leaflet remains relatively constant, and the posterior marginal chord is responsible for maintaining its placement (while the anterior one moves towards the posterior, until the line of coaptation is formed), so it needs a high degree of strength [96].

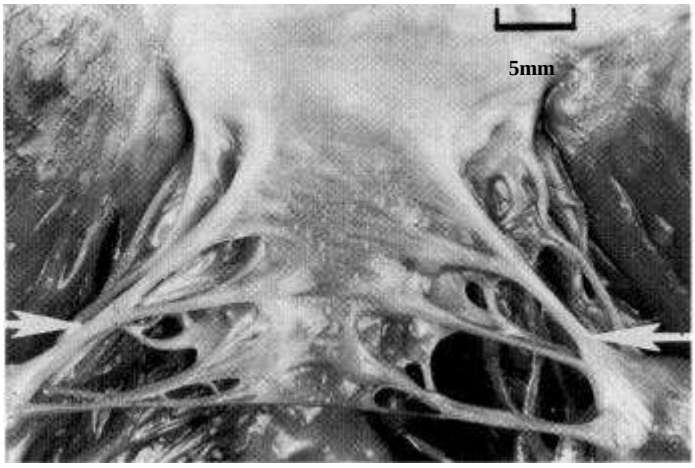

Fig.1.39: Ventricular surface of the anterior leaflet of the mitral valve: *strut chordæ* (arrows) [58]

Three distinct types of *chordæ tendineæ* insert into the posterior leaflet, whose free margin has indentations that give it a scalloped appearance (usually, it has one large middle scallop and two smaller lateral ones, near the commissures). Each chorda that forms a single strand arising from the posterior ventricular wall (Figs.1.40,a and 1.40,b) and flaring prior to its insertion into the basal portion of the leaflet is called "basal" chorda; the *chordæ* in this category vary a lot in number.

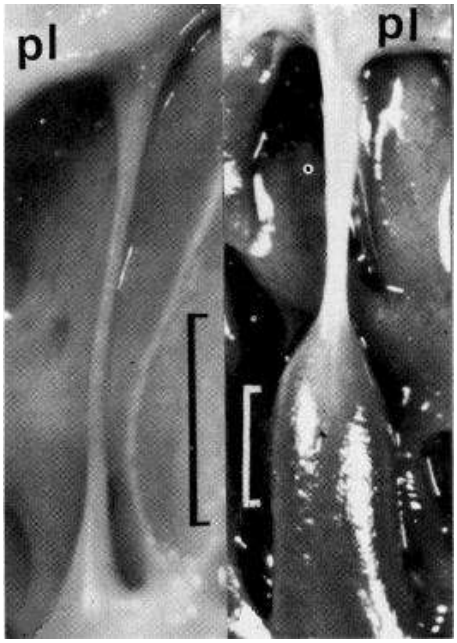

Fig.1.40: *Basal* chordæ of posterior leaflet (pl) arising (*a*) directly from the left ventricular wall, or (*b*) from the apices of small trabeculæ carneæ to insert near the annular attachment (scale: 5mm). [58]

A second type of *chordæ*, attached to the posterior leaflet, has a morphology similar to that of the anterior rough zone *chordæ*, but they are generally shorter and thinner (posterior leaflet does not have any strut *chordæ*).

A last type of *chordæ* (usually two) is termed "cleft", because they insert into the free margin of the cleft in the posterior leaflet: they divide it into three scallops, giving rise to tiny radial branches, like the struts of a fan [58]. These *chordæ tendineæ* are quite characteristic and their prior identification helps to define every different posterior scallops (Fig.1.41).

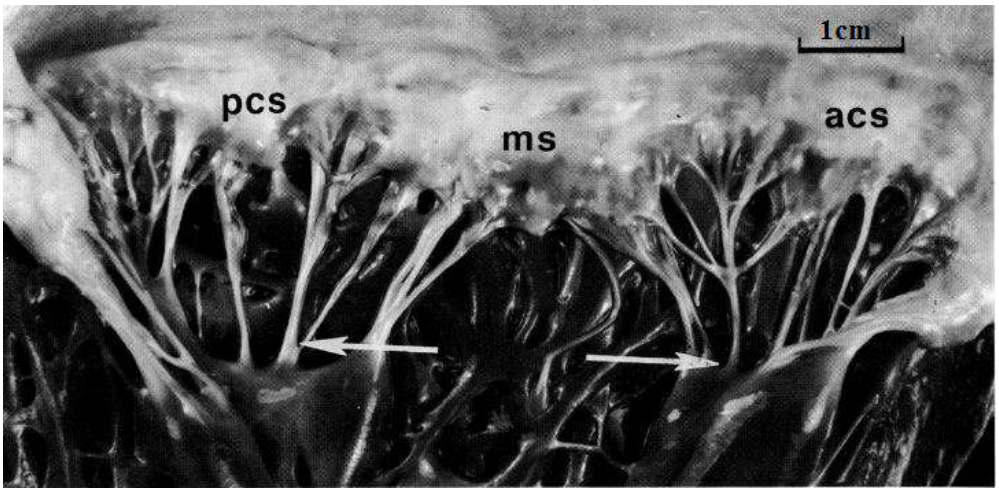

Fig.1.41: The tri-scalloped posterior leaflet: large middle scallop (ms) between two smaller, but comparable sized, semioval commissural scallops (pcs, posteromedial commissural scallop). *Cleft* chordæ (arrows) fan out to insert into the clefts, between the scallops [95]

Two cleft define three zones on the posterior leaflets (called, in fact, “tri-scalloped”): (1) the rough zone is defined, as in the anterior leaflet, by the line of leaflet closure and its free margin; (2) the narrow membranous or clear zone and (3) the basal zone, between the clear zone and the annulus, receives the insertion of the basal *chordæ tendineæ*, that originate directly from *trabeculæ carneæ* of the LV myocardium [58,95].

Fig.1.42 and Table2 summarize different classifications of the mitral valve chordæ tendineæ, also with their placement and typical characteristics:

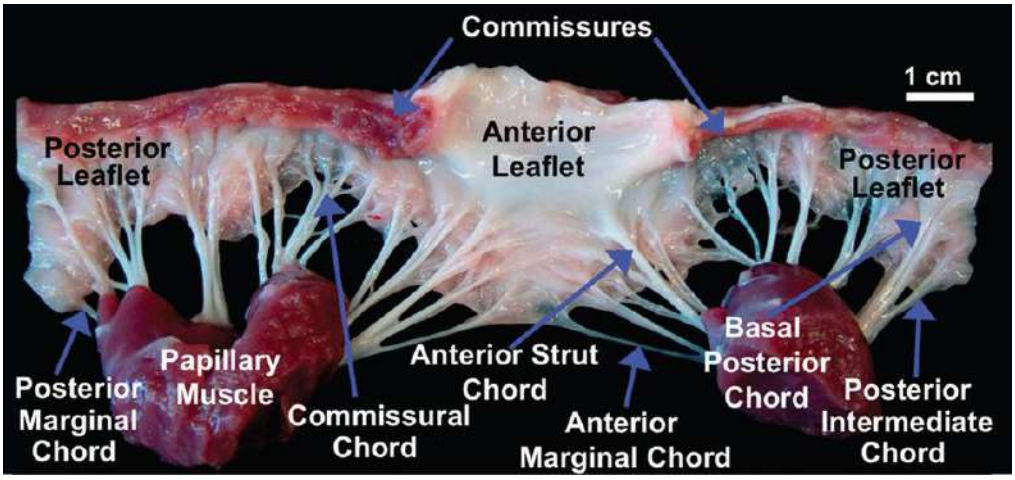

Fig.1.42: Excised porcine mitral valve [93]

The previously reported descriptions are just simplified classifications of the huge variety of the real *chordæ tendineæ* branches and manner of insertions existing in human mitral valve. In fact, there is a great variability among the examined cases in all above cited studies.

We have decided to create a summary table because, to our knowledge, it is quite difficult to orientate among different terminologies adopted in literature through the years, but also to facilitate a rapid comparison among all types of *chordæ tendineæ* and their characteristics. Different studies had classified the tendinous chords according on different criteria (chordal point of insertion on the leaflets, functions in the valve behavior, main features), thus also clinicians and surgeons still have nowadays some problems about understanding each other, because of the lack of standardized nomenclature.

Old terminology*[a]	**1st order**	**2nd order**	**3rd order**
Point of insertion*[b]	free edge (distal portion)	beyond the free margin, on the ventricular surface	base of the edge, proximal portion of the leaflet (directly from ventricular wall)
General Functions*[c]	- coaptation - prevent prolapse - MV competence: secure leaflets during closure	- coaptation - leaflet geometry, structure, function, mechanics	- ventricular geometry - annular reinforcement
New terminology*[d] and Main features of the Chordæ*[e]	**MARGINAL** C. *Ant*, *Post* RZ stiff, little extensible, thin; transmit contraction from papillary muscles to leaflets; collagen maintains placement of posterior leaflet (high degree of strength)	**INTERMEDIATE** *Post* no vessels	**BASAL** C. (MURAL)
	COMMISSURAL *AL*, *PM* fan-like arrangement; elastin prevents stress relaxation during constant strain	**STRUT** C. *Ant* maintain valve geometry; prevent prolapse; withstand high mechanical loads; lot of vessels little stiff, extensible and elastic, thick, large, few in number; from the tip of papillary muscle to the junction rough/smooth zone	**STRUT** C. (sustain)
	CLEFT C. *Post* branches	**CLEFT** C. main stem	

Tab.2: Ant=anterior; Post=posterior; RZ=rough zone; AL=anterolateral; PM=posteromedial; C.=chordæ.

*a [86]

*b [58]

*c [80,26,63]

*d [24]

*e [26,96,63,77]

1.2.1.2. Valvular Disease

Two main conditions can affect mitral valve: *Mitral Regurgitation* (MR) and *stenosis*.

The first one, the prevalent valvular disease in developed countries [12,49], is defined as a systolic retrograde flow from the left ventricle into the left *atrium*. Epidemiological data show that moderate or severe regurgitation is the most frequent valve disease in the USA [81] and the second most common form needing surgery in Europe, because it causes left ventricular overload and dysfunction, and yields poor outcome when it becomes severe. This disorder generally progresses insidiously, because the heart compensates by many redundant mechanisms acting to ensure leaflet closure -vast leaflet area, perimeter shortening, shape deformation, systolic aortic expansion- so its failure requires either catastrophic injury, such as chordal rupture or multiple structural changes [53]. Normal LV geometry and alignment of papillary muscles and *chordæ tendineæ* permit leaflets coaptation and prevent prolapse; dysfunctions of any one or more of components of the valvular-ventricular complex can lead to MR [18].

The main causes are classified as degenerative, usually related to valve prolapse, defined as an abnormal systolic valve movement into the left *atrium* [11] (evident in Fig.1.43), ischemic (chronic), due to the consequences of coronary disease, or rheumatic, that causes chordal and leaflet tissues retraction.

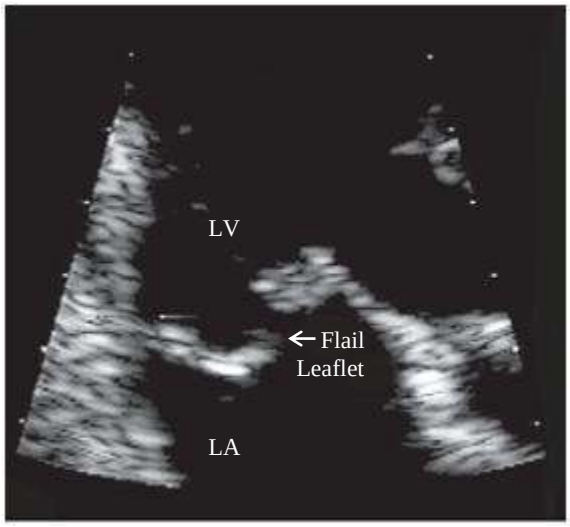

Fig.1.43: Echocardiographic apical view centered on the mitral valve: flail posterior leaflet, with the tip floating in the LA and grossly normal anterior leaflet [32]

A particular *cause* could produce regurgitation by different *mechanisms* (Tab.3), grossly classified as organic (resulting from intrinsic valve lesions) or functional (from remodeling of the left ventricle, which deforms a structurally normal MV), whose physiology is even more complex than the organic one [32]. In general, structural changes of the mitral valve apparatus can produce regurgitation: leaflet retraction (from fibrosis and calcification), annular dilatation, chordal abnormalities (rupture, elongation or shortening) and LV dysfunction (with or without papillary muscles involvement) [19,74,85].

	Organic			Functional
	Type I*	Type II†	Type IIIa‡	Type I*/Type IIIb‡
Non-ischaemic	Endocarditis (perforation); degenerative (annular calcification); congenital (cleft leaflet)	Degenerative (billowing/flail leaflets); endocarditis (ruptured chordae); traumatic (ruptured Chord/PM); rheumatic (acute RF)	Rheumatic (chronic RF); iatrogenic (radiation/drug); inflammatory (lupus/anticardiolipin, eosinophilic endocardial disease, endomyocardial fibrosis)	Cardiomyopathy; myocarditis; left-ventricular; dysfunction (any cause)
Ischaemic	--	Ruptured PM	--	Functional ischaemic

MR=mitral regurgitation. PM=papillary muscle. RF=rheumatic fever. *Mechanism involves normal leaflet movement. †Mechanism involves excessive valve movement. ‡Restricted valve movement, IIIa in diastole, IIIb in systole.

Tab.3: Causes and mechanisms of mitral regurgitation [32]

In the 80's, Carpentier et al. [15] classified Mitral Regurgitation into three main pathoanatomic types (described in Fig.1.44) based on leaflets and chordal motion; in Fig.1.45 the effects on leaflets coaptation are shown.

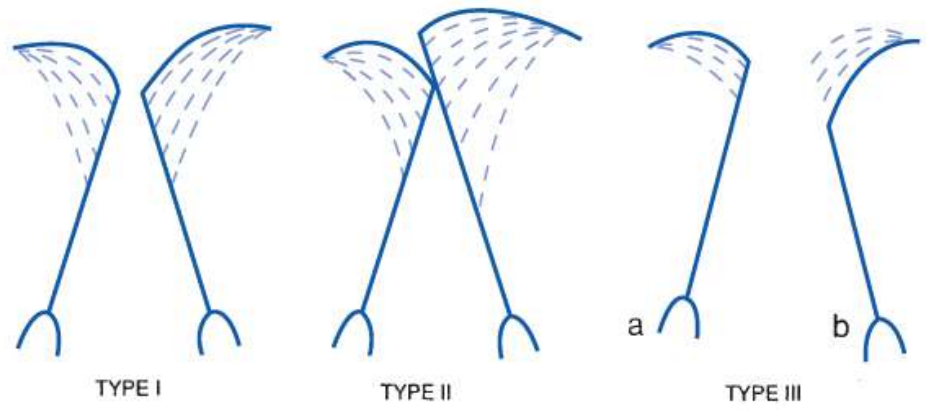

Fig.1.44: Carpentier's functional classification of leaflets and chordal motion associated with mitral regurgitation; dotted lines represent the course of the leaflets during the cardiac cycle [18]

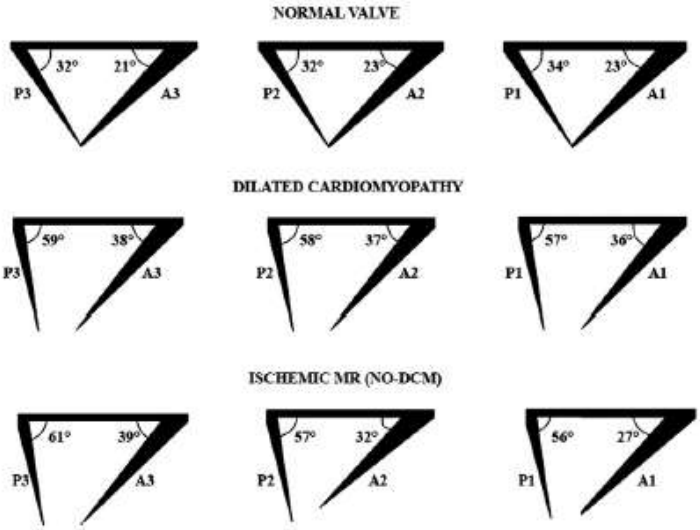

Fig.1.45: Comparison of angles between annular plane and leaflets scallops in different conditions [6]

In Type I MR, normal leaflet motion is often present in spite of frequent LV dilatation but the most common cause of MR in patients undergoing surgical evaluation is type II, characterized by leaflet prolapse or excessive motion [21,44,66]. It is also known as *Myxomatous Degeneration* and consists of excess spongy, weak fibroelastic connective tissue constituting leaflets and chordæ tendineæ [18], as shown in Fig.1.46 (typical in *Barlow's Syndrome*).

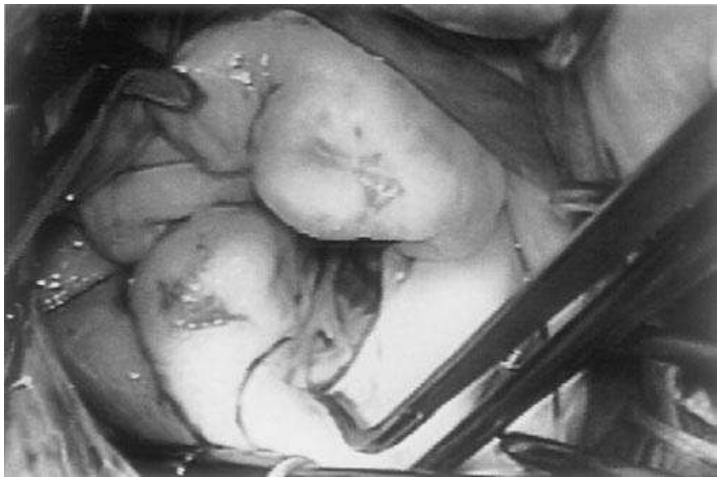

Fig.1.46: Intraoperative photography of mitral regurgitation owning to floppy mitral valve [18]

At last, type III results from papillary muscle dislocations in restricted leaflet motion.

Recent studies have highlighted that, compared with normal subjects, patients with *Functional Mitral Regurgitation* (FMR) have larger annulus along the septo-lateral diameter with more relaxed saddle shape, as indicated by its greater area, longer perimeter and reduced height [131]. This is an adaptive mechanism to cover the orifice area when the left ventricle dilates, but often it is insufficient because the leaflets become more stretched than normal, thicker and more redundant, the cords stiffer and globally less extensible. However, the most important morphological change concerns papillary muscles displacement, reflected in abnormally increasing imbalance between closure and tethering forces, which reduce the MV leaflet coaptation as shown in Fig.1.47 [45,53,26].

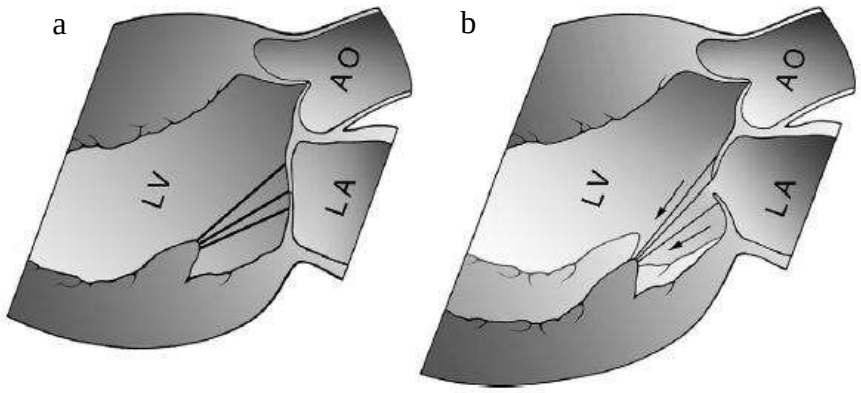

Fig.1.47: Relationship between papillary muscles and mitral leaflet: (*a*) Normal; (*b*) Large LV, greater tethering upon leaflets, any coaptation. [26]

The second condition that affects the MV is an obstruction of the left-ventricular inflow at the level of the valve as a result of rheumatic heart disease or structural abnormalities of the valvular apparatus, which prevents proper opening of the valve during diastole, known as *Stenosis* [12]. Non-rheumatic causes include severe mitral annular and/or leaflet calcification, congenital deformities, malignant carcinoid syndrome, neoplasm and LA thrombus [33]. Pathoanatomic characteristic changes include commissural fusion, leaflet fibrosis with stiffening and retraction, chordal fusion and shortening, and mitral annular calcification, that may progress to mitral sclerosis. Calcific protrusions into the ventricle or on the leaflets can further narrow the valve orifice, make the leaflets thicker and immobile (Fig.1.48) [18].

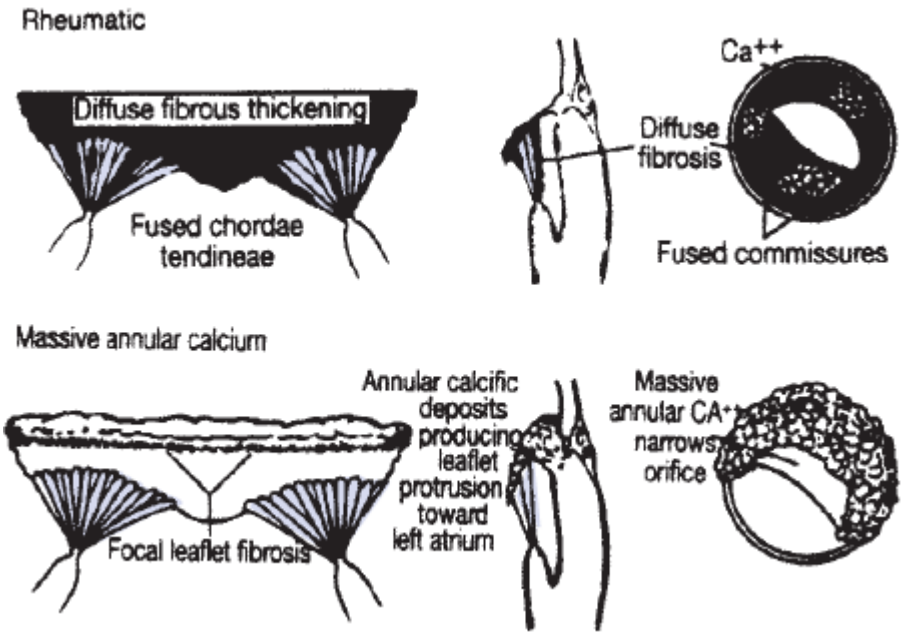

Fig.1.48: Different causes of mitral stenosis [18]

Mitral Regurgitation and Stenosis are intimately related and affect each other. In a regurgitant valve, fluid dynamic alterations cause vortices and blood stagnation near the leaflets; this phenomenon encourages blood coagulation and Calcium accumulation, making the valve stenotic. Vice versa, stiffening of a stenotic valve reduces leaflets efficient coaptation and causes a retrograde flow from the left ventricle into the *atrium*.
In both cases, there is a positive feedback, i.e. an initial injury can cause further damage and progressively worsen valve performance [73].

Surgical treatment is the only approach with defined clinical success [11]: valvular repair is preferred over replacement procedure for eighty-nine percent of patients with degenerative mitral valve and ischemic heart diseases because of greater freedom from reoperation and from several risk factors associated to endocarditis, thromboembolism or anticoagulant treatments, aside from better preservation of left ventricular function [40]. For valve prolapse, typical repair is resection of the prolapsed posterior leaflet segment, while subvalvular support can be obtained by chordal transfer, or artificial chords, and by using annuloplasty.

Consistent anatomical and functional descriptors of mitral lesions and geometry are essential to diagnose valvular disease and assess surgical reparability [11].

2. CARDIAC IMAGING TECHNIQUES

Over the last decades, different imaging techniques have been developed for the increasing request by surgeons and interventional cardiologists of detailed information about cardiac morpho-pathologies prior to any procedure. The introduction of early imaging tools into clinical practice contributed to provide unique information in improving the knowledge of cardiac structures. Particularly, accurate studies of the cardiac valves functional anatomy and their relationships with surrounding parts are of utmost importance in understanding patient conditions, identifying any pathologies and planning surgical interventions, when necessary.

2.1. Echocardiography

Echography is an imaging modality that exploits the ultrasounds behavior and, in the last 30 years with advances in both hardware and software technologies, has developed to become the most widely used diagnostic tool for many reasons. Images are generated by a scan converter that counts the time between the emission of ultrasound and return of the reflected wave to the same crystal, and calculates the distance from transducer to reflective structure, assuming a constant speed of progression.

In many cases conventional echography provides an initial and useful guide to study different organs, because blood allows excellent penetration of ultrasonic energy at high-frequency, from 2.0 to 20.0 MHz (penetration is minor through fat and air, while bones are such strong reflectors that no energy is left to progress). It has proved to be particularly suitable for cardiac disease because of its excellent temporal resolution, high sensitivity and accuracy in measurement on moving organs (*M-Mode*). Furthermore, other advantages are portability of echographic instruments, low cost of exam, which is rapid and painless, so easy repeatable, its lack of ionizing radiation and widespread availability. For all these reasons, echocardiography has become the gold standard in diagnosis of most adult cardiovascular pathologies and in monitoring their progression over time [53,18]. However, it also has some limitations, that include variations in image quality as the result of the individual body habitus (transthoracic echocardiography might be difficult in obese patients, in the presence of wall deformities or chronic lung disease [2]), expertise needed to manipulate the ultrasound probe, and potential measurement variability due to plane selection [98]. While measurements of depth are excellent, lateral resolution is less precise

because strong reflectors tend to diffract the ultrasound energy, which rebounds not only toward the original crystal but also toward the adjoining ones, so that artifacts may be generated.

2.1.1. Echographic Techniques for Mitral Valve Assessment

Today, transthoracic or transesophageal echocardiography (*TTE* or *TEE*) are commonly the primary diagnostic tools for a clear general understanding of the anatomy and pathologies of the Mitral Valve because they are usually satisfactory, often obviating further cardiac imaging exams.

Conventional two-dimensional echocardiography (*2DE*) is the clinical mainstay for patients with MV disease in many echocardiography laboratories, but it is severely limited in studying with precision three-dimensional structure of the valve. 2DE is limited in that all points of interest cannot be localized in one plane [107]: usually, two-dimensional examination of the mitral valve requires to combines multiple redundant views of all parts of the valve to identify each mitral segment, also using internal recognizable cardiac landmarks (such as the Aortic Valve) [134]. Annular dimensions are often erroneously assessed using 2D transthoracic echocardiography because it visualizes the mitral annulus in slices perpendicular to the plane on which it lies, due to the tomographic nature of echography (Fig.2.1) [5,18]. Just a slight flexion of the probe makes it not perfectly perpendicular to the plane of the mitral annulus, so its dimensions can be overestimated or underestimated. Also studies of the *chordæ tendineæ* are traditionally neglected in 2D echocardiography because they are linear structures, with a thickness often less than 1 mm, which generally can be seen only as small lines. When the echocardiographic image is of good quality, it is possible to see some *chordæ tendineæ* from the insertion of the papillary muscle to that of the mitral valve, but it is almost impossible to distinguish the different cords types, nor to identify their precise branches localization on the leaflets surface. Neither three-dimensional echocardiography provides additional information compared to two-dimensional techniques (Fig.2.2): the *chordæ* appear joined more often than they are in reality (only with the transgastric approach it is possible to see them fairly easily) [35].

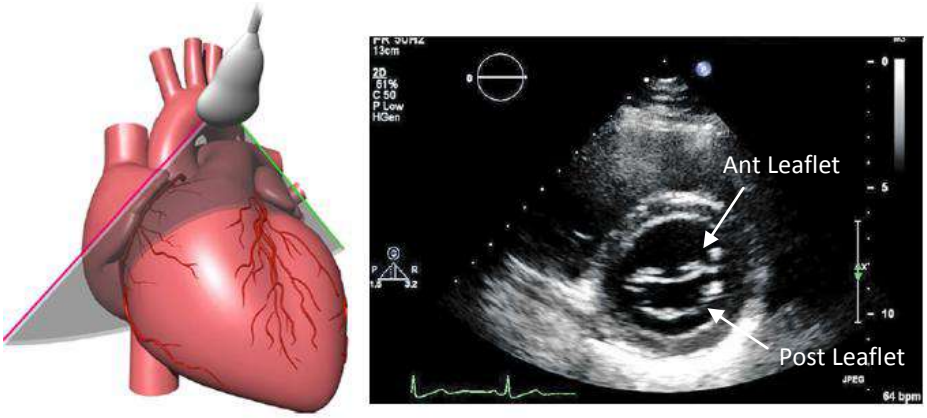

Fig.2.1: Parasternal basal Short Axis (Para SAx) view of the MV [25]

TTE is completely noninvasive and safe, it can usually provide detailed description of complete etiologies and mechanisms of valvular disease, important and useful classifications (85% to 90% of cases), but it may require *TEE*, which provides superior quality in imaging the heart, owing to excellent ultrasound penetration from the esophagus with higher ultrasonic frequencies. Moreover, *transesophageal* transducer is much closer to the posterior portions of the heart, so structures with high acoustic impedance, such as lungs or ribcage, do not appear between the transducer and the heart. This approach enables more precise measurements then *transthoracic* two-dimensional echocardiography [35], but it is more invasive: the risks attached to TEE are extremely low but not absent. This procedure is contraindicated in patients with recent oral intake, prior esophageal surgery or unstable cervical spine injuries, and presents possible effects of conscious sedation or anesthesia on the evaluation of cardiac diseases, limited ability to modify position of the transducer and loss of image quality in the distant field.

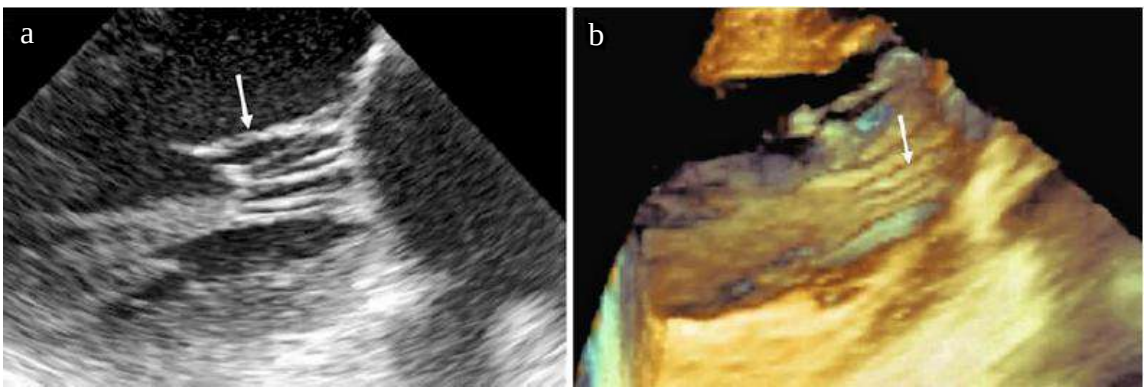

Fig.2.2: (*a*) TE2DE: Anterolateral papillary muscle and *chordæ tendineæ*; (*b*) 3DE of the same patient: The number of *chordæ* appears to be less than in 2D view. They are seen as single and thicker *chordæ* because the resolution is insufficient to distinguish them [35]

Despite some advantages, routine transesophageal echocardiographic evaluation of the mitral valve remains challenging for several reasons: (1) a systematic examination using standardized views is needed; (2) surgical and transesophageal echocardiographic descriptions of the mitral anatomy and associated abnormalities often differ substantially: a surgeon views the mitral valve in a non-physiologic state because the heart has been decompressed during cardiopulmonary bypass whereas transesophageal echocardiography shows the mitral valve in its normal dynamic and physiologic state, prior the cardiopulmonary bypass; (3) the currently used nomenclature for the anatomic description of the mitral valve is neither standardized nor universally accepted [38].

Atlases of echocardiography describe some standard echographic views, probe position and the corresponding expected image of mitral portion (see Tab.4), but it is very difficult to obtain these precise images during a MV examination in real clinical practice.

5-Chamber Allows localization of pathology to the anterior or posterior leaflet. Specific scallops difficult to identify based only on this view, but generally shows anterior elements of the valve.		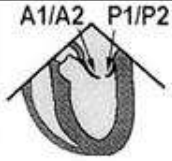
4-Chamber Allows localization of pathology to the anterior or posterior leaflet. Specific scallops difficult to identify based only on this view, but generally shows posterior elements of the valve.	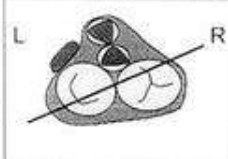	
2-Chamber Anterior Shows a long anterior leaflet (A2/A3) and a short segment of the posterior leaflet (P3). Note that the part of the anterior leaflet that coapts with the P3 scallop is the A3 segment.	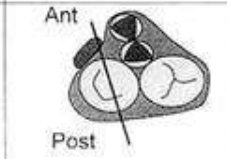	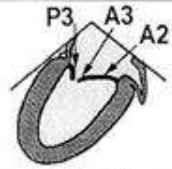
2-Chamber Mid Three scallops and two coaptation points are seen: P3, P1, and a variable amount of A2, which disappears during diastole.	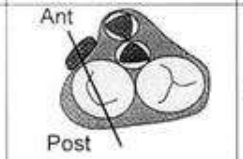	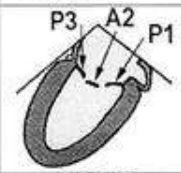
2-Chamber Posterior No coaptation point seen. The plane cuts through the posterior leaflet only. Usually demonstrates mostly P2, with some P1 and P3.	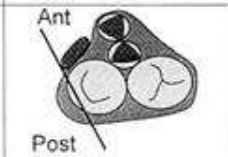	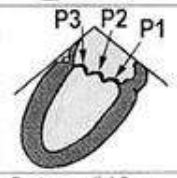
Short Axis This view is most useful with color Doppler to localize the site of regurgitation. However it rarely demontrates the nature of the pathology.	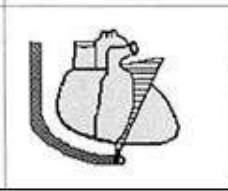	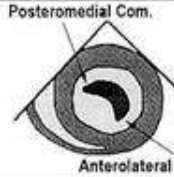

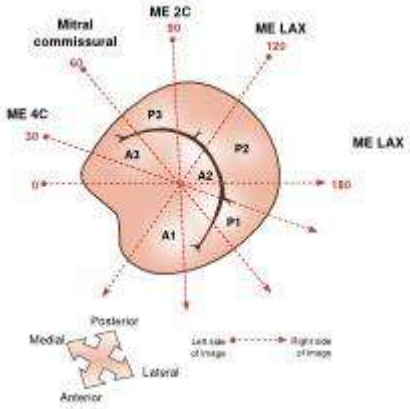

Tab.4: *left*: the most common echocardiographic views for two-dimensional TEE; *right*: orientation of transesophageal probe (degrees). [142,144]

Our meeting with Dr. Gambarin F., cardiologist echographist at St. Pio X Clinic in Milan, has highlighted the principal and important difficulties in studying mitral leaflets geometry by two-dimensional techniques. Moreover, if it was necessary to measure the length of a leaflet scallop by TTE, it will be almost impossible to distinguish the end of its rough zone by the beginning of the point of attachment of the chordal branches on the its surface, even if we had a good image quality (Figs.2.3).

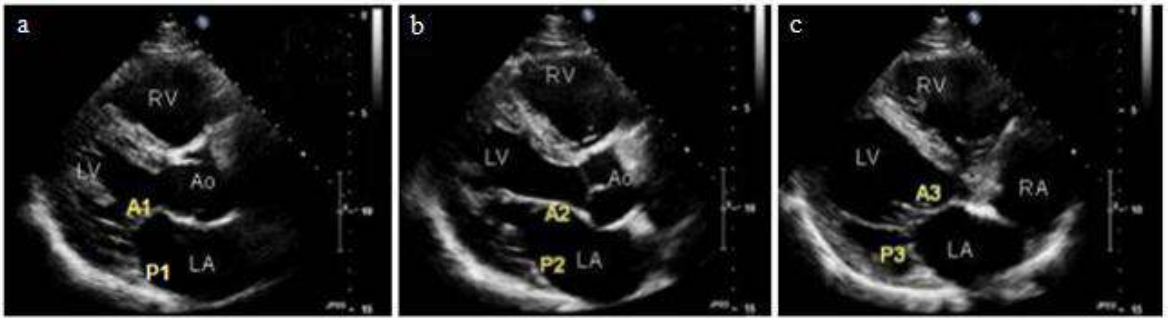

Fig.2.3:*Chordæ tendineæ* are visible under the leaflets. Parasternal Long Axis (plax) view of (*a*) Anterior scallops, (*b*) Middle scallops and (*c*) Posterior scallops. RA=Right *Atrium*, RV=Right Ventricle, LA=Left *Atrium*, LV=Left Ventricle, Ao=Aorta [138]

While by TTE it is quite easy to visualize the mitral annulus with anterior and posterior leaflets profile (see Fig.2.1), it is also possible to image the central scallops A2 and P2 (Fig.2.4), but it is almost impossible to separately identify the other single scallops (A1 and P1, A3 and P3) because there isn't any well defined boundary or landmark: adjacent scallops of a leaflet merge each other as shown in Figs.2.5.

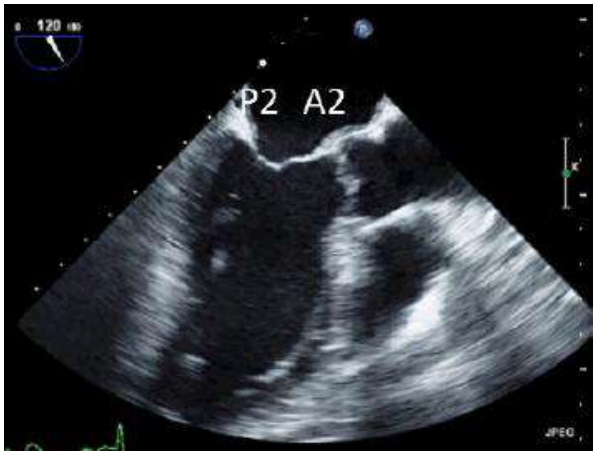

Fig.2.4: Mid-Esophageal Long Axis view [31]

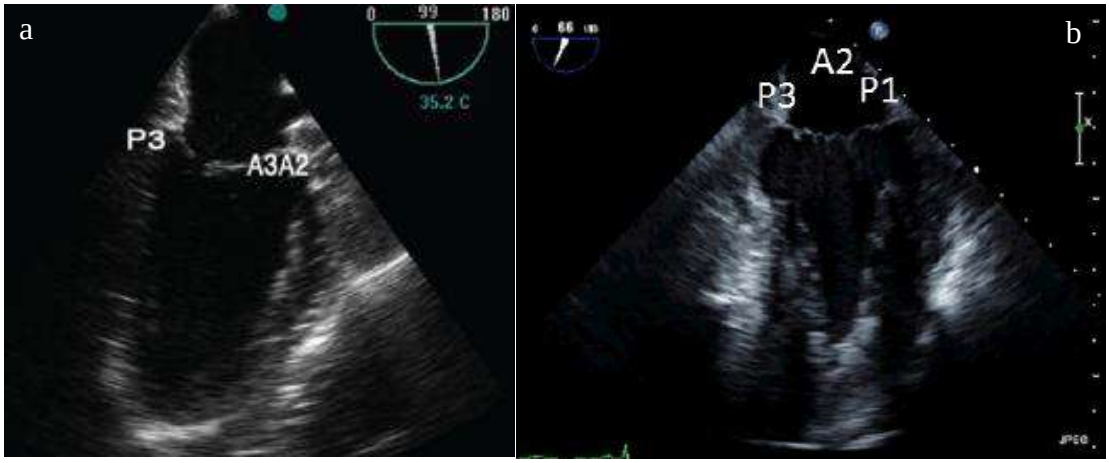

Fig.2.5: It is impossible to understand where one scallop ends and another one begins: (*a*) 2-Chamber (2C) view; (*b*) Mid-Esophageal (ME) Mitral Commissures (MC) view [7,31]

Furthermore, we must remember that transthoracic and surgeon's views are mirror, as depicted in Fig.2.6,a.

In conclusion, 2D echocardiography has facilitated the advancement of mitral valve knowledge and repair, but consensus is increasing that a dynamic, anatomically correct 3D view of the valve is crucial.

Three-dimensional echocardiographic (*3DE*) imaging has been developed with the aim of providing additional anatomic detail and improved spatial relationships that were not available from 2D images [59].

Almost 30 years ago, Levine et al. [62] used nascent 3D echocardiographic technology to describe the non-planar saddle shape of the mitral annulus for the first time, and Abraham and coworkers demonstrated that 3D transesophageal echocardiography could detect new morphologic findings not seen on 2D TEE [68]. Subsequently, this technique has been used to accurately quantify its geometry [98]. To date it is also possible to locate the areas of fibrous thickening that correspond to the trigones (Fig.2.7,a).

With the *same prospect of surgeon* (true and real revolution of the scope of echocardiography) anatomical details that have never been seen before can be easily observed, such as the commissures or the variable morphology of the posterior leaflet with its incisions that divide the leaflet itself (Fig.2.7,b) [35].

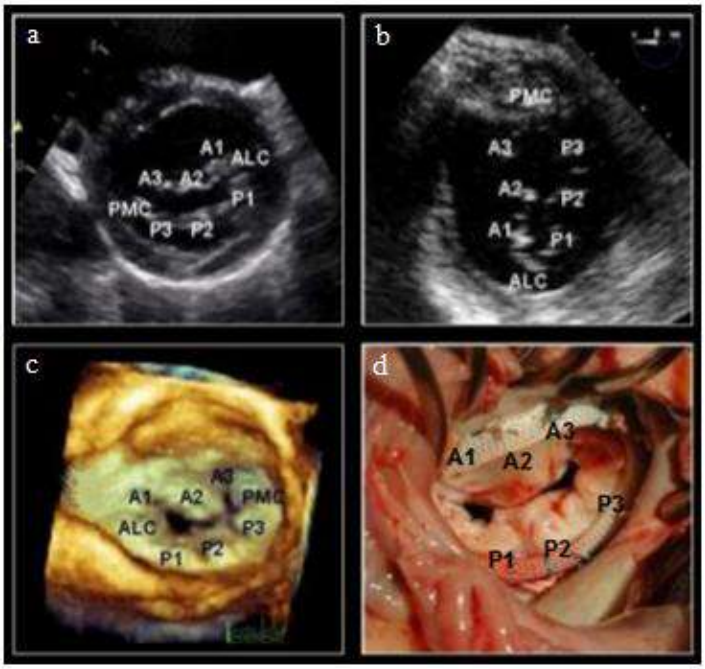

Fig.2.6: Short Axis (Sax) view from (*a*) 2D TTE, (*b*) 2D TEE, (*c*) 3D TTE, (*d*) surgeon's view. ALC=Anterolateral Commissure, PMC=Posteromedial Commissure [138]

Three-dimensional echocardiography has the potential to overcome the difficulties of erroneously perceiving spatial relationships of 2D images, also because the entire valve is in the field of view, avoiding measurements underestimation due to foreshortening. In addition, no geometric assumptions are needed to compute volumes, measurements can be made in true 3D space [98] and the differing depth of a structure compared to another is noticed by the observer thanks to variations in gray or color.

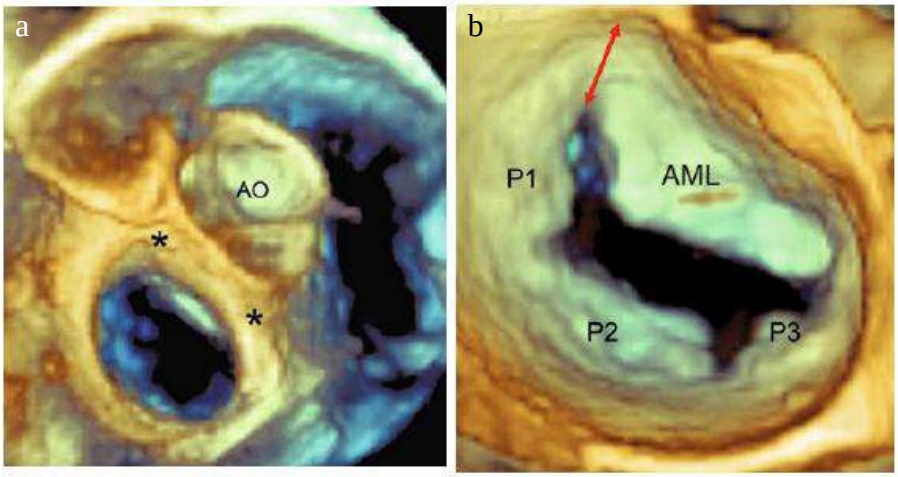

Fig.2.7: 3D TE view: (*a*) the asterisks indicate locations of the two trigones; Ao=Aorta. (*b*) the red arrow indicates the distance between the commissure and the insertion of the leaflet on the annulus; AML=Anterior Mitral Leaflet. [35]

Real-time 3D echocardiography (*RT-3DE*) can potentially have a significant impact: the visualization of all MV scallops is excellent for both leaflets [112]. Advances in echocardiographic technology have improved the detail in which the mitral leaflets can be examined in real time. With multiplane imaging probes, the entire mitral valve can be visualized with relatively little instrument manipulation, allowing [38] fast datasets acquisition during a single breath-hold, without the need for off-line reconstruction. Potential benefits could also be the absence of motion artifacts, realistic "surgeon's views" of the mitral valve but, above all, the lack of dependence on geometric modeling and image plane positioning, resulting in more accurate quantification [59]. This technique has been in continuous development for approximately 10 years making its use increasingly common, not only for research purposes but also in daily clinical practice.

Moreover, transesophageal real-time 3-dimensional echocardiography (*TE-RT3DE*) offers a unique opportunity to completely image and quantify mitral annulus full-volume, size and motion [42]. Its principal advantage over 2D transesophageal echocardiography is that it enables the visualization of specific structures from various angles: the whole structure may be imaged and subsequently mapped from one single view without the need for mentally reconstruction [107].

2.2. Echocardiography vs. Computed Tomography and cMRI

Accuracy of measurements achieved by either Computed Tomography and Magnetic Resonance is superior compared to the echocardiographic ones [106].

Multi-Detector row Computed Tomography (*MD-CT*) has emerged as an imaging technique that can fully evaluate both cardiac structure and function: it has the advantage of 3-dimensional volumetric data sets allowing unlimited plane reconstructions. It is able to provide direct visualization of the mitral valve and correctly identify its anatomy and geometry in 49 of 50 cases (98%) [2,34]. The high spatial resolution of MD-CT and current rotation techniques permit to obtain different anatomical planes in order to accurately assess dimensions and spatial relationships of the mitral valve complex as well as the highly variable subvalvular apparatus (e.g. number of heads of papillary muscles, type of insertion to the ventricular wall) [34,23].

Mainly in patients with a poor acoustic window or contraindications to Magnetic Resonance, MD-CT, which approximates the level of MR in terms of measurements

precision, is an ideal modality to calculate the mitral annulus area, the anteroposterior and intercommissural diameters (SAx, i.e. short axis view, Fig.2.8), but also the tenting heights (coaptation depths, defined as the distance between the leaflet coaptation and the mitral annulus plane) and angles at which each leaflet meets the annular plane can be accurately performed in all three planes (Fig.2.9) [23,34,106,108]. Furthermore, orientation across the modified short axis view of the mitral valve provides the 4-chamber view at the anterolateral (A1–P1), central (A2–P2) and posteromedial (A3– P3) levels, allowing to assess the length of the valvular leaflets [2,34].

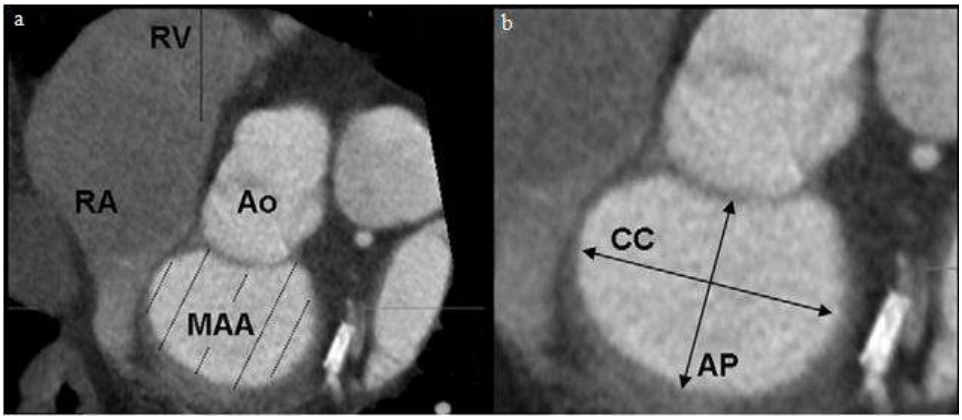

Fig.2.8: Four-Chamber (4C) view: from SAx view at the level of the annulus the (*a*) Mitral Annulus Area (=MAA) and (*b*)annular diameters (CC=intercommissural, AP=Anteroposterior) can be assessed. Ao=Aorta, RA=Right *Atrium*, RV=Right Ventricle [23]

However, the use of CT scan is limited by the administration of a contrast agent, the X-ray exposure and a relatively low temporal resolution [106,108]. Multi-Detector Computed Tomography may emerge as a technique that can evaluate both cardiac structure and function [2], but main limitations are image noise, requirement for regular rhythm and slow heart rate during imaging, lot of time for post-processing the acquired data because of images complexity, the exam duration, which increases probabilities of patient movements causing distortion effects, and the radiation dose; nonetheless, this technology is very promising [18].

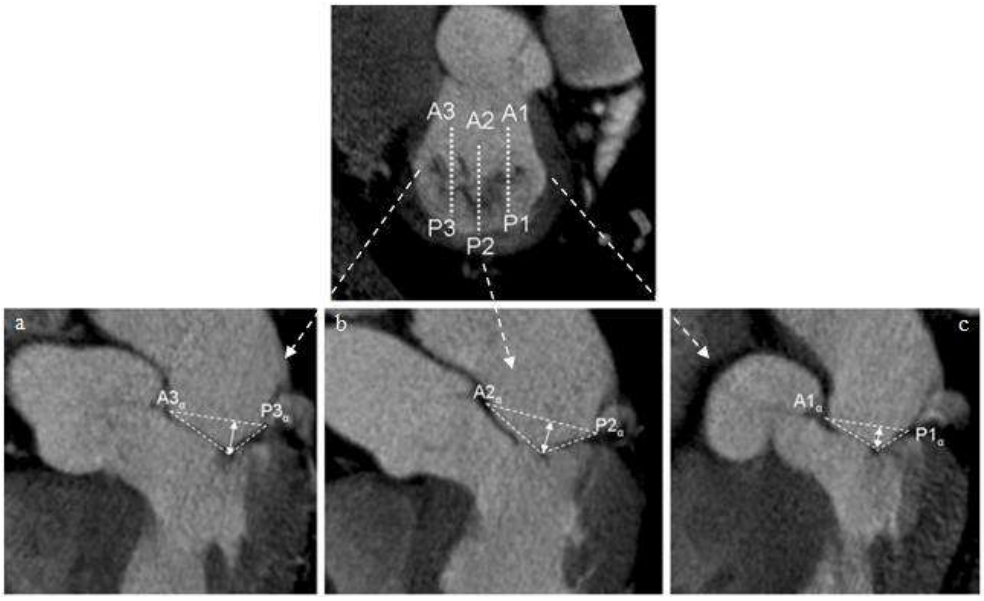

Fig.2.9: *Top*: SAx view at the level of the mitral leaflets and commissures; *Down*: the orthogonal planes provide the Apical views (*a*), (*b*), (*c*). Double headed arrows measure the leaflet tenting heights [34]

Cardiac Magnetic Resonance Imaging (*cMRI*) is generally accepted as the most accurate technique for monitoring adaptational changes in chamber dimensions associated with valvular disease, quantitatively evaluating regurgitant valves and assessing ventricular function and volumes. The advantage of this technique is its non-invasiveness and the possibility of examination without the administration of a contrast agent with absence of X-rays exposure but its inherent constraints such as pacemaker implants, morbid obesity, and claustrophobia, with its high costs hinder MRI in becoming a clinically relevant technique for imaging cardiac valves in healthcare facilities [2,106].

CMRI can be effectively used as an alternative source of data to TT-RT3DE in order to obtain images with higher time resolution and better blood-to-tissue contrast [52]. The use of a rotational sequence of acquisition allows to capture the complete end-diastolic profile of the MV leaflets, and the time-dependent position of papillary muscles tips (Fig.2.10) throughout the entire cardiac cycle, otherwise unavailable. However, it is necessary to post-process the images for every frame, in each cut-plane: valvular substructures of interest are manually selected, in order to reconstruct them by approximating points on the annulus with empirically determined adequate functions, as described by some research groups [52,110,128].

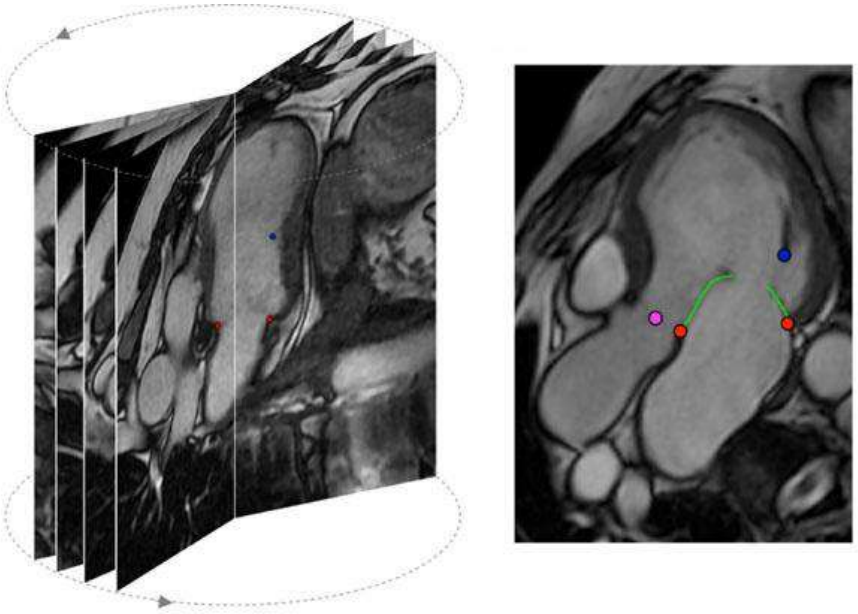

Fig.2.10: long-axis multiple cMRI cut-planes: pointing of annulus (red), leaflets (green), papillary muscle tip (blue) and position of the Aorta (pink) [110]

In conclusion, echography remains the best early approach to cardiac pathologies, thus all cardiac specialists need to understand the basic principles, physiologic determinants and expected results to make an appropriate interpretation of it.

Echocardiographers use particular "windows" (among ribs, sternum, and lungs) to ensure good penetration of ultrasounds into the heart and thus good images of the cardiac structures. Like all complex testing modalities, echocardiography is subjected to operator-dependent factors and Bayesian interpretation of results. Hence it is essential that quality of imaging and integration of reported results be challenged critically by clinicians, to indicate and plan surgery and anesthesia, to manage patients intraoperatively and to monitor them postoperatively to ensure the best possible outcome. However, there are multiple echocardiographic modalities that can respond to different clinical questions [18].

Although 2D transthoracic and transesophageal echocardiography provide precise information regarding MV anatomy, they suffer from the limitation of need for mental reconstruction of the three-dimensional valve anatomy by the examiner. On the contrary, both 3D TTE and TEE are more accurate and very promising techniques, which could increase the understanding of more complex abnormalities of the valvular apparatus and individual scallops identification; they may provide a detailed anatomic depiction of the MV and exact spatial localization of pathological structures, close to surgical findings, in a relatively short time. Limitations of the transthoracic 3D technology are mainly related to

the quality of images in one-third of cases, in comparison with the transesophageal approach; it has an accuracy similar to that of 2D TEE so, to the best of our knowledge, they both remain the ideal techniques for the valve geometry investigation [87].

In the near future, one of the most promising uses of these technologies is in planning mitral repair procedures, designed and customized for each patient preoperatively using data obtained from echographic images. Such virtual surgery automated tools will allow the surgeon to design optimal operations through a detailed analysis of the valve geometry before ever entering the operating room [98].

3. MITRAL VALVE GEOMETRY

The complex physiology and three-dimensional anatomy of the mitral valve, besides its surrounding structures, present substantial challenges for cardiac specialists because it is critical to understand their in vivo mechanics [126]. In life, there is a wide variation in annular size, not only during the cardiac cycle, but also under different hemodynamic conditions, so it is difficult to relate mitral annular dimensions measured at autopsy to those measured during life. Moreover, different annular size is often due to different methods of specimen preparation. For instance, for formalin-preserved hearts, the annuli may be probably considered in the systolic state [97], whereas if hearts are fresh or examined after perfusion fixation [28], annuli may be regarded as in diastolic phase [84].
Some research groups have obtained *in vivo* mitral valve measures, but there are several inconsistencies in annular size dimensions, likely due to the predominant use of echocardiography, which cannot identify and track distinct anatomic landmarks in time, therefore it is more subjective than other imaging methods. A study by Anwar et al. [5] demonstrated that mitral annulus diameter measured by 3D echocardiography and MRI is larger if compared with values from 2D echography (Fig.3.1), while there was no significant difference between MRI and 3DE. The frequent underestimation of true anteroposterior diameter may be explained by the slant of and measurement from two-dimensional echocardiography, since its changes in size mainly occur along the axis represented by the perpendicular line suggested in figure below [115].

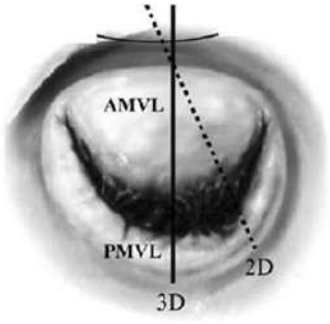

Fig.3.1: Real-time three-dimensional echocardiography (3D) and 2DE (dashed line) measurement of mitral annulus diameter, defined as the perpendicular line from the top of the curvature to the middle of the straight mitral annulus border. AMVL, anterior mitral valve leaflet; PMVL, posterior mitral valve leaflet. [5]

In order to understand complexity of the mitral valve geometry, it is necessary to take into account all these cited aspects: many difficulties in estimating *in vivo* valvular dimensions and some limits related to the inadequate spatial resolution of imaging methods available in everyday clinical activities make hard any geometric reconstruction. This causes widespread lack of standardized models of the mitral valve and its functioning, human data and rigorous validation of simulation results [125].

In Tab.5, some measurements in human studies are shown, as an example, to point out the discrepancies among ranges of values obtained by different imaging techniques. In literature, mitral annulus dimensions are considered to be normal in patients without left-sided heart disease, with normal left atrial and ventricular dimension, mitral valve and ventricular function [5] but, in analyzing the reported results, it must be also taken into account of the small numbers of some studies [28,54].

	Area[cm²]		**Circumference**[cm]		**Diameter**[cm]
	Systole	*Diastole*	*Systole*	*Diastole*	*Diastole*
2DE	3.7 – 5.1 [131] 3.6 – 6.8 [84]	6.1 – 7.7 [131] 5.3 – 8.9 [84]	7.0 – 9.0 [84]	8.5 – 10.1 [84]	2.5 – 3.5 [5]
3DE	_	5.8 – 11.6 [5]	_	_	2.8 – 3.8 [5]
MRI	5.8 – 8.0 [54]	6.7 – 11.3 [5] 8.1 – 10.9 [54]	_	_	2.9 – 3.9 [5]
Autopsy	_	8.2[28]	7.5 – 11.0 [97]	10.2[28]	_

Tab.5: Underestimation of mitral annular area and diameter measured by 2D echocardiography compared to MRI (and 3DE)

If compared with average maximal mitral annular area measured using 2D transthoracic echocardiography, in normal control subjects, also other recent studies report large mitral annular sizes measured using 3D TEE, similar to values in table [37,84].

The estimation of the annular area is strongly dependent also upon the definition of the annular border and the conversion of the non–planar geometry (3D area) into a planar area (see Fig.3.2) [57], but it is a clinical measured parameter used in classification of dysfunctions such as mitral stenosis [61].

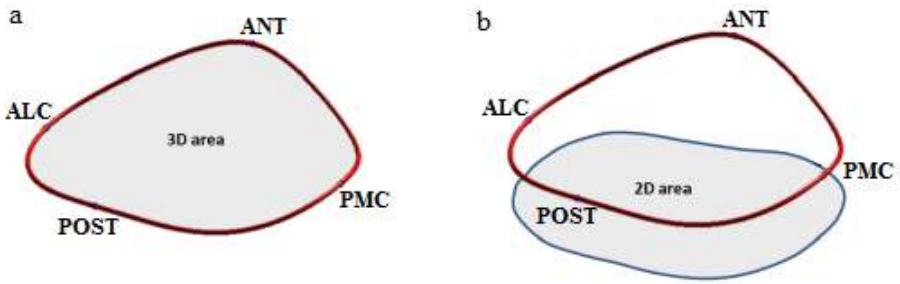

Fig.3.2: Scheme of 3D mitral annular apparatus: ANT=Anterior leaflet, POST=Posterior leaflet, PMC=Posteromedial Commissure, ALC=Anterolateral Commissure [111]

3.1. The Diastolic Phase: Comparison between Geometric Assumptions and Feasibility of Parameters Assessment

3.1.1. Mitral Annulus

As highlighted in previous chapters, the mitral valve has a very complex morphology, hence it is preferred to analyze its different components separately and make some assumptions about its geometry during first steps on studying it.

The perimeter of the valvular orifice is defined by the annulus of the valve: its accurate assessment would be of very great importance for the diagnosis and treatment of mitral valve disease, but information available in literature are yet limited and discordant.

This flexible structure varies a lot in size and shape during cardiac cycle and its out–of–plane motion is not uniform, as the anterior portion exhibits larger displacements than the centre of the posterior one [61]. Although the annulus is a dynamic substructure of the valve, if we look at it from the left atrium at first, by considering only the short axis (SAx) view, it can be described as a planar structure in order to reduce the numerical complexity of the problem. The end-diastolic configuration (completely open valve) and the corresponding geometry could be assumed as the initial, unloaded (i.e. undeformed) one [110].

In her first-generation model, Kunzelman [55] assumed an annulus profile which appeared D-shaped and smoothed, divided into two parts that corresponded to the insertions of the leaflets [61,69]: the top of the "*D*" represented the anterior portion of the annulus, while the inferior tract represented the posterior one [123]. In most of the models available in literature, the physiological profile of the mitral orifice is defined as an idealized line, with a simplified shape, that represents the union of two semi-ellipses with a shared major axis represented by an ideal line which connects the commissures of the valve. Due to this particular shape, the annulus extent is often described in terms of its two main diameters: the septolateral (SL) and the intercommissural (IC) ones [84]. The geometric center corresponds to the intersection of two axes at the middle of the IC distance: the mitral valve orifice can be assumed approximately symmetric about the septolateral midline [29], as shown in Fig.3.3.

Below each figure, a table summarizes the accuracy of geometric parameters assessment by different methods, if available in literature, and clinical images illustrate the best one.

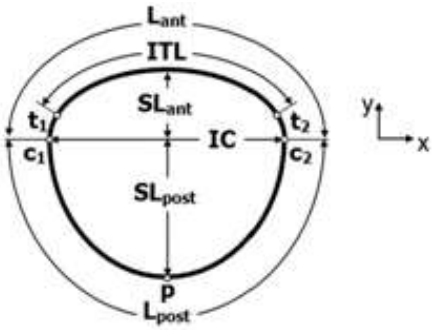

Fig.3.3: Geometrical parameters of the annular profile, atrial view: L_{ant} =anterior annular portion length, L_{post} =posterior annular portion length, ITL=intertrigonal length, IC=intercommissural distance, SL_{ant} =septolateral dimension of the anterior annular tract, SL_{post} =septolateral dimension of the posterior annular tract, c_1 and c_2=commissures, t_1 and t_2=trigones [109]

	MRI	CT	3DE	2DE	Autopsy
L_{ant}	X	X*[a]	X	X*[b]	X*[d]
L_{post}			X		
ITL		X	X		
SL_{ant}	X	X	X	X*[c]	
SL_{post}	X	X	X		
IC	X	X	X		

Tab.6: By evaluating the major diameters (*SL* and *IC*) the circumference (sum of L_{ant} and L_{post}) can be obtained, and vice versa [13,30,35,42,56,70,125].
*[a] Accuracy: 98% [34]
*[b] Accuracy: 72±12% [2]
*[c] Underestimation: 10-15% [5]
*[d] Overestimation: 9.6% [84]

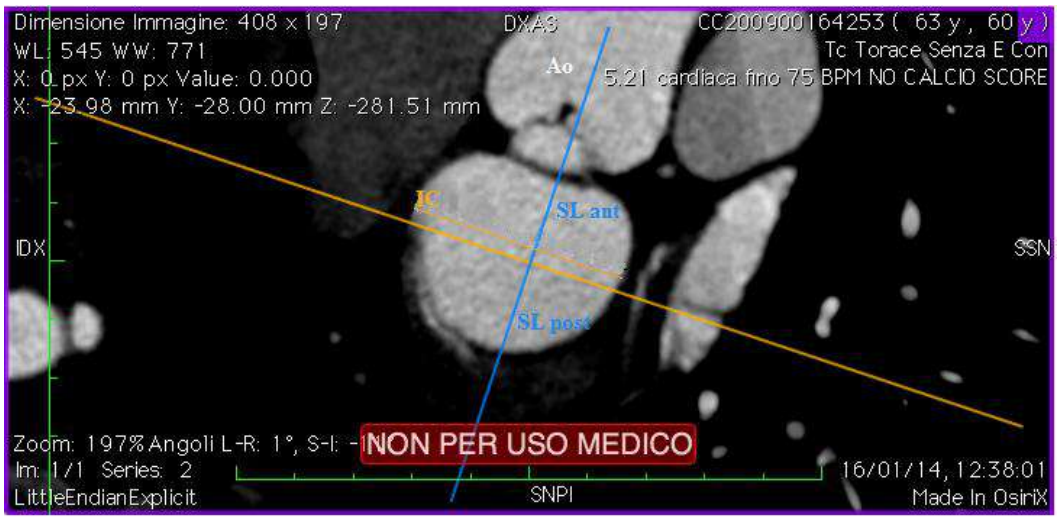

Fig.3.4: Mitral valve SAx view by CT: it permits better estimation of annular dimensions than echocardiography because the latter one is unable of exact appreciation of the limits of the ring in order to measure intercommissural and septolateral diameters

Where the accuracy values were not available, *X*s indicate the most used methods to easily visualize and assess each parameter, as reported in literature (references in square brackets). Often, some of them are not measured because their values are not significant in clinical practice, except for mitral annulus area and circumference as markers of pathological dilations. More often, the routine images aim to point out leaflets prolapse and chordal rupture, but several pathological conditions are due to or can cause alterations in valvular morphology then variations in mitral valve dimensions, if compared with physiological range. Unfortunately, the accuracy of the most widespread imaging technologies in everyday clinical practice is limited, especially that one of echocardiographic methods.

Three dimensional techniques has allowed for appreciation of the typical, real non-planarity of the mitral annulus and enabled accurate measurements of the saddle-horn height (H) [53], reported in Fig.3.5, defined as the maximal vertical distance between the highest and lowest annular points, perpendicular to the mitral annulus fitting plane.

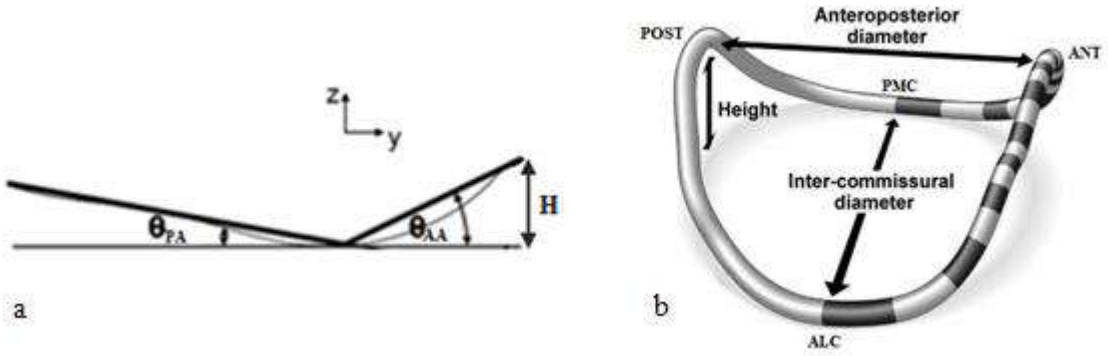

Fig.3.5: (*a*) Geometrical parameters of the annular profile from lateral view: θ_{AA} =rotation angle of the Anterior portion and θ_{PA} = rotation angle of the Posterior tract of the mitral Annulus, around the IC axis. (*b*) Mitral ring feature as a result of the above-mentioned rotation; ANT=anterior leaflet, POST=posterior leaflet, ALC=Anterolateral commissure, PMC=Posteromedial commissure [42,109]

	MRI	**CT**	**3DE**	**2DE**	**Autopsy**
H		X	X		
θ_{AA}			X		
θ_{PA}			X		

Tab.7: If septolateral lengths are known, it is possible to estimate the annulus height (*H*) by the rotation angles θ_{AA} and θ_{PA}, and vice versa [9,57,120]

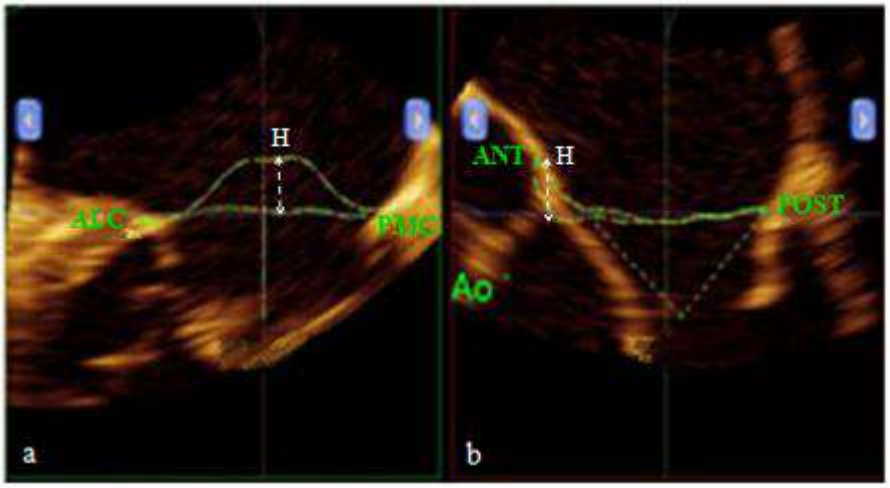

Fig.3.6: 3DE images of the MA: principal axes correspond to main diameters (ALC and PMC=Anterolateral and Posteromedial Commissures, ANT and POST=Anterior and Posterior annulus); it is well visible the height (*H*) of anterior tract of the annulus [70]

3.1.2. Mitral Leaflets

Generally, the anterior leaflet consists of a single wide cusp inserted on a shorter tract of the annulus but more extended in the annulus-to-free edge direction; instead, the posterior one is more variable, often having three cusps, it inserts on a longer tract of the annulus but is shorter in the annulus-to-free edge direction [123].

In early 90's, Kunzelman et al. investigated mitral valve anatomy with the goal to provide consistent terminology to be used throughout its analysis and determine an acceptable animal model of the valve, consisting of an entire membranous structure, formed by the leaflets, which includes two commissural regions, as depicted in Fig.3.7. Anterior and posterior annular lengths are labeled in different manner (*A* or *C* and *B* or *D*) even if they indicate the same morphological features because it has been outlined a 20.9% increase in total annular length from the intact to the excised state of the human mitral valve [56]. The leaflets heights *G* and *H* can be defined as the distances of leaflets free edges from the annulus.

In initial conditions the mitral valve is not totally open: both leaflets lie on a nearly conical surface that originates from the annulus profile and tilt at its insertion in order to reproduce their end-diastole position, as provided by echocardiographic data. Two rotation angles, θ_{AL} and θ_{PL} (Fig.3.9), describe the orientation of central portions of the leaflets towards the center of the valve orifice.

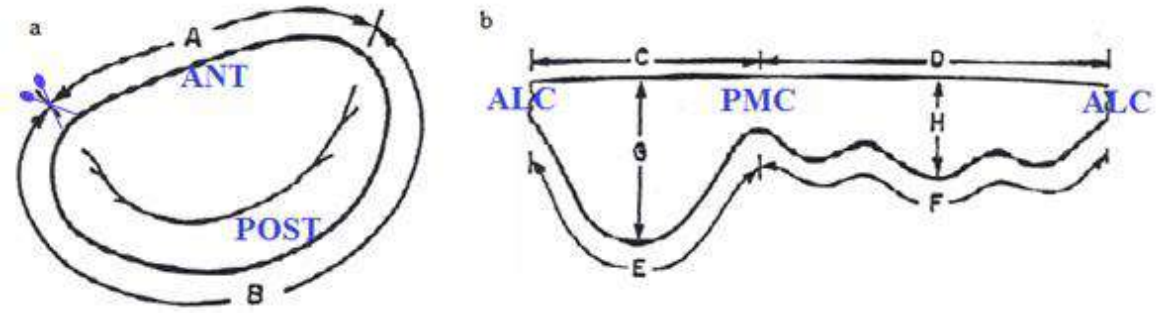

Fig.3.7: (*a*) Intact and (*b*) Excised valve measurements: lengths and heights of the mitral leaflets; cut point is indicated at the level of Anterolateral Commissure. A and C = Anterior Annular Lengths, B and D = Posterior Annular Lengths, E = Anterior Edge Length, F = Posterior Edge Length, G = Anterior Leaflet Height, H = Posterior Leaflet Height [56]

	MRI	CT	3DE	2DE	Autopsy
E					X
F					X
G	X	X	X*[a]	X*[b]	X
H	X	X			X

Tab.8: It is impossible to assess the length of the free margins *in vivo* because of the movement of the valvular leaflets [27,56,100,110,125].
*[a] Accuracy: 87-95% [68]
*[b] Accuracy: 84-87% [68]

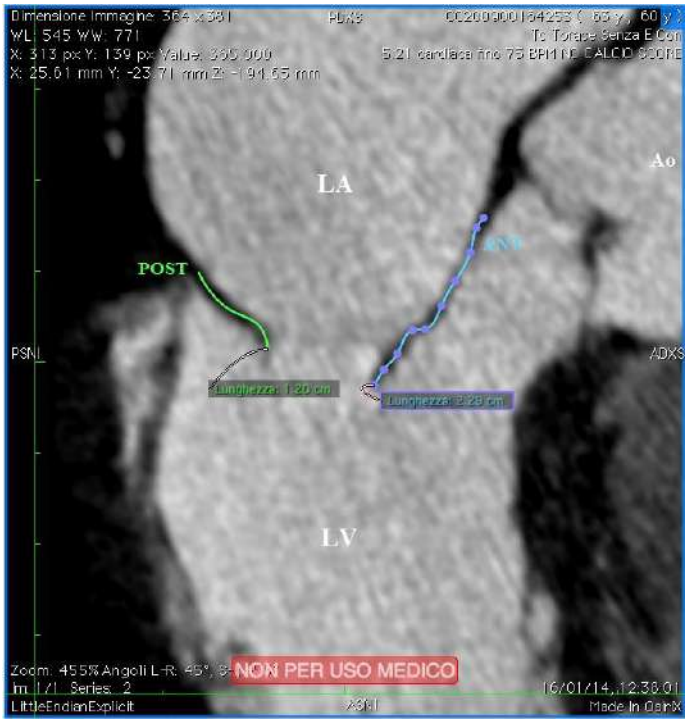

Fig.3.8: CT of the mitral valve: leaflets scallops A2 and P2; besides central portions, also lateral scallops have their dimensions

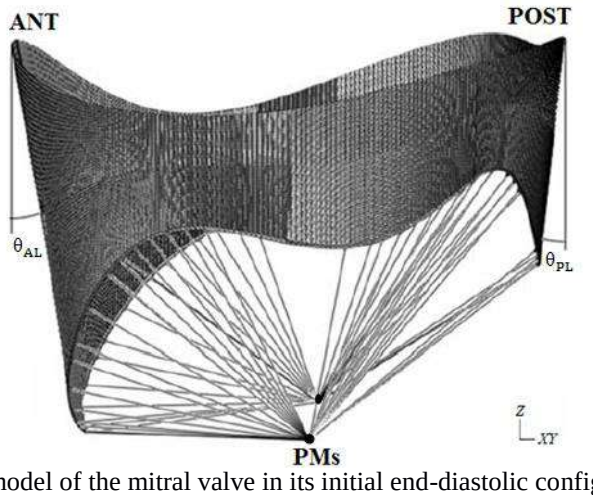

Fig.3.9: Geometrical model of the mitral valve in its initial end-diastolic configuration. ANT and POST=Anterior and Posterior leaflets, respectively; θ_{AL} and θ_{PL} =tilting of Anterior and Posterior Leaflets; PMs=Papillary Muscles tips. [123]

	MRI	CT	3DE	2DE	Autopsy
θ_{AL}	X	X	X	X	
θ_{PL}	X	X	X	X	

Tab.9: Very few information are available in literature about the tilt of the leaflets and their methods of assessment [18,107,110]

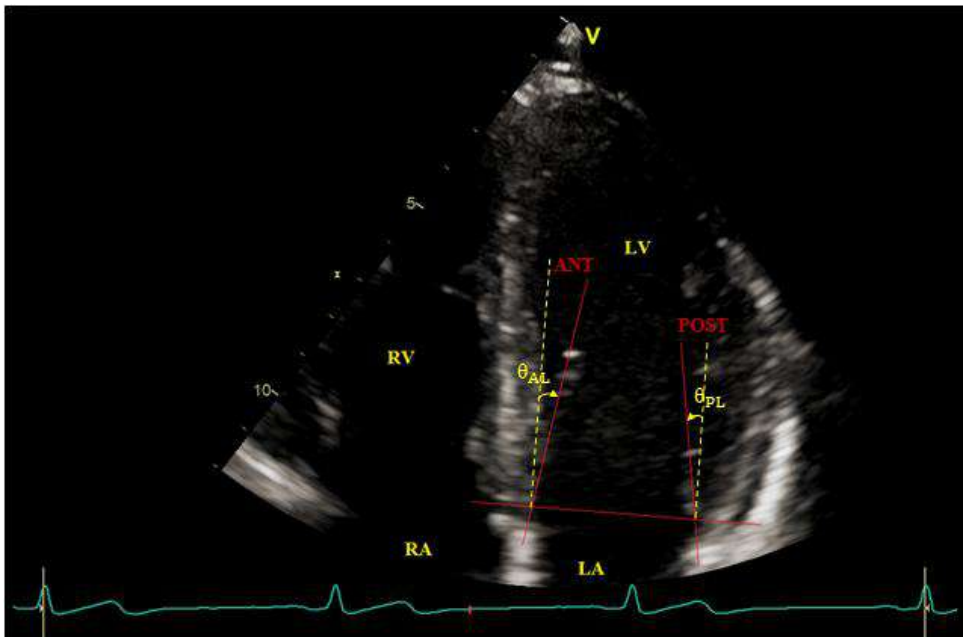

Fig.3.10: Unfortunately, medical experience says that different 2D echocardiographic views of the same patient's leaflets tilt could provide different measures of angles, which are therefore not much reliable

4. PARAMETRIC MODEL

The increasing sophistication of surgical solutions necessitates the development of quantitative patient-specific computer simulation tools to aid surgical planning through the assessment of preoperative scenarios and prediction of postoperative outcomes. For a computational model, to evolve into a clinically relevant simulation tool, critical prerequisite is the integration of the state-of-the-art imaging techniques with biomechanical computational approaches [124].

Different MV patient-specific studies differ by the type of clinical imaging, i.e. ultrasound methods [71,90,123,130], cardiac MRI [110,128] or multi-slice CT [125], level of automation, and completeness of the morphological reconstruction. The key features are summarized in Table 10.

Study	Data source	Automation	Patient-specific features
Votta 2008	TT-RT3DE	Semi-automated	Leaflets extent and inclination, MA profile, PMs tips position
Wenk 2010	CMR	Manual	Leaflets surface, MA profile, LV + PMs
Stevanella 2011	CMR	Manual	Leaflets extent and inclination, MA profile, PMs tips position
Mansi 2012	TE-RT3DE	Fully automated	Leaflets surface + thickness, MA profile, PMs tips position
Xu 2012	TE-RT3DE	Manual	Leaflets surface, MA profile, PMs tips position
Pouch 2012	TE-RT3DE	Semi-automated	Leaflets surface + thickness, MA profile, PMs tips position
Wang 2012	MSCT	Manual	Leaflets surface + thickness, MA profile, PMs tips position chordal insertions

Tab.10: Different approaches to tackle MV patient-specific morphological reconstruction for biomechanical simulations. MA=mitral annulus; PMs= papillary muscles; TT/TE-RT3DE=trans-thoracic/esophageal real-time 3D echocardiography; cMR=cardiac magnetic resonance; MSCT=multi-slice computed tomography [124]

The work of Mansi et al. [71] represents the gold standard in automation: he used machine-learning algorithms to fully automate MV detection; instead, regarding the completeness, the use of MS-CT [125] made it possible for the first time to account for the patient-specific description of the distribution of chordal origins on the papillary muscles tips and their insertions into the leaflets. On the other hand, only Wenk and coworkers [128] accounted for the patient-specific LV wall, but using manual segmentation of a series of orthogonal short and long-axis cine-cMR sequences.

Therefore, none of the currently available geometric models realistically takes into account all of the aspects that characterize the function of the mitral valve, with the best imaging method, and generating a completely automated modeling tool. It is a matter of finding the best trade-off among these aspects in order to provide the best model to the specific goal. In fact, every model is based on simplifying assumptions (often regarding mitral valve geometry or material properties), whose nature, number and impact varied from model to model, depending on the degree of complexity of the latter and on its particular application [123]. Some general limitations have been shared by nearly all of the available models, and also assumed as starting point in our geometric reconstruction.

4.1. Rhinoceros 5.0 and Grasshopper Plug-In

To realize our three-dimensional mitral valve model, it has been used *Rhinoceros 5.0*, a commercial 3D graphics and Computer-Aided Design (CAD) application software developed by Robert McNeel & Associates. *Rhino* makes it possible to create almost any tree-dimensional object: it is a free-form surface modeling tool that utilizes NURBS mathematical model. It is highly versatile: it can create, edit, analyze, document, render, animate and translate NURBS curves, surfaces, solids, point clouds and polygon meshes. It is easy to learn and use, fast and very accurate, compatible with every other design, analysis, rendering and animation program, it doesn't need to any particular hardware. It enables the user to customize the interface and create custom commands and menus; furthermore, it has an interesting interface, allowing you to display the object you are working on from four separate angles; this ensures that all sides of your project are fully visible at all time, sparing you from having to switch between various modes of display. *Rhinoceros* is used in a lot of different specific fields, such as engineering, architecture, 3D printing, industrial, marine, automotive or jewelry design, as well as multimedia and graphic design, rendering, animation, prototyping. It can handle complex models by visualizing them quickly and without wasting too much memory; aside from all the features and functions, it also offers a series of utilities that can come in handy when designing 3D models. This application hasn't any running cost and tools and assistance are free. Dozens of plug-ins are available to complement and expand *Rhinoceros*' capabilities in structural analysis, simulation, visualization and fabrication of design [136]: among them the one called *Grasshopper*.

Grasshopper (adopted version: 0.9.0076) is a visual programming language developed by David Rutten, that runs within and tightly integrated with *Rhinoceros* 3D application; it is a comprehensive and reliable graphical algorithm editor that requires no knowledge of programming or scripting [135]. It features a fairly advanced user interface that contains various feature you can make use of, but the layout is still kept to minimal so even beginners can easily learn how to master their designs. *Grasshopper* can create complex associated geometries and solutions that otherwise would be very difficult, if not impossible to construct in *Rhino*. Its strength is the ability to edit the model real-time: you can change and update original model and parameters, and refine your rules definition as you work [141].

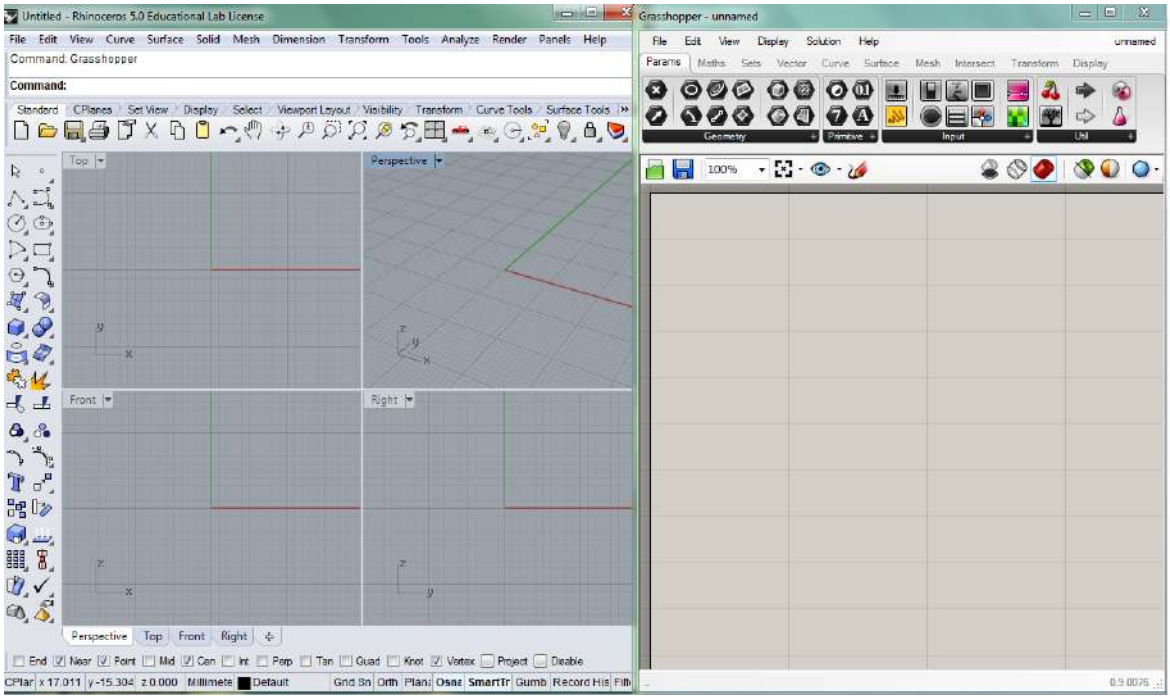

Fig.4.1: *Rhinoceros* (*left*) and *Grasshopper* (*right*) windows

The main window consists of specific options, in different sections such as *Parameters*, *Vector*s, *Curve*s, *Surface*s and *Mesh*es, apart from standard elements in tool bars: it is possible to navigate through menus and access new objects and shapes you are interested in. Programs are created by dragging components onto a canvas and setting parameters to each object: the outputs to these components are then connected to the inputs of the subsequent ones, so all data are passed from component to component via connected wires;

they can be either defined locally as constants or imported from a document or file [139].

4.2. Reconstruction of Geometric Model: Step-by-Step Procedure

As seen in the previous paragraph, none of the referred models fulfilled two mandatory conditions in order to be compatible with the use by clinicians in their current practice: being patient-specific, and readily set and usable in an automated, fast and user-friendly fashion [110]. In this scenario, our parametric model of the mitral valve has been developed.

In this first geometrical reconstruction, the valve substructures accounted for are the saddle-shaped annulus, the anterior leaflet, consisting of a single cusp and the posterior one, which is tri-scalloped, instead. The model has been developed to simulate its structure during diastole in both normal and pathological states; it incorporates macroscopic anatomic information because the main target is to make the use by clinicians as easy as possible, just employing data supplied by routinely imaging assessment. Ventricular and atrial geometries are not here modeled and leaflets thickness is neglected.

4.2.1. Mitral Annulus Reconstruction

The model has been developed starting from the following main assumptions, illustrated in Fig.4.2:

- in diastolic configuration, the annulus can be considered as a combination of two semielliptical profiles that share one of the main diameters (at the same time, *IC diameter* is the major axis of the smallest ellipse and the minor diameter to the biggest one);
- to limit the complexity associated with modeling the mitral valve, symmetry conditions have been applied: the annulus is considered as symmetrical to the plane perpendicular to the valve orifice, as shown in the figure below.

The mitral annulus (MA) was generated by a two-step procedure (see point 1. and 3.).

Initially, it has been constricted to a fixed planar geometry and it has not been taken into account its contraction. For simplicity it has been always considered a limited time-frame of the simulated phenomenon: the end-diastolic configuration has been assumed as the

unloaded one, being the time point within the cardiac cycle which is characterized by a nearly zero transvalvular pressure drop.

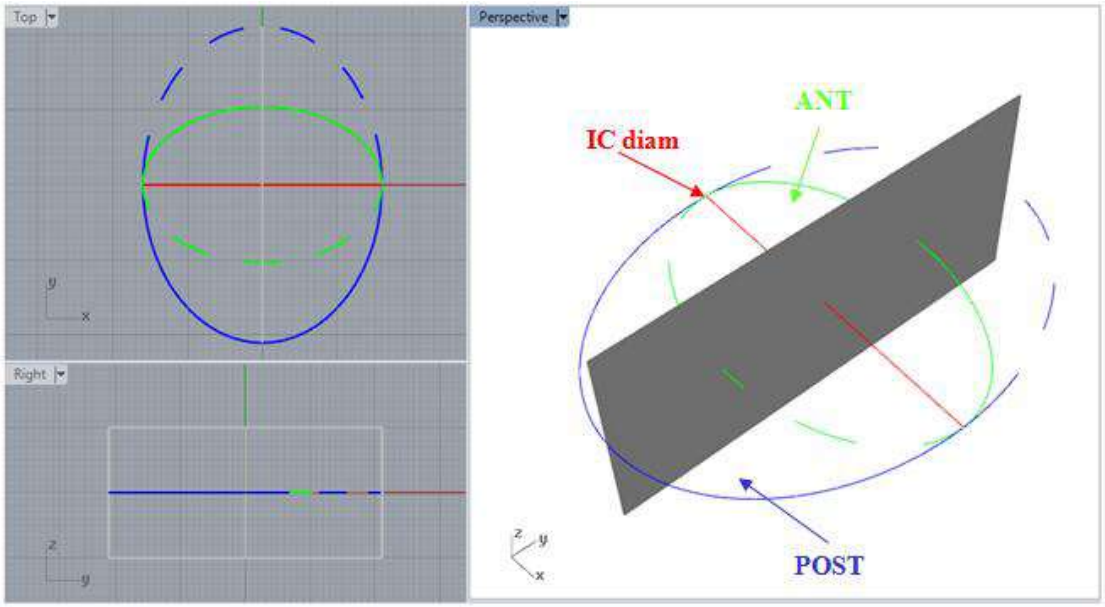

Fig.4.2: Perspective view (*right*): ANT=anterior portion of the reconstructed mitral annulus profile (*green*), POST=posterior annulus (*blue*), IC diam=intercommissural diameter (*red*). The geometric annulus profile is made up of the junction of the two halves ellipses and traced by a solid line, while dashed curves indicate the remaining geometries, not considered. The grey plane of analysis is defined at the center of the mitral valve, perpendicular to the plane passing through the valve orifice. (Image processed by *Rhinoceros 5.0*)

The model is characterized by an intercommissural (***IC***) distance and an anteroposterior (septolateral, *SL*) dimension, split in its anterior and posterior portions ($\boldsymbol{SL_{ant}}$ and $\boldsymbol{SL_{post}}$, respectively) by the IC diameter. We temporarily assume the IC axis 32 mm long and set SL_{ant} = 10.4 mm and SL_{post} = 21.1 mm, as reported in literature, obtaining a 31.5 mm septolateral diameter. Remaining dimensions, such as the anterior and posterior annular lengths and the orifice area, are consequently obtained, consistently with the experimental data reported by Stevanella et al. [109]. The mitral annulus has been defined in the Cartesian *xy* plane.

For greater clarity, every step of the geometric reconstruction is listed below with identification of corresponding parameters on clinical images provided by Dr. Gambarin (in every figure "*ANT*" means anterior leaflet, while "*POST*", is the posterior one).

1. We set numerical values of two main diameters, *IC* and *SL*, which intersect at the origin (***O***) of the *xy* axes: for convenience, the *IC* diameter has been put on the *x* axis,

symmetrically to the septolateral (*y* axis) one, whose two portions, on the contrary, have different lengths. In fact, the anterior tract of *SL* diameter is typically shorter than the posterior one, hence they have been constructed in order to lie on positive and negative part of the *y* axis, respectively, as shown in Fig.4.3,b. A range of possible values of annular diameters (and other geometrical parameters), found in literature, are reported in Appendix A and set in the properties of the *Slider* components of *Grasshopper*, allowing to vary dimension of every object visualized in *Rhinoceros*. The output of every component might be the input for the subsequent one.

After setting the diameters lengths, we detect their extreme points (red crosses in the figure below) and draw four segments starting from the origin of the plane. The end points are labeled ***A***, ***B***, ***C*** and ***D*** in order to make more understandable also next steps.

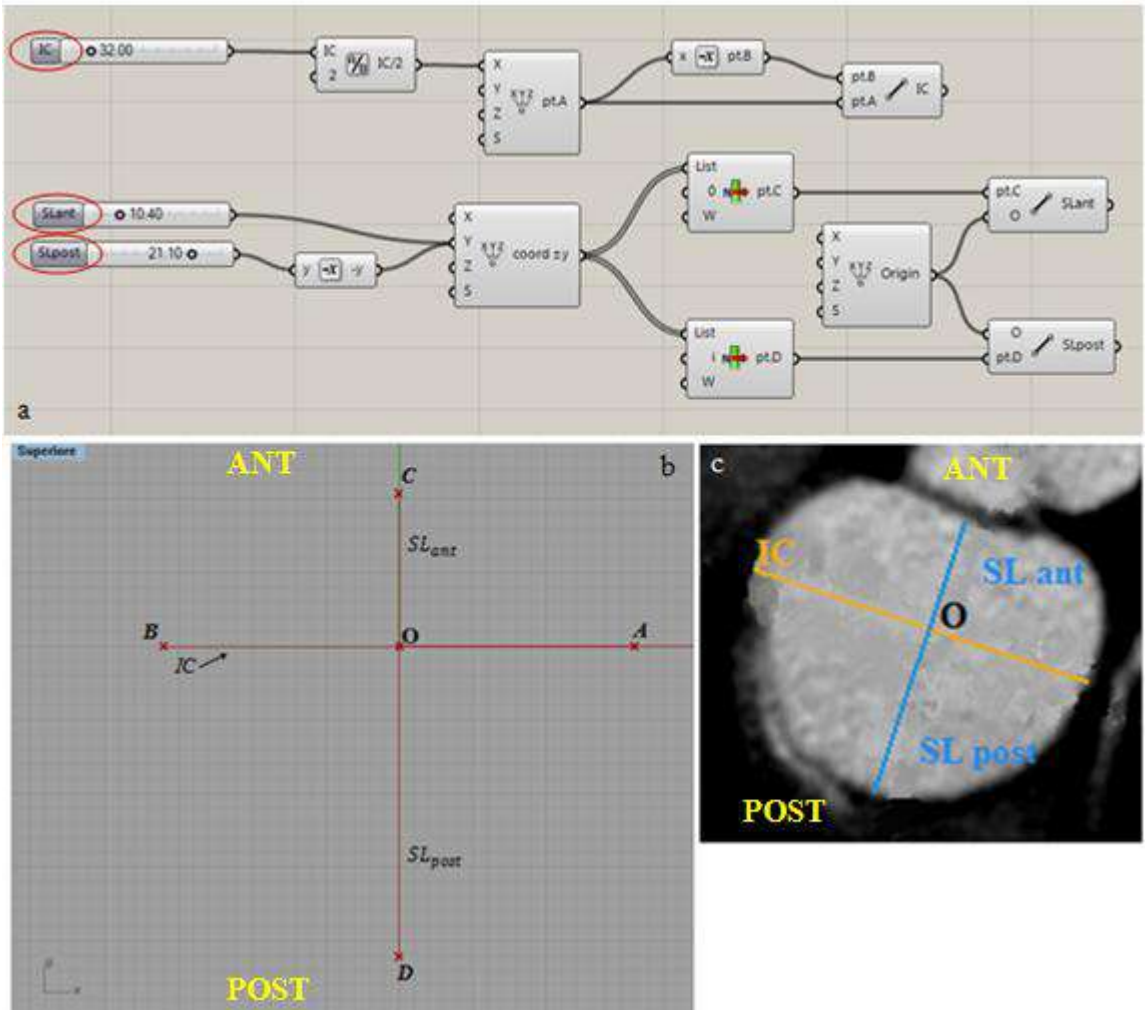

Fig.4.3: (*a*) *Grasshopper* geometrical components and (*b*) *Rhinoceros* atrial view visualization of the two main diameters: *A*, *B*=Commissural points, *C*=Anterior leaflet midpoint, *D*=posterior leaflet midpoint; (*c*) CT of mitral annulus: identification of diameters in Short Axis view.

2. We draw a closed curve which interpolate four end points, starting from point *A*, counterclockwise: we obtain a "D-shaped profile", as the annulus appears in bi-dimensional images.

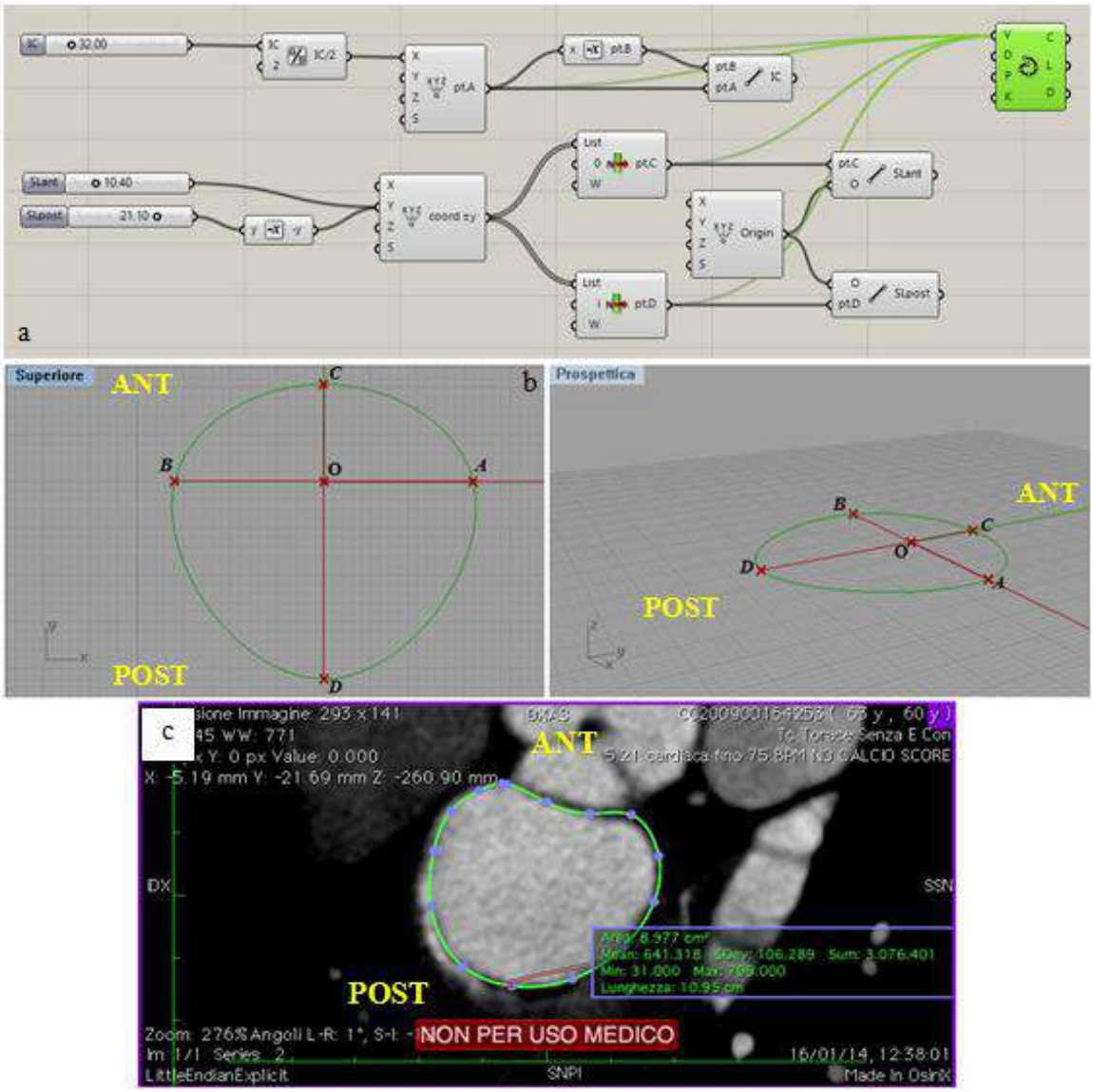

Fig.4.4: (*a*) *Grasshopper* programming: the green component points the new operation out; (*b*) *Rhino* views; (*c*) Comparison with CT image of a real annular profile.

3. However, out of the *xy* plane, the mitral annulus is described by the height (*H*) of the annular "saddle" so, as second phase in this modeling, it must be taken into account its three-dimensional features.

The anterior and posterior tracts of the *SL* diameter ($\overline{CO}$ and $\overline{OD}$) were properly rotated around the *IC* axis, in +*z* direction, with fixed point in ***O***, by 40 deg ($\boldsymbol{\theta_{AA}}$) and 13 deg ($\boldsymbol{\theta_{PA}}$) respectively (red circles in Fig.4.5,a identify setting values), as reported in Stevanella's work [109]: we obtain a saddle-horn height consistent with experimental findings from literature [20].

Grasshopper allows only rotations in *radians*, hence *degrees* values selected by user are always converted by the expression

$$A * \pi/180,$$

where *A* is the angle input value (*deg*).

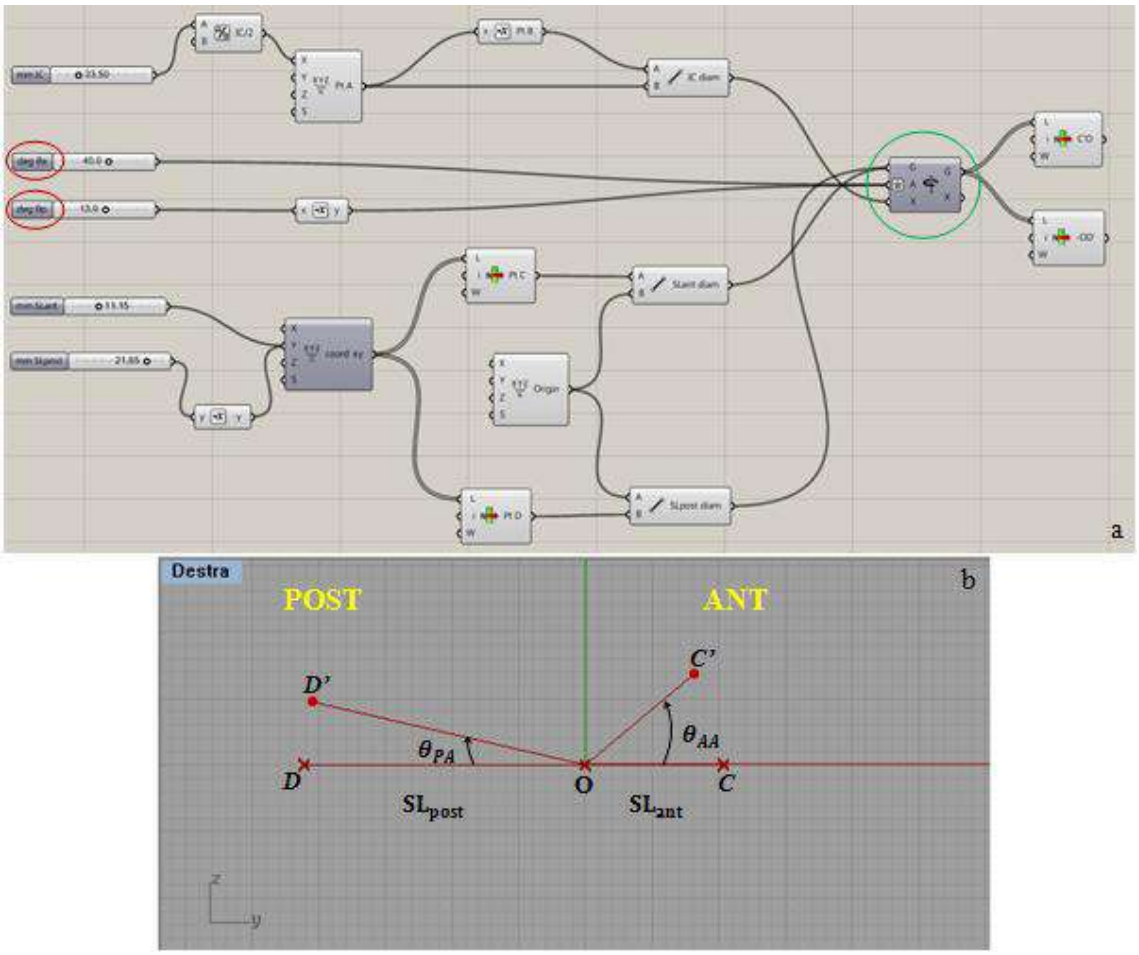

Fig.4.5: (*a*) Operations for the *SL* segments rotation (*Rotate Axis* component in green circle); (*b*) Right view of the rotation angles θ_{AA} and θ_{PA}: ***C'*** and ***D'*** points are consequent end points of the *SL* diameter; LAx view.

Obviously, if measures of septolateral diameter are assessed from a long axis view of echocardiographic or tomographic image, the above-mentioned reconstruction technique is correct, while it underestimates annulus dimensions if we measure the *SL* length in a short axis view. In fact, in top view, the visualized annulus profile corresponds to its perimeter when passing through the highest points of the saddle shape (see Figs.4.3,c and 4.4,c), while we represent its planar projection on *y* axis. Therefore, it is necessary to take into account these different aspects during annulus reconstruction and compute right *SL* diameter values in case, as shown by Fig.4.6.

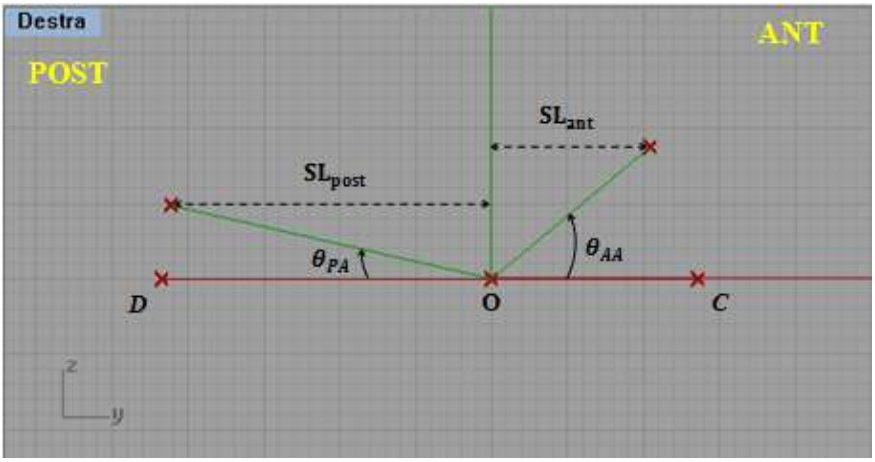

Fig.4.6: Compared with Fig.4.5,b, dashed lines indicates true dimensions of *SL* tracts assessed by SAx view, so the length of rotated segments (green lines) are obtained by the expressions $\overline{CO} = \frac{SL_{ant}}{\cos\,\theta_{AA}}$ and $\overline{OD} = \frac{SL_{post}}{\cos\,\theta_{PA}}$.

By typical imaging methods, it is almost impossible to assess these rotation angles. A few studies used surgically implanted ultrasounds crystals [64] or radiopaque markers [48] to reconstruct the annular profile (considering the saddle height) in sheep, by converting them in 3D coordinates. These techniques are too invasive for human investigations, but they have been useful to provide a quantitative idea about the annular curvature.

4. Now we can redraw the closed curve that represents the annulus profile (green line in Fig.4.7): this time, the curve passes through two new points found tilting the anterior and posterior portions of *SL* diameter, named ***C'*** and ***D'*** to distinguish them from the previous ones.

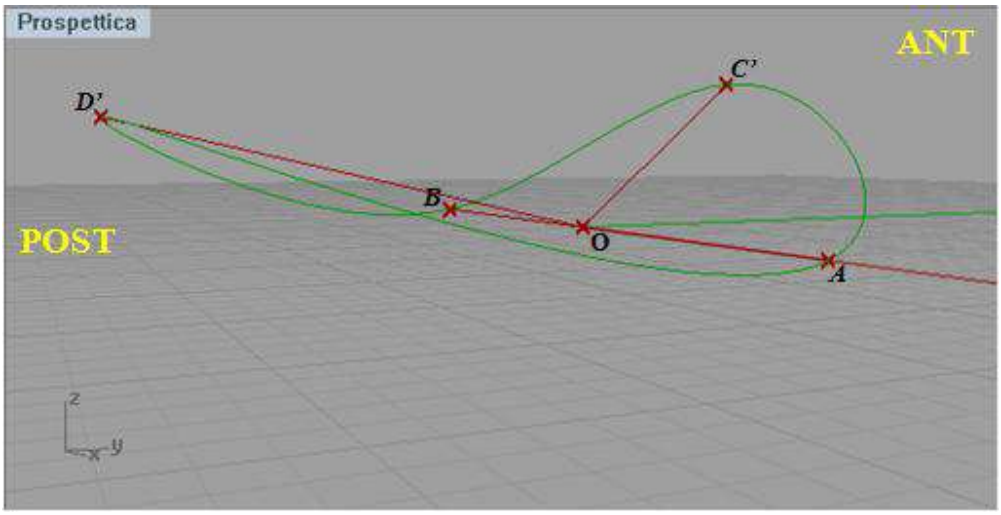

Fig.4.7: Resulting annular profile after *SL* diameter rotations: Perspective view

4.2.2. Mitral Leaflets Reconstruction: Method 1

At first, the simplest approach we adopted to geometrical modeling of mitral leaflets consists in describing them as a single membrane whose free margin does not have any cusps. In completely open valve configuration, the leaflets lay on the lateral surface of a hypothetical cylinder whose superior cross-sectional plane (cylinder generatrix) corresponds to the valve orifice.

We generated first mitral valve leaflets profile according to data reported in literature [97]: anterior and posterior leaflets heights were assumed to be 21.5 mm and 13.8 mm respectively, whereas the anterolateral and posteromedial commissural heights were set as equal to 8.5 mm and 8.2 mm, respectively.

1. We assume that mitral leaflets surface could be obtained by a linear extrusion of the MA profile: the final leaflets profile will not be necessarily identical to the annular one, but it will maintain the same configuration, i.e. a saddle shape composed by two semiellipsis. However anterior and posterior leaflets have usually different dimension, so it is necessary

to know their variable heights, in order to identify corresponding end points on the leaflets free edges.

To do that, we set the values of leaflets and commissures heights by *Grasshopper Slider*s and we trace four vectors, starting from *A*, *C'*, *B*, *D'* points and moving in negative *z* direction, by assuming maximum heights in correspondence of previously defined end points (steps in yellow box, Fig.4.8).

Thus we identify four new points which will lie on the leaflets profile (Fig.4.9).

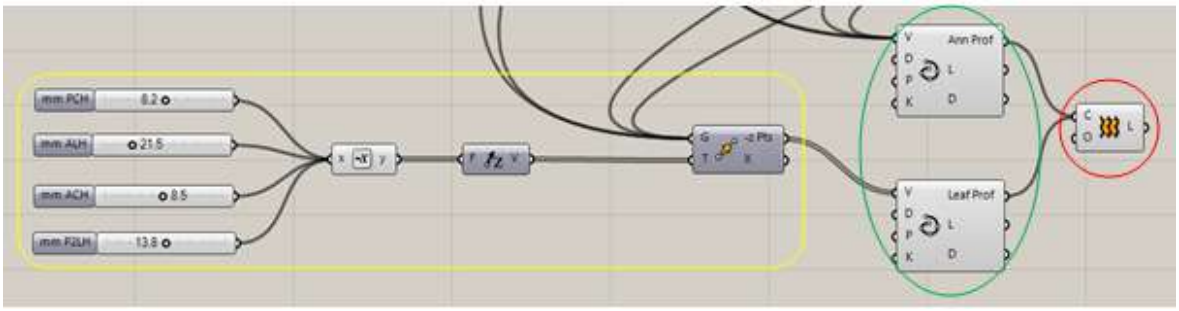

Fig.4.8: *Green* oval: *Interpolate* components; *Red* circle: *Loft* component.

2. We draw a second curve representing the leaflets profile, identified by interpolating new 3D coordinates points (see *Grasshopper* components in Fig.4.8, *Rhinoceros* geometrical reconstruction in Fig.4.9).

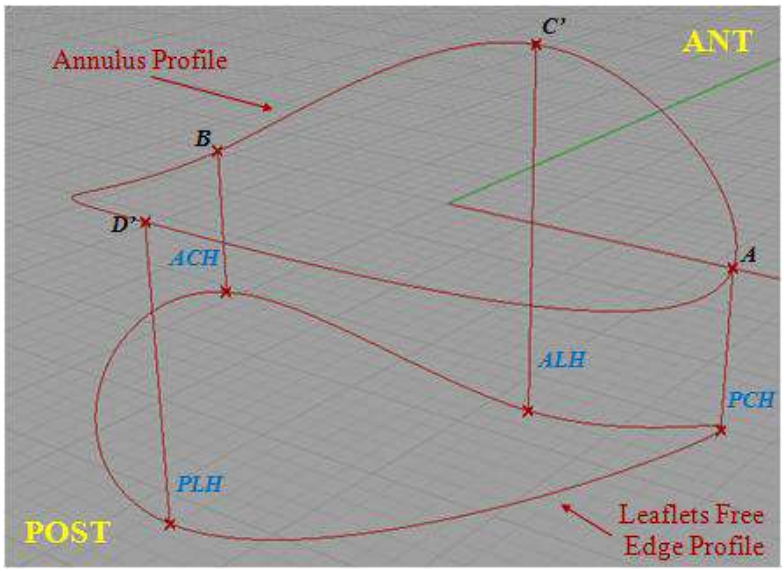

Fig.4.9: ***A→PCH***=Posteromedial Commissural Height
C'→ALH=Anterior Leaflet Height
B→ACH=Anterolateral Commissural Height
D'→PLH = Posterior Leaflet Height

ALH and ***PLH*** are defined as distances between leaflets insertions on the annular ring and their free margins, as well as ***PCH*** and ***ACH*** for the commissures, as shown in Fig.4.9.
Then, we can generate a *Loft* surface between the curves (Fig.4.10).

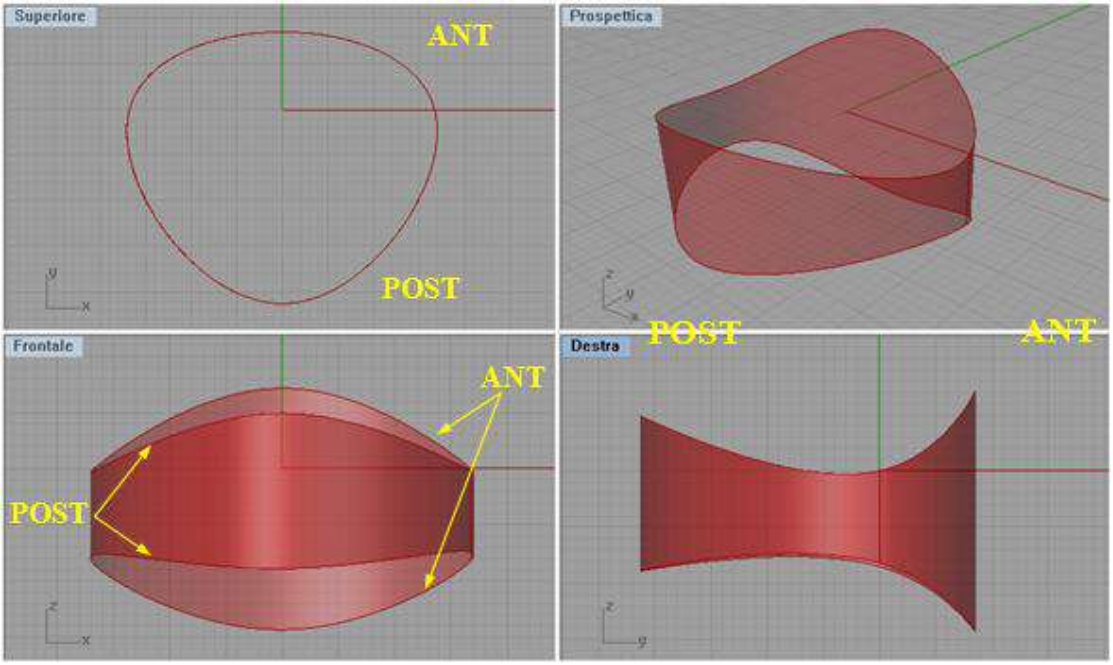

Fig.4.10: Diastolic configuration of the MV geometrical reconstruction with ANT and POST leaflets: surface extrusion between annular and leaflets profiles

3. Subsequently, we tilt the anterior and posterior leaflets towards the center of the valve orifice: in fact, it is easy to see, even with 2D echocardiography (see Fig.4.11,b), that in real mitral valves they are not perfectly perpendicular to the annular ring even when the valve is completely open.
For our modeling, the anterior leaflet was tilted by 8.3 deg with respect to a parallel plane to the *z* axis, while the posterior one was tilted by 5.3 deg, consistently with data reported in literature [123] and measured in real clinical cases, provided by Dr. Gambarin.
We obtain this tilting by rotating segments of anterior and posterior leaflets heights *ALH* and *PLH* (illustrated in Fig.4.8,a), and by using *C'* and *D'* points as pivot, respectively. We found two new points, labeled ***ALH'*** and ***PLH'***, to redefine the leaflets free edges profile, as shown in Fig.4.11,a.

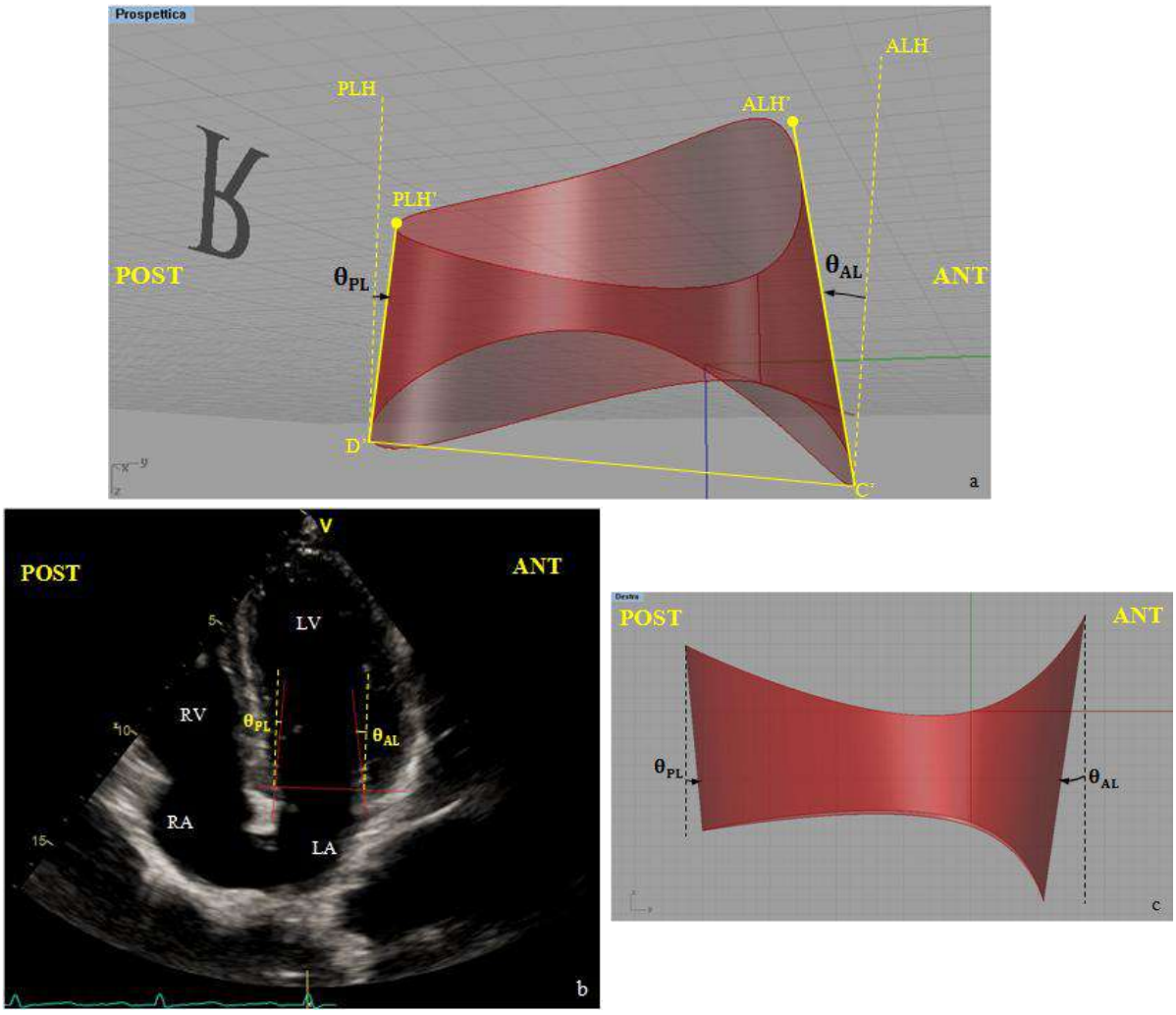

Fig.4.11: In every image are shown the rotation angles $\boldsymbol{\theta_{AL}}$ (AL=anterior leaflet) and $\boldsymbol{\theta_{PL}}$ (PL=posterior leaflet): (*a*) and (*b*) represent the same view of the MV in 3D geometrical reconstruction and from 2D-TTE, 4-chambers view (RA=right *atrium*, RV= right ventricle, LA=left *atrium*, LV= left ventricle). In *a*, the reversed "*R*" suggests the position of the right heart chambers compared to the MV, to make more evident the parallelism with the echocardiographic image. (*c*) Lateral view of the mitral leaflets profile and their tilts.

4. At last, we define the characteristic three-scalloped profile of the posterior leaflet, while we consider the anterior one as a whole unit.

We hypothesize the posterior leaflet composed by a greater central scallop, which we will name P_2, and two smaller lateral cusps, P_1 (anterior) and P_3 (posterior). Literature and clinical experiences report a great variability within the scallops, both in height and width, not so easy to measure by imaging techniques; in order to characterize every scallop, we need to know these dimensions, represented in Figs.4.12.

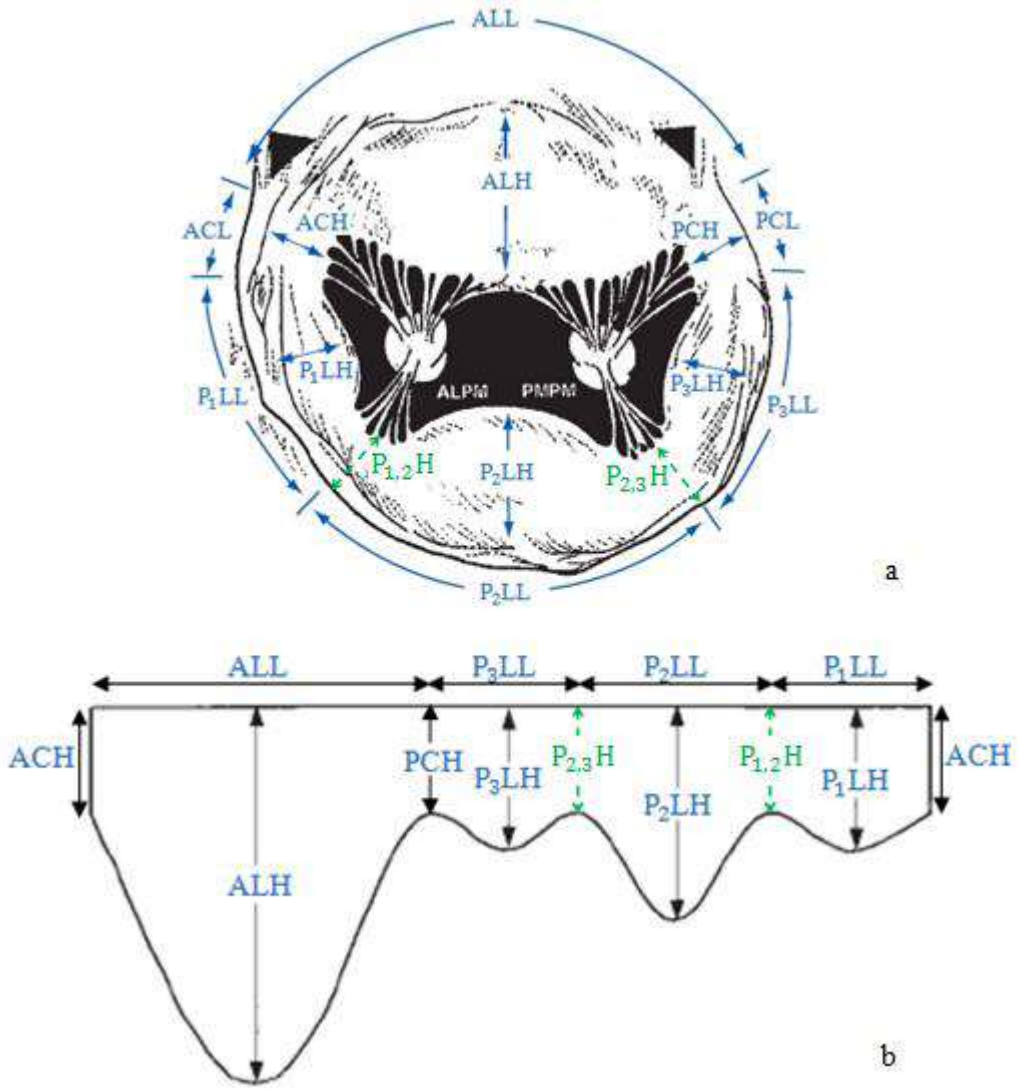

Fig.4.12: (*a*) Atrial view representation of the mitral valve: every measure necessary to our geometrical reconstruction is reported; ALPM and PMPM=Anterolateral and Posteromedial Papillary Muscles [100]. (*b*) Same parameters for the excised mitral valve (only *ACL* and *PCL* are neglected). Green arrows indicate minimum leaflets heights.

PCL=Posteromedial Commissure Length
ALL=Anterior Leaflet Length
ACL=Anterolateral Commissure Length
$\boldsymbol{P_1LL}$=Posterior Leaflet Length, anterior scallop
$\boldsymbol{P_2LL}$=Posterior Leaflet Length, central scallop
$\boldsymbol{P_3LL}$=Posterior Leaflet Length, posterior scallop

PCH=Posteromedial Commissure Height
ALH=Anterior Leaflet Height
ACH=Anterolateral Commissure Height
$\boldsymbol{P_1LH}$=Posterior Leaflet Height, anterior scallop
$\boldsymbol{P_{1,2}H}$=Posterior leaflet Height between anterior and central scallops
$\boldsymbol{P_2LH}$=Posterior Leaflet Height, central portion
$\boldsymbol{P_{2,3}H}$=Posterior leaflet Height between central and posterior scallops
$\boldsymbol{P_3LH}$=Posterior Leaflet Height, posterior portion

Besides *PCH*, *ACH*, *ALH* and P_2LH (heights of both commissures, anterior leaflet and central portion of the posterior one,) previously defined, we also set $\boldsymbol{P_1LH}$ and $\boldsymbol{P_3LH}$ values, which represent maximum heights of parietal and septal scallops of posterior leaflet, respectively, while $\boldsymbol{P_{1,2}H}$ and $\boldsymbol{P_{2,3}H}$, are the minimum heights between central cusp and the lateral ones.

Leaflets profile (red curve in Fig.4.13) passes through the end points defined by leaflets heights, whom coordinates are identified starting from the corresponding points along the annulus profile (Fig.4.13). Therefore, values necessary to our geometric reconstruction are points of maximum and minimum heights of every scallop, which allow to describe the amplitude of the leaflets curve by the annulus, and the distances among them (leaflets lengths of attachment to the annular ring, shown in Fig.4.12) by supposing that every cusp reaches its maximum height exactly at the middle of its width (i.e. every scallop is symmetrical to its own maximum height, perpendicular to the annulus). To do that, we refer to numeric values from cadaveric samples, reported by Sakai et al. [100], even if measures from excised valves are slightly different from those ones of an intact valve.

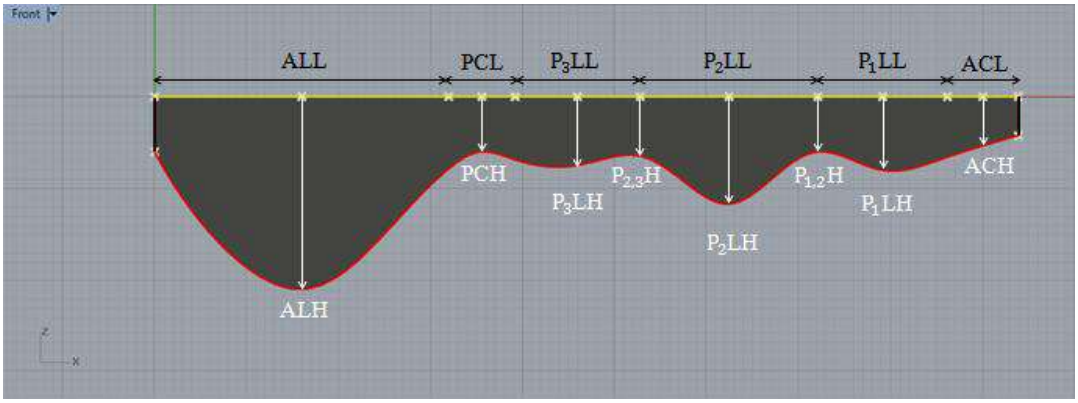

Fig.4.13: Same frontal view of the mitral leaflets surface for an excised valve as the picture Fig.4.12,b: our geometrical reconstruction. Yellow line: annulus profile; red curve: leaflets profile.

Values assessed by Sakai and colleagues, and also used in our modeling, are reported in Table 11; wider ranges of values from literature are summarized in Appendix A, except for $P_{1,2}H$ and $P_{2,3}H$ parameters, that we suppose 7.5 mm long, by studying anatomy proportions of the mitral valve and previous geometrical simulations by other research groups.

Measures	Mean ± SD [mm]	Measures	Mean ± SD [mm]
ALL	32.0±4.0	**ALH**	23.4±2.9
PCL	7.2±2.1	**PCH**	8.3±2.0
P_3LL	13.6±3.3	**P_3LH**	13.0±2.3
P_2LL	19.3±4.1	**P_2LH**	13.8±2.9
P_1LL	14.1±3.6	**P_1LH**	11.2±2.3
ACL	7.7±2.1	**ACH**	8.7±2.4

Tab.11: Values of 57 human mitral valves with annular diameters 29.7±3.5 mm long studied at autopsy [100] and adopted in our geometrical reconstruction.

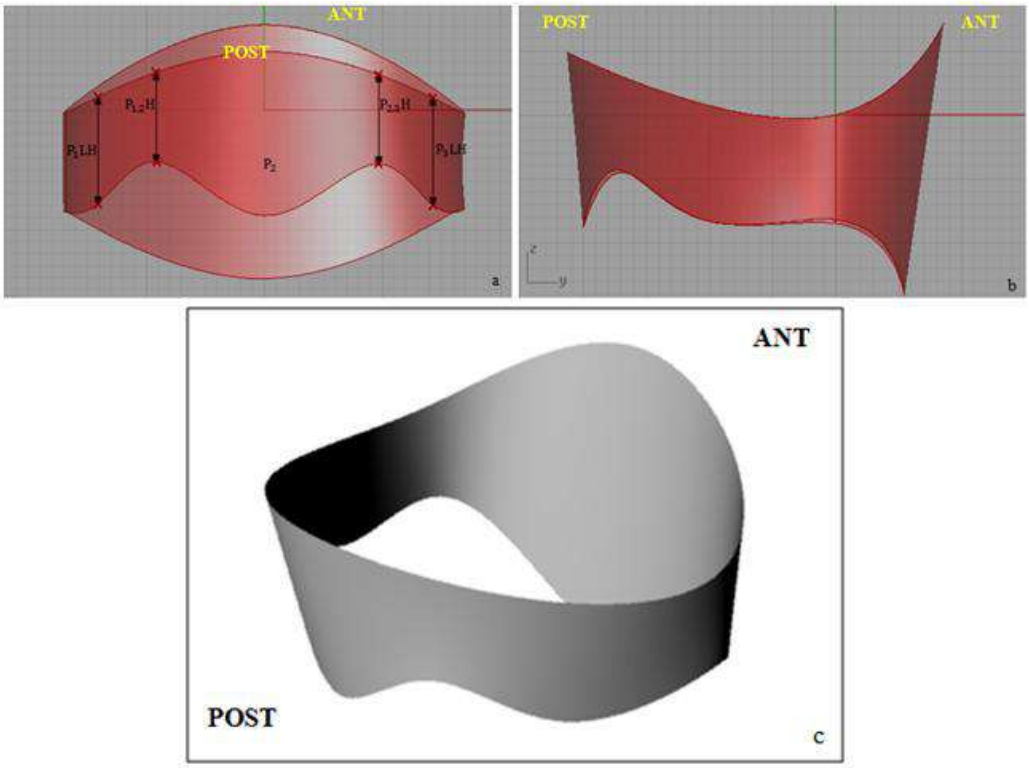

Fig.4.14: Result of the first 3D geometrical reconstruction of the MV (subvalvular apparatus is neglected). (*a*) Frontal view; (*b*) Lateral (right) view; (*c*) Perspective rendering.

However, several limits are related to imaging techniques and, consequently, to the assessment of geometrical parameters. In order to make useful our mitral valve model in a future clinical practice as predictive tool, it would be desirable to use the smallest possible number of parameters to generate a patient-specific model and to get all values just from one routinely, not invasive and not expensive imaging exam, if possible. In this case, the gold standard is three-dimensional echocardiography.

4.2.3. Improved Mitral Leaflets Reconstruction: Method 2

In this second parametric model, the mitral annulus has been defined by its two main diameters, provided by echocardiographic images, as previously described, as well as tilting of anterior and posterior tracts of the saddle-shaped annulus and central portions of the mitral leaflets remain unchanged. Instead, leaflets profile and their heights are obtained by a different method.

We originally generated leaflets by extruding the annulus along the negative *z*-axis, i.e. perpendicularly to the annular plane, and then tilting them at their insertion on the annulus in order to reproduce their end-diastolic position as provided by echocardiographic data; now, leaflets free margin profile is described through a harmonic function, which expresses the annulus-to-free edge distance (i.e. leaflets heights, referred as *y* in the formula below) as a function of the position on the annulus (*x*), described for the first time by Votta et al. [121]. This is a linear combination of sinusoids:

$$y(x) = k + \sum_{n=1}^{12} a_n * \sin(n\omega x), \qquad (1)$$

where values from literature [122] are ω=0.0356999 for frequency, *k*=6.0, constant, and a_1=5.40814, a_2=4.2918, a_3=5.30630, a_4=3.06855, a_5=−0.09161, a_6=−0.5986, a_7=−0.30913, a_8=−1.15527, a_9=1.0269, a_{10}=0.25297, a_{11}=−0.64712, a_{12}=0.11715 are the adopted amplitudes of the Sine wave. Votta et al. experimentally derived these particular values starting from clinical measurements reported by Kunzelman and colleagues [56] for an excised porcine mitral valve: data were interpolated and scaled according to different dimensions of the valves in both studies.

Even if the intact valve is not planar, we can consider the annulus profile of an excised valve as lying on the *x*-axis of a two-dimensional plane, as previously shown in Fig.4.13; our main target is to reduce the number of anatomical parameters required to implement our geometric model of the mitral valve, so we decide to adopt this new method in order to derive leaflets heights just from coordinates of certain points on the annulus profile. Therefore, first of all, it is necessary to understand how to get the correct scale factor for our parametric model, the meaning of each term in *(1)* and how they influence the model geometry of the valve.

Also considering our previous model, besides some literature data, it is obvious to presume that the leaflets size should proportionally change if the annulus dimensions increase or reduce, in order to preserve leaflets proper coaptation.

In figure below, a Sine wave obtaining from *(1)* and representing the leaflets profile is shown:

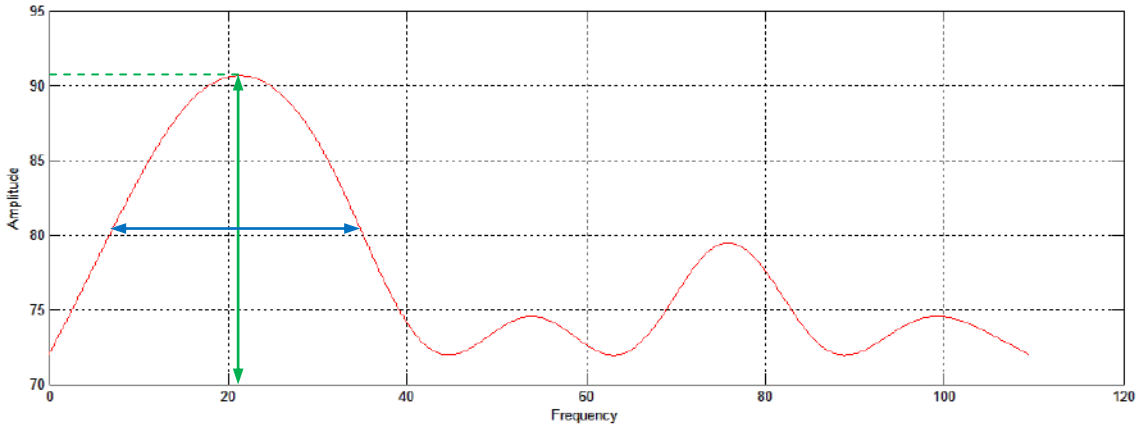

Fig.4.15: MATLAB plot of sinusoidal wave described by *(1)*: values of frequency (*x*) and amplitude (*y*) for a 109.5 mm annulus length; green and blue double-headed arrows indicate the anterior leaflet height and its width, respectively.

by using a simple custom software implemented in MATLAB (The MathWorks Inc., Natick, MA, United States), attached in Appendix C, we can read values corresponding to the length of the mitral annulus (in millimeters) on the *x*-axis, while the amplitude of the wave, on the *y*-axis, describes relative distance between mitral ring and leaflets free edges (i.e. leaflets heights, see green arrow in Fig.4.15).

As suggested by Votta et al. [121], who adopted a factor to scale up the diameter dimension of his modeled valve compared to the first value reported by Kunzelman, at first we use a scale factor defined as follow:

$$\mathrm{f_{scale}} = \frac{\mathrm{circ_2}}{\mathrm{circ_1}}, \qquad (2)$$

where $circ_1$ is the (constant) length of the annulus profile in Votta's work, while $circ_2$ is the annulus perimeter of our geometric models (it will be different for various models). Resulting function is shown in Fig.4.16: the amplitude remains unchanged while the frequency ranges in a directly proportional manner to the annular circumference. However, it is easy to understand that greater circumferences cause greater valve orifices, thus it is

reasonable to assume that leaflets with unchanged highs will not be able to thoroughly coapt both in physiological and pathological conditions.

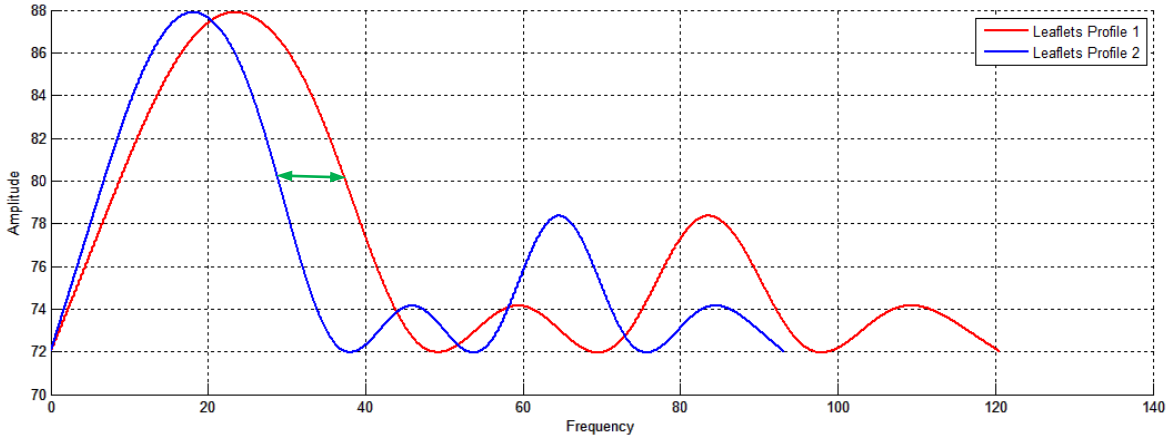

Fig.4.16: Leaflets profiles for annular circumferences of 120.6 (red curve) and 93.2 mm long (blue curve): only the leaflets width is proportionally changed (see green double-headed arrow).

Similarly, it is not sufficient to rescale only the amplitude (Fig.4.17), but it is important to separately analyze these different effects of the linear combination of sinusoids in order to understand how they influence curve morphology. This points us out that it is necessary to modify something else in the previous formula *(1)*, in addition to adopting a proper scale factor *(2)*.

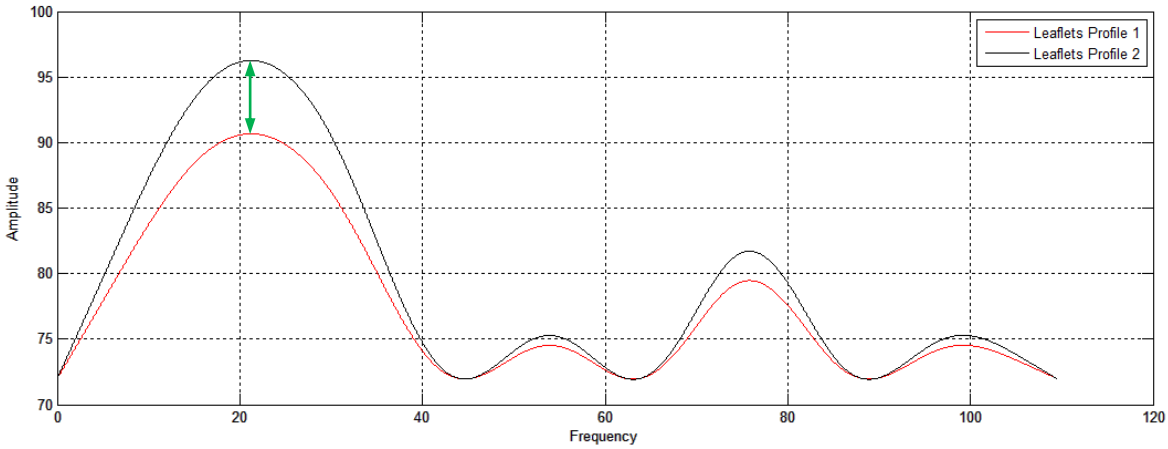

Fig.4.17: Leaflets profiles for annular circumferences of 109.5 mm with different amplitudes of the Sine waves (see green double-headed arrow).

After some experimental tests with real dimensions of mitral valves taken from literature [122], we found that the particular value of ω parameter by Votta derives from

$$\omega = \frac{\pi}{circ} = \frac{\pi}{88} = 0.0356999, \qquad (3)$$

where *circ* is the length of the mitral annulus modeled by Votta's research group and 0.0356999 is the exact value used to implement his first harmonic function describing the leaflets free edges.

Hence, we tried to obtain some correct sinusoidal waves for different annular lengths by using a function defined as *(1)*, scaling our circumference dimension by analogous factor to *(2)* and replacing Votta's value of *circ* (88 mm) in *(3)* with the mitral annulus size of our model. The results are shown in Fig.4.18: sine amplitudes and frequencies (i.e. leaflets heights and widths, respectively) change proportionally to ranges of *x* values (i.e. annular lengths).

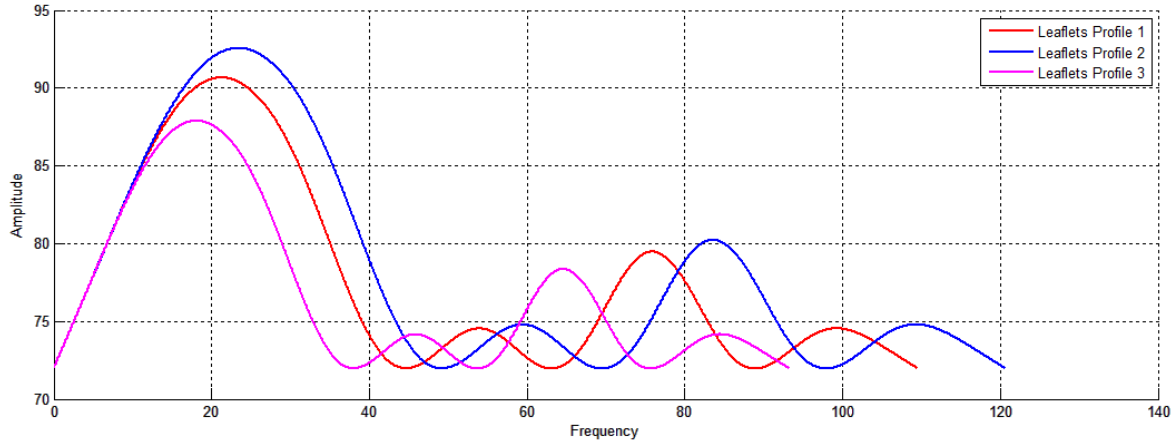

Fig.4.18: Sinusoidal curves representing leaflets profiles for annular circumferences of 93.2, 109.5 and 120.6 mm (magenta, red and blue curves, respectively)

Regarding amplitude values a_n, n = 1:12, achieved through Votta's group tests and employed to implement *(1)*, in our experience, we suppose that they are related to 12 particular points on the annular ring. By comparing curves of leaflets profile obtained from MATLAB code with our first model of the mitral valve, we notice that it was necessary also to us to identify exactly 12 points on the annulus circumference to find space coordinates corresponding to the main points describing the leaflets free edges curve (Fig.4.19).

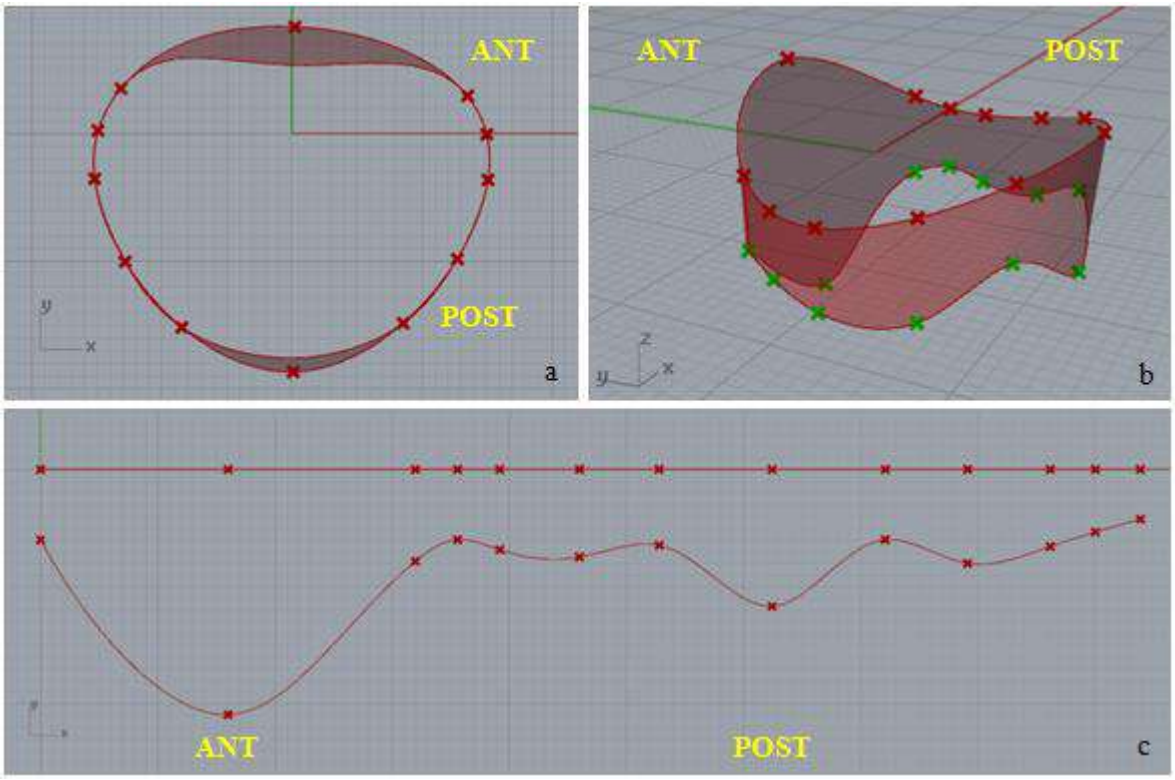

Fig.1.19: 12 red crosses suggest derived points from echocardiographic data on the annulus profile: (*a*) Superior view of the new MV model; (*b*) Perspective view of the same modeled valve with 12 points suggested by green crosses, obtained by implementing *(1)* in *Grasshopper* in order to define the leaflets profile. (*c*) Excised MV shows 13 points because the first and the last one will overlap.

We perform this second model of the mitral leaflets by using their values of lengths of attachment to the mitral ring, which will be measurable by three-dimensional TEE (Fig.4.20 by Dr. Magrini G., San Matteo Hospital, Pavia).

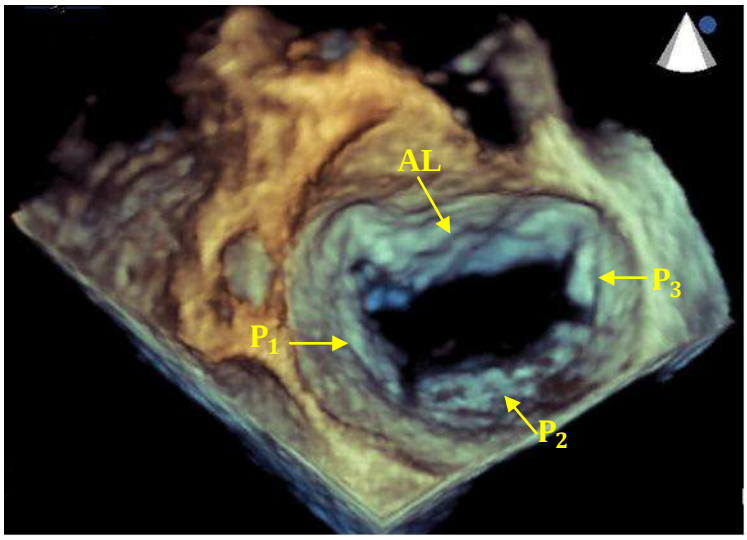

Fig.4.20: Short axis view of the MV by 3D TEE; *AL*=Anterior Leaflet; P_1=anterior scallop, P_2=middle scallop and P_3=posterior scallop of the Posterior Leaflet

1. We provide these measurements of length to our *Grasshopper* program and calculate also their midpoints. Then, we transform all values in corresponding spatial 3D coordinates on the annulus profile (Fig.4.21): they all will be the *x* inputs to implement the sinusoidal function using expression *(1)*, with suitable scale factors, as previously described (see Fig.4.22).

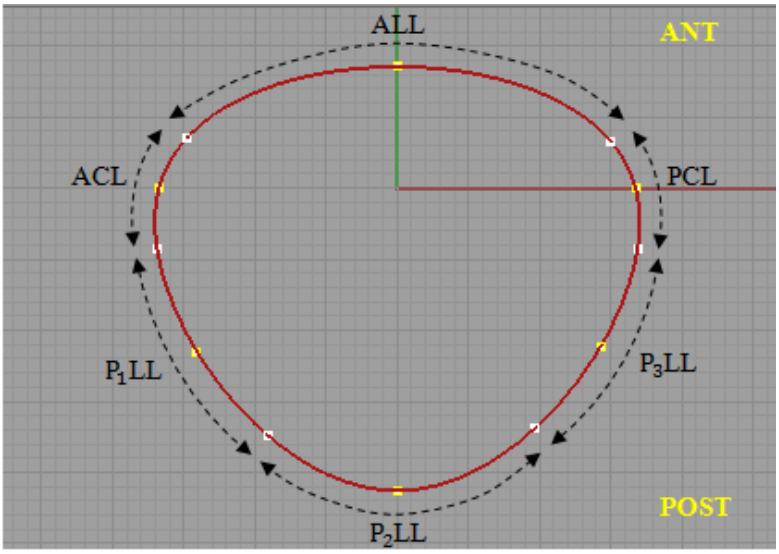

Fig.4.21: Superior view of the curve describing the annulus profile: yellow little squares represent computed midpoints of every measured lengths

After evaluating the expression, as result we obtain 12 values, which are equivalent to the valve heights at every point shown in the figure above. In order to describe this particular sine wave, we need to know not only its maximum amplitudes, but also the minimum ones. In fact, mitral posterior leaflets particularly show quite a recurrent and characteristic conformation in physiological conditions: they approximately reach their maximum height at the middle of their width and the least value between each couple of scallops. For this reason we decided to accept geometrical approximations deriving from using *(1)*, with midpoints of every circumferential portion, besides their extreme points.

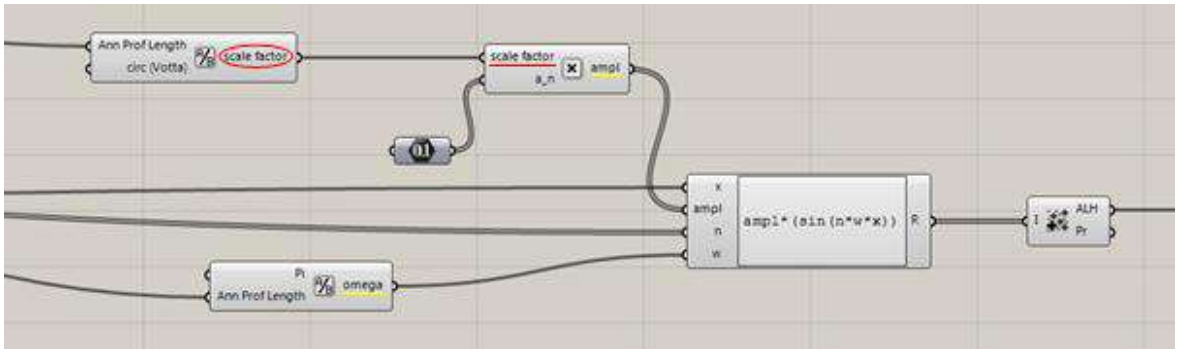

Fig.4.22: Implementation of harmonic function *(1)* with *Grasshopper* Expression component

2. Now, we can associate every computed height value of leaflets scallops and commissures to the corresponding point along the annular circumference: because we know their space coordinates, we project annular points in negative *z*-direction by an amount equal to the obtained lengths, in order to identify 12 points coordinates (see green crosses in Fig.4.23), which are necessary in order to define the leaflets profile.

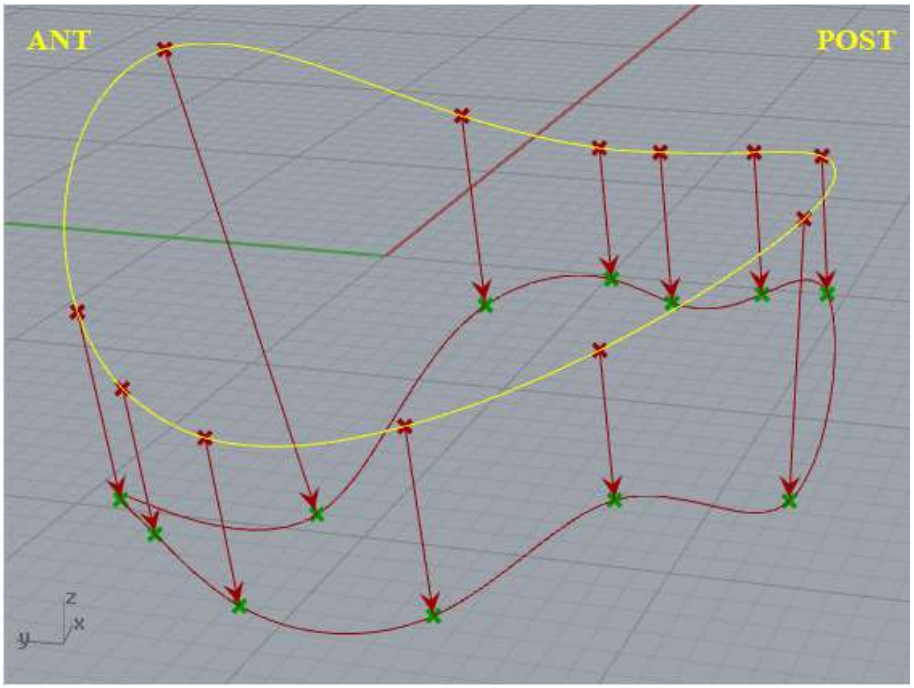

Fig.4.23: Green crosses show 12 points determined by *(1)*, red arrows indicate the direction of points projection, yellow and red curves are annulus and leaflets profiles, respectively

3. Leaflets orientation is maintained: their tilting has been obtained as described at step 3. in the previous paragraph.

The resulting valvular surface is shown in Fig.4.24:

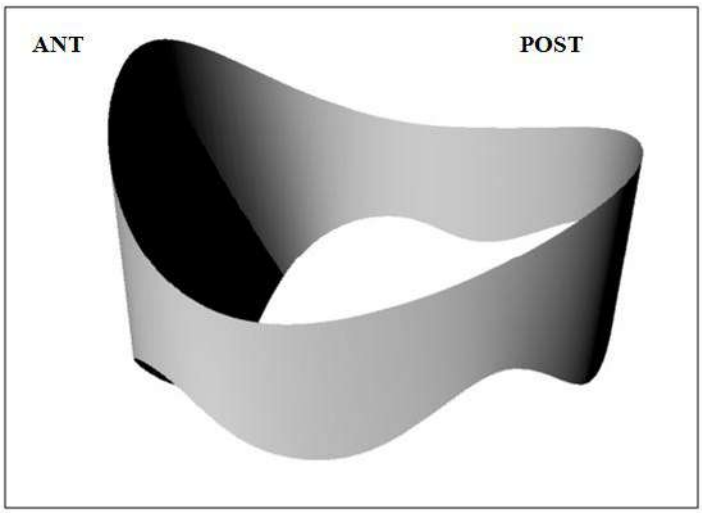

Fig.4.24: *Rhinoceros 5.0* render of our second model of a mitral valve: description of mitral leaflets by harmonic function

Tab.12 shows all necessary lengths parameters to our parametric models reconstructions: this comparison highlights mitral valve dimensions which could be avoided if we use this new method. Parameters regarding annulus and leaflets tilting have not been added to the table below because they are necessary in both model and, in clinical practice, it is very difficult to assess rotation angles of anterior and posterior tracts of the saddle-shaped annulus particularly, so we always take these values (θ_{AA} and θ_{PA}) from literature [109]. However, they have been reported in Appendix A.

During our meeting with Dr. Magrini G., echocardiographist at San Matteo Hospital in Pavia, we had confirmation that three-dimensional investigation modality supplies the best-quality mitral valve images, even if artifacts due to patient breath can be present. Nowadays, trans-esophageal 3DE is a routine exam to study heart valvular pathologies; particularly, 4-Chamber Full-Volume results to be the best mode of acquisition because it allows to get the whole volume of the structure of interest, by preserving spatial relationships among different parts. Then, we can select a particular sections for following examinations: by a 3D probe, it is possible to obtain anatomical reconstructions which can be decomposed in every possible orientation of planes (*Frontal*, *Sagittal* and *Transversal* views, Fig.4.25). The *X-Plane* modality is particularly useful because provides couples of two-dimensional planes, perpendicular to each other, which allow to observe *SAx* (Short

Axis), *LAx* (Long Axis) *LVOT* (*L*eft *V*entricular *O*utflow *T*ract; or 3-Ch.), and Bicommissural projections, and which are suitable to measure geometric dimensions necessary to implement our parametric model.

Parameters [mm]	Model 1	Model 2
IC diam	x	x
SL_{ant}	x	x
SL_{post}	x	x
ALL	x	x
P_1LL	x	x
P_2LL	x	x
P_3LL	x	x
ACL	x	x
PCL	x	x
ALH	x	-
P_1LH	x	-
$P_{1,2}$LH	x	-
P_2LH	x	-
$P_{2,3}$LH	x	-
P_3LH	x	-
ACH	x	-
PCH	x	-

Tab.12: "*x*" indicates which parameters are necessary to the valve model implementation for each of two methods

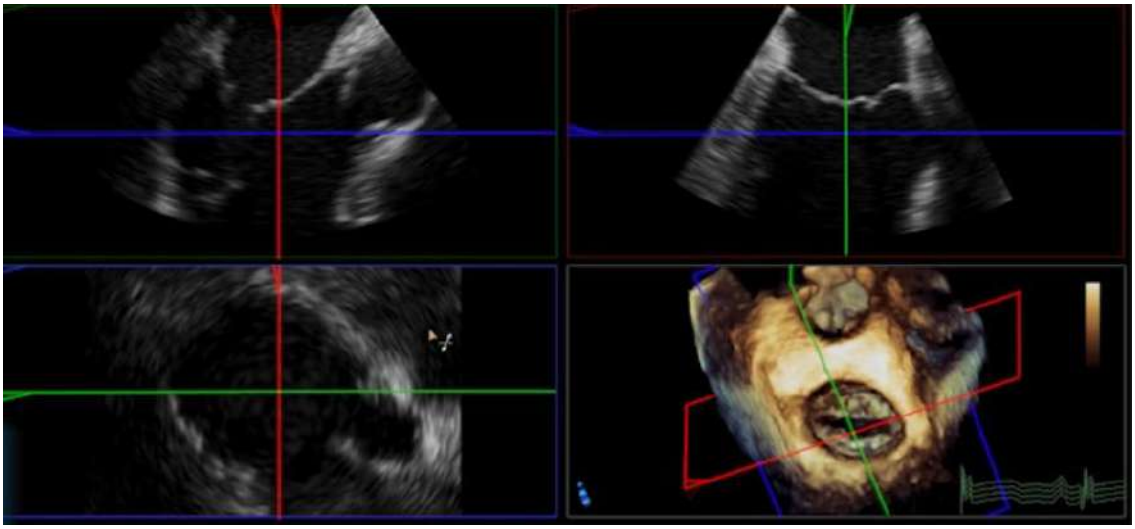

Fig.4.25: *Multiplanar Reconstruction* (MPR) with *Philips Epiq 7 Affiniti* Ultrasound System

At last, by way of example, we use clinical data (provided by Dr. Gambarin F.) to develop patient-specific MV models (Figs.4.26) to show the software ability to model also pathological geometries: their parameters values are reported in Tab.13.

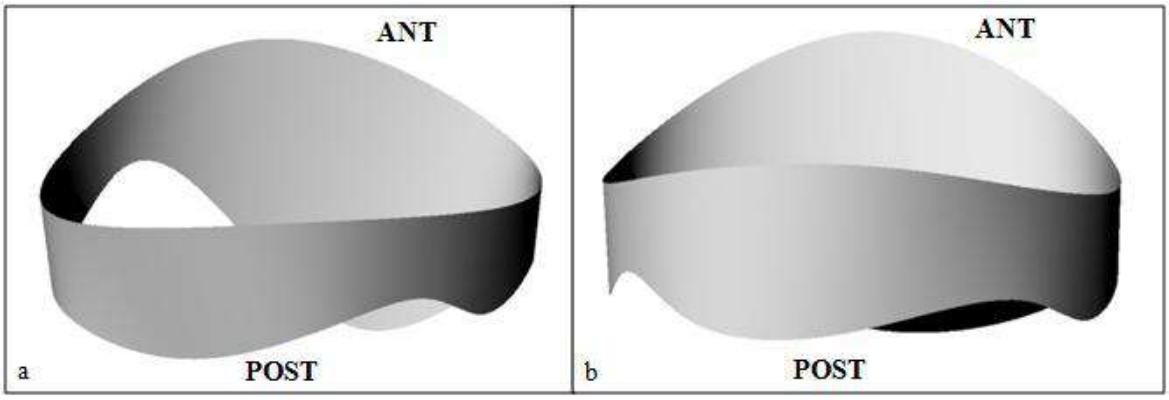

Fig.4.26: (a) Patient 01; (b) Patient 02

Parameters	Patient 1	Patient 2
IC diam	38.45	36.06
SL_{ant}	8.95	10.01
SL_{post}	19.23	19.57
ALL	45.01	45.98
P_1LL	18.95	12.62
P_2LL	27.15	24.4
P_3LL	12.55	12.3
ACL	7.5	6.2
PCL	9.43	5.8
θ_{AA}	*N.A.*	*N.A.*
θ_{PA}	*N.A.*	*N.A.*
θ_{AL}	*N.A.*	*N.A.*
θ_{PL}	*N.A.*	*N.A.*

Tab.13: Necessary parameters to the valve modeling. Parameters dimensions measured in *mm*; rotation angles not available (*N.A.*) have been replaced with before mentioned values from literature

ALH	23.9	22.9
P_1LH	11.6	12.2
$P_{1,2}$LH	10.36	6.22
P_2LH	10.4	12.0
$P_{2,3}$LH	6.23	7.36
P_3LH	11.4	10.44
ACH	6.0	8.41
PCH	6.04	6.09

Tab.14: Parameters measured after reconstruction (*mm*)

5. A PRELIMINARY FINITE ELEMENT ANALYSIS

5.1. Introduction to FEM

A Finite Element Method (FEM) is a numerical method for solving problems in different areas of Engineering sciences, such as branches of Solid and Fluid mechanics, Structure analysis, Thermodynamics, and Biomaterials, Bio-mechanics and Bio-medical engineering. This method can be applied to solve almost all multiphysics problems encountered in practice, steady or transient, in linear and nonlinear regions for one-, two- and three-dimensional domains. To comprehensively understand and quantify any physical phenomena, it is necessary to use mathematics because most of these processes are described using Partial Differential Equations (PDEs).

Nowadays, Finite Element Method has become one of the most powerful and frequently used tools for solving such equations. It consists of finding solutions that locally approximate the exact original equations to be studied, by converting PDEs into a set of algebraic equations, easy to solve, in order to simulate the complex behavior of physical system.

A typical work out of this method involves the use of mesh generation techniques for dividing the domain of a large problem into a collection of smaller, simpler parts, that represent different areas in the physical system and are described by a set of element equations to the original problem with initial values (Boundary Conditions, BCs).

The simple equations that model these finite elements are a good choice for analyzing problems over complicated domains that need to be solved numerically: hence, through the before-mentioned discretization, the integral form is converted to a summation that can be solved at discrete number of points over the domain.

Finite Element Analysis (FEA) yields approximate values of the unknowns then recombining all sets of element equations into a global system for the final calculation.

This procedure is summarized in the diagram below (Fig.5.1).

In many instances three-dimensional finite element approach is employed for the analysis of soft biological tissues, that show a large deformation behavior.

These structural models are able to solve the equations of continuum mechanics in order to compute tissue field variables (e.g. displacements, stresses and strains) at each material point, and have been increasingly adopted in the last two decades to study heart and its valves biomechanics in order to provide powerful insight into clinically relevant patient-specific situations.

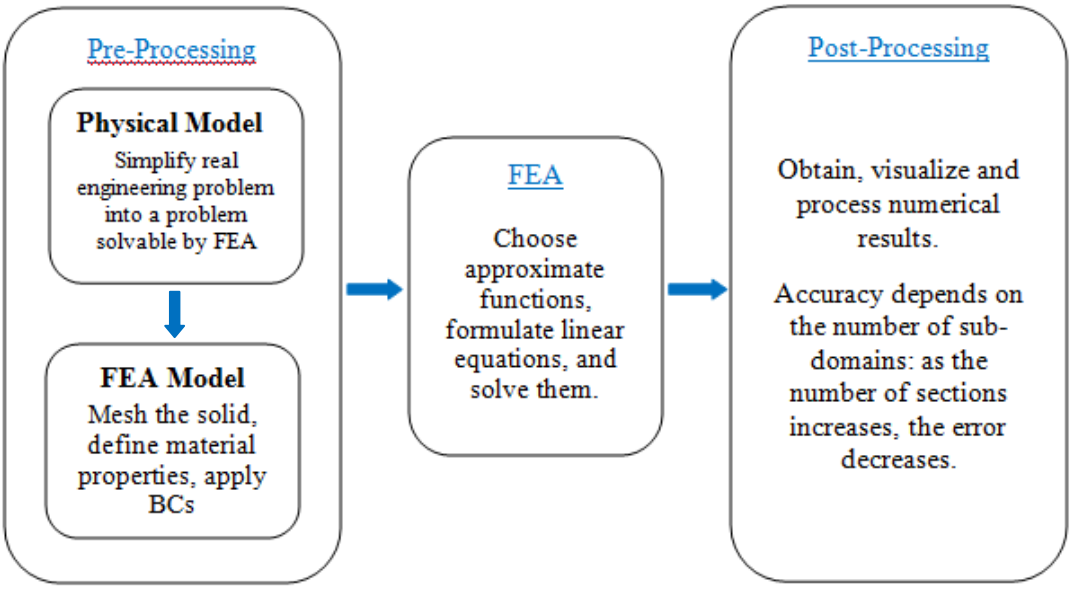

Fig.5.1: General FEA procedure

Particularly, MV finite element models could be a valuable tool, since they allow the virtual simulation of a hypothetical scenario and the assessment of associated valvular biomechanics both in physiological and pathological conditions [110]. However, every developed model is based on simplifying assumptions, depending on the degree of complexity of the model and on its particular application. Different groups have developed three-dimensional structural FE models of the human mitral valve, but the implementation of a fully realistic model represents a challenging task, owing to the high complexity of the different aspects to be modeled [91].

For this purpose, the commercial solver *Abaqus 6.12* (SIMULIA, Dassault Systèmes, Providence, RI, USA, 2011) serves as an appropriate tool.

5.2. Abaqus 6.12

ABAQUS is a software for Finite Element Analysis and computer-aided engineering, used in many application fields, due to its wide material modeling capability and ability to be customized [133].

Any complete *Abaqus* analysis usually consists of some distinct stages, detailed below.

We have imported from *Rhinoceros* our parametric model of the mitral valve (file *.iges*) developed by *Grasshopper* plug-in: this one will be our **Part**, i.e. the geometry of the structure to be analyzed (Fig.5.2). Every aspect of the modeling process (e.g. properties of **material** and mesh, besides the visualization of results) can be defined by different Modules in *Abaqus/CAE* (Complete Abaqus Environment), that is a software application with interactive graphical interface.

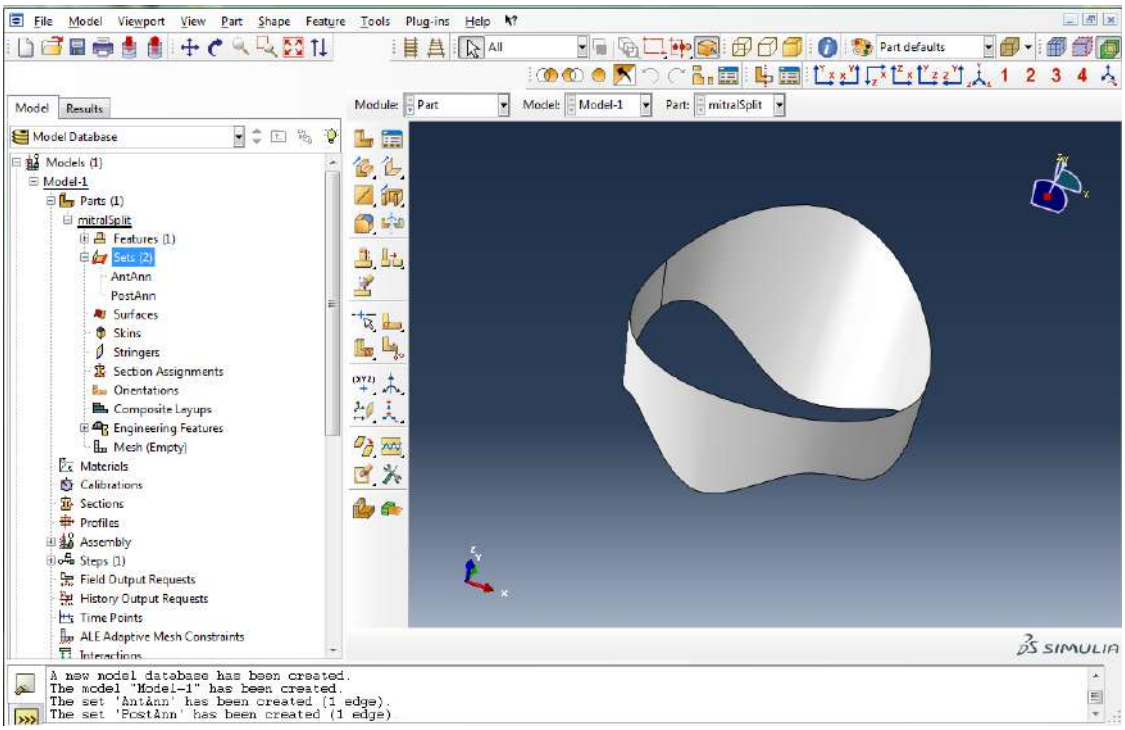

Fig.5.2: **Part** of the MV model (end-diastolic phase) in *Abaqus/CAE* interface

After having partitioned the model into its anterior and posterior *Sections* (see Fig.5.3,a), corresponding to the anterior and posterior leaflets, respectively, physical properties can be assigned to the geometry, together with **loads** and **boundary conditions**. The next step consists in decomposing the actual geometry into a collection of *finite elements* joined by shared *nodes*: they all form a **Mesh**, made up of 4-nodes 3D deformable *shell* elements (ABAQUS S4R element type), as shown in Fig.5.3,b.

Physiologically, MV opening and closure are mainly driven by the transvalvular pressure drop; for this reason, we have simulated its systolic biomechanics by assuming that the effect of surrounding blood can be simplistically described through a pressure load applied to the ventricular side of the leaflets for a total simulation time of 0.8 seconds.

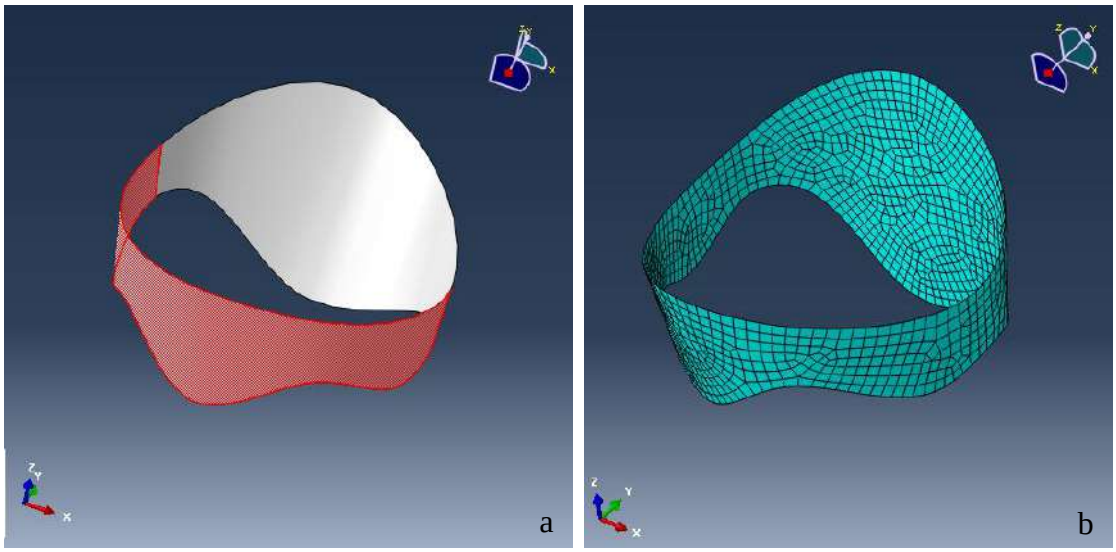

Fig.5.3: (*a*) Partitioned geometry in anterior and posterior sections: the latter one is pointed out in red; (*b*) Discretized model.

Different literature data report changes in annular length, saddle-horn height and orifice area [20,54,84] from end-diastole to systolic peak so, in order to analyze the role played by the contraction of annulus, we have suppressed its motion by defining initial BCs, which are represented in Fig.5.4 together with loads.

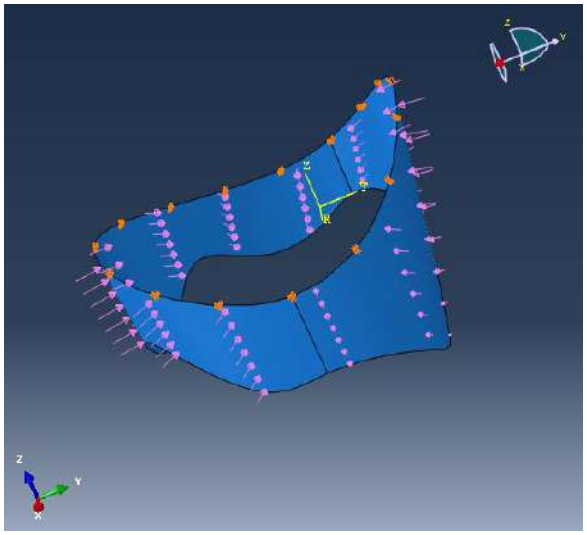

Fig.5.4: Pink arrows perpendicular to the ventricular side (external surface) of the mitral leaflets represent the blood pressure, while orange nodes on the annulus perimeter suggest the boundary conditions.

All tissues were assumed as homogeneous (density ρ=10.4 g/cm^3) and we have approximated MV leaflets response through the elastic constitutive model, described by

Young's Modulus (E_{Ant}=2.1-2.35 MPa, E_{Post}=1.887-1.99 MPa for the anterior and posterior portions of the valve, respectively) and Poisson's Ratio (υ=0.45) (parameters values from literature [129]).

In order to perform this first simulation, we have used *Abaqus/Explicit*, a special-purpose Finite Element analyzer that employs explicit integration scheme to numerically solve highly nonlinear systems with many complex contacts under transient loads [131].

In general, in a stress analysis, the displacements of the nodes are the fundamental variables that *Abaqus* calculates; once the nodal displacements are known, stresses and strains in each finite element can be determined.

In the present preliminary analysis, we don't want to numerically compute the elastic stress-strain relationship for fibers in mitral valve tissues, but we aim to better comprehend and show the leaflets qualitative behavior during valvular closure (Fig.5.5,a).
As we expected, it is impossible to perform a correct leaflets coaptation because of the lack of the subvalvular apparatus: this simulation highlights the importance of presence of the *chordæ tendineæ*. In particular, we prove that, by applying also much lower loads than the physiological pressures on the external surfaces, mitral leaflets have excessive rotation. For example, in Fig.5.5,b, we show the posterior leaflet prolapsing into the *atrium*, as it happens in pathological conditions, after chordal rupture (see echocardiographic image in Fig.1.43). This test lets us deduce that *chordæ tendineæ* play an essential role in valvular closure dynamics, as supposed in literature and previously enounced.

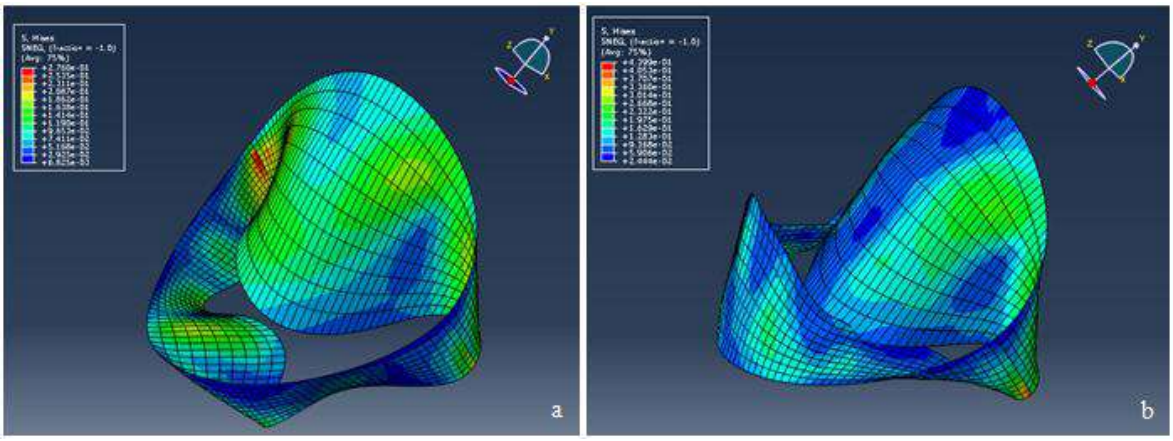

Fig.5.5: (*a*) First steps simulation of valvular dynamics toward systolic phase; (*b*) Prolapsed posterior leaflet in subsequent steps.

Future Developments

The present work is the first step towards the development of a three-dimensional patient-specific model of the mitral valve, with aim of becoming a predictive tool available to clinicians in everyday practice.

We have identified a series of essential anatomical values necessary to our model implementation, so it will be straightforward to set up a standardized protocol in collaboration with heart specialists. Particularly, it would be useful to point out 3D echocardiographic views from which it is possible to accurately quantify these geometrical parameters. This step is necessary because, in heart valves routine evaluation, these peculiar measurements are not usually performed, so it is necessary to establish most suitable planes projections in order to achieve them.
Moreover, we expect the ability to extend our parametric model through volumetric data from 3D echocardiography, by locating the papillary muscles tips (visible by transgastric view), some *chordæ tendineæ* and left ventricular wall, which is an integral part of the subvalvular *apparatus* and its movements.

With a precise and more complete geometrical model, it would be possible to perform more accurate Finite Element Analysis (FEA) so we could provide a useful tool for medical operators in investigating and predicting surgical outcomes or planning, with heart surgeons, the best patient-specific strategy before entering the operating room. In particular, it would be of great interest to know the exact location of the chordal insertions on the leaflets in order to study their contribution to the correct valve coaptation and simulate their possible restoration effects.
At last, it would be important to have clinical data regarding a large number of cases in order to validate our modeling process.

Conclusion

In the present work we have described the software developed to implement a three-dimensional parametric model of patient-specific mitral valves, useful for the visualization of this anatomical structure and validation of modeling procedure.
In particular, after an extended literature review aimed to deep comprehension of valvular geometry, we used a powerful and quite recent commercial software for parametric modeling (*Grasshopper*), which interfaces with a common CAD tool (*Rhinoceros*), to realize our parametric model.
Both origin and development of this work required direct interactions with medical operators routinely performing heart valves ultrasound evaluations, in order to lay the basis of a protocol definition of specific anatomical 3D echocardiographic measurements.
At first, this work has been encouraged by Heart Surgery staff of University-Hospital in Padua, looking for a patient-specific tool able to predict surgical outcomes, because knowledge of parametric data could beforehand permit an accurate planning of the most appropriate surgical strategy. During the model development, we obtained clinical images and valuable information by cardiologists at St. Pio X Clinic in Milan (Dr. Gamabrin F.) and St. Matteo Hospital in Pavia (Dr. Magrini G.).

Even though we have run into some limitations, such as measuring geometrical parameters not usually assessed during routine clinical practice, and high inter-patients variability of valvular dimensions that makes almost impossible to set any ratio between different parts of the valve, a parametric software for building patient-specific models of the mitral valve has been successfully developed.
It is a user-friendly tool for evaluations of normal or abnormal geometry of the valve: it allows to obtain different models depending on entered values of parameters measured during 3D echocardiographic exams, which is the most widely used tool in clinical practice for assessing cardiac pathomorphology.

Future works could be developed in different directions, such as the increase of valvular geometry complexity in order to simulate its correct functioning, improve its faithfulness to physiological structures and be used as a predictive tool in realistic numerical simulations. Moreover, having already indentified all necessary measurements to the model implementation, writing a protocol reporting corresponding echocardiographic

parameters is straightforward because, even if not ordinary echocardiographic views are required, all values can be obtained by a routine exam.

References

[1] Ahmad R.M., Gillinov A.M., McCarthy P.M., Blackstone E.H., Apperson-Hansen C., Qin J.X., Agler D., Shiota T., Cosgrove D.M., "Annular Geometry and Motion in Human Ischemic Mitral Regurgitation: Novel Assessment with Three-Dimensional Echocardiography and Computer Reconstruction". *Ann Thorac Surg*, 2004; 78: 2063-68.

[2] Alkadhi H., Bettex D., Wildermuth S., Baumert B., Plass A., Grunenfelder J., Desbiolles L., Marincek B., Boehm T, "Dynamic Cine Imaging of the Mitral Valve with 16-MDCT: A Feasibility Study". *AJR*, 2005; 185: 636-46.

[3] Anastasi G., Capitani S., Carnazza M.L., Cinti S., De Caro R., Donato R.F., Ferrario V.F., Fonzi L., Franzi A.T., Gaudio E., Geremia R., Lanza G.G., Grossi C.E., Gulisano M., Manzoli F.A., Mazzotti G., Michetti F., Miscia S., Mitolo V., Montella A., Orlandini G., Paparelli A., Renda T., Ribatti D., Ruggeri A., Sirigu P., Soscia A., Tredici G., Vitale M., Zaccheo D., Zauli G., Zecchi S., "Trattato di Anatomia Umana", 4th Ed. *Edi-Ermes Milano*, 2006; vol.1, pp.290-300.

[4] Angelini A., Ho S.Y., Anderson R.H., Davies M.J., Becker A.E., "Histological Study of the Atrioventricular Junction in Hearts with Normal and Prolapsed Leaflets of the Mitral Valve". *Br Heart J*, 1988; 59: 712-16.

[5] Anwar A.M., Soliman O.I.I., ten Cate F.J., Nemes A., McGhie J.S., Krenning B.J., van Geuns R.J., Galema T.W., Geleijnse M.L., "True Mitral Annulus Diameter is Underestimated by Two-Dimensional Echocardiography as Evidence by Real-Time Three-Dimensional Echocardiography and Magnetic Resonance Imaging". *Int J Cardiovasc Imaging*, 2007; 23: 541-47.

[6] Asselta C., "Analisi Morfometrica Comparativa della Valvola Mitrale in due Banchi Prova per Cuori Battenti Passivi". Thesis, Politecnico of Milano, 2014-15.

[7] Banakal S.C., "Intraoperative Transesophageal Echocardiographic Assessment of the Mitral Valve Repair". *Ann Card Anaesth*, 2010; 13(1): 79-85.

[8] Bello A., "Sviluppo di un Algoritmo Semiautomatico di Segmentazione e Quantificazione della Funzione Atrio-Ventricolare Sinistra da immagini MRI in Asse Lungo". Thesis, Politecnico of Milano, 2011-12.

[9] Blanke P., Dvir D., Cheung A., Ye J., Levine R.A., Precious B., Berger A., Stub D., Hague C., Murphy D., Thompson C., Munt B., Moss R., Boone R., D., Pache G., Webb J., Leipsic J., "A Simplified D-Shaped Model of the Mitral Annulus to

Facilitate CT-Based Sizing Before Transcatheter Mitral Valve Implantation". *J Cardiovasc Comput Tomogr*, 2014; 8(6): 459-67.

[10] Bonizzoni F.M., Fazio M., "MRI-Based Simulation of Intra Ventricular Fluid Dynamics". Thesis, Politecnico of Milano, 2013-14.

[11] Bonow R.O., Carabello B.A., Chatterjee K., de Leon Jr A.C., Faxon D.P., Freed M.D., Gaasch W.H., Lytle B.W., Nishimura R.A., O'Gara P.T., O'Rourke R.A., Otto C.M., Shah P.M., Shanewise J.S., "2008 Focused Update Incorporated Into the ACC/AHA 2006 Guidelines for the Management of Patients With Valvular Heart Disease". *J Am Coll Cardiol*, 2008; 52(13): e1-142.

[12] Bonow R.O., Carabello B.A., Chatterjee K., de Leon Jr A.C., Faxon D.P., Freed M.D., Gaasch W.H., Lytle B.W., Nishimura R.A., O'Gara P.T., O'Rourke R.A., Otto C.M., Shah P.M., Shanewise J.S., "ACC/AHA 2006 Guidelines for the Management of Patients With Valvular Heart Disease: A Report of the American College of Cardiology/American Heart Association Task Force on Practice Guidelines (Writing Committee to Revise the 1998 Guidelines for the Management of Patients With Valvular Disease)". *Circ*, 2006; 114(5): e84-231.

[13] Brandao C.M.A., Abdouni A.A., Rochitte C., Veronese E., Melo R.J., Sanctis A., Tarasoutchi F., Pomerantzeff P.M.A., Jatene F.B., Heart Institute, University of Sao Paulo Medical School, "Mitral Annular Dynamics After Mitral Valve Repair – Cardiac Magnetic Resonance Analysis". HVS Annual Meeting, 2016, March; New York, USA.

[14] Carpentier A., Chauvaud S., Fabiani J.N., Deloche A., Relland J., Lessana A., D'Allaines C., Blondeau P., Piwnica A., Dubost C., "Reconstructive Surgery of Mitral Valve Incompetence: ten-year Appraisal". *J Thorac Cardiovasc Surg*, 1980; 79(3): 338-48.

[15] Carpentier A., Guerinon J., Deloche A., Fabiani J.N., Relland J.. "Pathology of the mitral valve. The Mitral Valve: A Pluridisciplinary Approach". *Edward Arnold*, 1976; ch.7, pp.65–77.

[16] Chandra S., Salgo I.S., Sugeng L., Weinert L., Tsang W., Takeuchi M., Spencer K.T., O'Connor A., Cardinale M., Settlemier S., Mor-Avi V., Lang R.M., "Characterization of Degenerative Mitral Valve Disease using morphologic analysis of Real-Time Three-Dimensional Echocardiographic Images: Objective insight into complexity and planning of Mitral Valve Repair". *Circ: Cardiovasc Imaging*, 2011; 4(1): 24-32.

[17] Chen L., May-Newman K., "Effect of Strut Chordæ Transection on Mitral Valve Leaflet Biomechanics". *Ann Biomed Eng*, 2006; 34: 917-26.

[18] Cohn L.H., "Cardiac Surgery in the Adult", 3rd Ed. *McGraw-Hill Medical*, 2008; Ch.41, p.1006.

[19] Dagum P., Timek T., Green G.R., Daughters G.T., Liang D., Ingels N.B., Miller D.C., "Three-Dimensional Geometric Comparison of Partial and Complete Flexible Mitral Annuloplasty Rings". *J Thorac Cardiovasc Surg*, 2001; 122(4): 665-73.

[20] Dagum P., Timek T.A., Green G.R., Lai D., Daughters G.T., Liang D.H., Hayase M., Ingels N.B. Jr, Miller D.C., "Coordinate-Free Analisys of Mitral Valve Dynamics in Normal and Ischemic Hearts". *Circ*, 2000; 102(suppl III): III-62-9.

[21] David T.E., Ivanov J., Armstrong S., Rakowski H., "Late Outcomes of Mitral Valve Repair for Floppy Valves: Implications for Asymptomatic Patients". *J Thorac Cardiovasc Surg*, 2003; 125(5): 1143-52.

[22] De Cobelli F., Natale L., "Risonanaza Magnetica Cardiaca". *Springer-Verlag Italia*, 2010; Ch.2, 4.

[23] Delgado V., Tops L.F., Schuijf J D., de Roos A., Brugada J., Schalij M.J., Thomas J.D., Bax J.J., "Assessment of Mitral Valve Anatomy and Geometry With Multislice Computed Tomography". *JACC: Cardiovasc Imaging*, 2009; 2(5): 556-65.

[24] Derobertis S., "Procedura Mitraclip: Simulazione agli Elementi Finiti della Tecnica su Modelli di Valvola Mitrale Ricostruiti da MRI Cardiaca". Thesis, Politecnico of Milano, 2013-14.

[25] Desai M., Jellis C., Yingchoncharoen T., "Atlas of Mitral Valve Imaging", *Springer*, 2015; pg.12.

[26] Di Mauro M., Gallina S., D'Amico M.A., Izzicupo P., Lanuti P., Bascelli A., Di Fonso A., Bartoloni G., Calafiore A.M., Di Baldassarre A., "Functiona Mitral Regurgitation from Normal to Pathological Anatomy of Mitral Valve". *Int J Card*, 2013; 163: 242-48.

[27] Du Plessis L.A., Marchand P., "The Anatomy of the Mitral Valve and its Associated Structures". *Thorax*, 1964; 19(3): 221-27.

[28] Einstein D.R., Kunzelman K.S., Reinhall P.G., Nicosia M.A., Cochran R.P., "Hemodynamic Determinants of the Mitral Valve Closure Sound: A Finite Element Study". *Med Biol Eng Comput*, 2004; 42: 832-46.

[29] El Sabaie M.H., Abdelatti M.N., Zarea A.A., Farag A.M., Hashem A.A., Fadel A.M., "Assessment of Mitral Valve Geometric Deformity in Patients With Ischemic Heart

Disease Using Three-Dimensional Echocardiography". *The Egypt Heart J*, 2017; 69(1): 13-20.

[30] Ender J., Sgouropoulou S., "Value of Transesophageal Echocardiography (TEE) Guidance in Minimally Invasive Mitral Valve Surgery". *Ann Cardiovasc Surg*, 2013; 2(6): 796-802.

[31] Enriquez-Sarano M., Akins C.W., Vahanian A., "Mitral Regurgitation". *Lancet*, 2009; 373: 1382-94.

[32] Essop M.R., Nkomo V.T., "Rheumatic and Nonrheumatic Valvular Heart Disease: Epidemiology, Management, and Prevention in Africa". *Circ*, 2005; 112: 3584-91.

[33] Ewe S.H., Klautz R.J., Schalij M.J., Delgado V., "Role of Computed Tomography Imaging for Transcatheter Valvular Repair/Insertion". *Int J Cardiovasc Imaging*, 2011; 27: 1179-93.

[34] Faletra F.F., "Echocardiography in Mitral Valve Disease", *Springer*, 2013; Ch.1.

[35] Fenoglio J.J., Pham T.D., Wit A.L., Bossett A.L., Wagner B.M., "Canine Mitral Complex". *Circ Res*, 1972; 31: 417-30.

[36] Flachskampf F.A., Chandra S., Gaddipatti A., Levine R.A., Weyman A.E., Ameling W., Hanrath P., Thomas J.D., "Analysis of Shape and Motion of the Mitral Annulus in Subjects With and Without Cardiomyopathy by Echocardiographic 3-Dimensional Reconstruction". *J Am Soc Echocardiogr*, 2000; 13: 277-87.

[37] Foster G.P., Isselbacher E.M., Rose G.A., Torchiana D.F., Akins C.W., Picard M.H., "Accurate Localization of Mitral Regurgitation Defects Using Multiplane Transesophageal Echocardiography". *Ann Thorac Surg*, 1998; 65: 1025-31.

[38] Galderisi M., "Diastolic Dysfunction and Diastolic Heart Failure: diagnostic, prognostic and therapeutic aspects". *Cardiovasc Ultrasound*, 2005; 3: 9.

[39] Gillinov A.M., Faber C., Houghtaling P.L., Blackstone E.H., Lam B.K., Diaz R., Lytle B.W., Sabik J.F., Cosgrove D.M.III, "Repair versus Replacement for Degenerative Mitral Valve Disease with Coexisting Ischemic Heart Disease". *J Thorac Cardiovasc Surg*, 2003; 125: 1350-62.

[40] Gogoladze G., Dellis S.L., Donnino R., Ribakove G., Greenhouse D.G., Galloway A., Grossi E., "Analysis of the Mitral Coaptation Zone in Normal and Functional Regugitant Valves". *Ann Thorac Surg*, 2010; 89: 1158-62.

[41] Gómez de Diego J.J., García-Orta R., Mahía-Casado P., Barba-Cosials J., Candell-Riera J., "Update on Cardiac Imaging Techniques 2012". *Rev Esp Cardiol*, 2013; 66(3): 205-11.

[42] Grewal J., Suri R., Mankad S., Tanaka A., Mahoney D.W., Shaff H.V., Miller F.A., Enriquez-Sarano M., "Mitral Annular Dynamics in Myxomatous Valve Disease: New Insights With Real-Time 3-Dimensional Echocardiography". *Circ*, 2010; 121(12): 1423-31.

[43] Hall R.J.C., Julian D.G., "Diseases of the Cardiac Valves". *Edinburgh: Churchill Livingstone*, 1989.

[44] Hayek E., Gring C.N., Griffin B.P., "Mitral Valve Prolapse". *Lancet*, 2005; 365: 507-18.

[45] He S., Fontaine A.A., Schwammenthal E., Yoganathan A.P., Levine R.A., "Integrated Mechanism for Functional Mitral Regurgitation". *Circ*, 1997; 96(6): 1826-34.

[46] Iaizzo P.A, "Handbook of Cardiac Anatomy, Physiology, and Devices", 2nd Ed. *Humana Press*, 2009; pp.125–8.

[47] Iaizzo P.A., Bianco R.W., Hill A.J., St. Louis J.D., "Heart Valves, from Design to Clinical Implementation". *Springer*, 2013.

[48] Impl-Pappalardo O.A., "Implementazione di un Modello Biomeccanico Masse-Molle della Valvola Mitrale per la Simulazione di Interventi Chirurgici di Riparazione". Thesis, Politecnico of Milano, 2013-14.

[49] Itoh A., Krishnamurthy G., Swanson J.C., Ennis D.B., Bothe W., Kuhl E., Karlsson M., Davis L.R., Miller D.C., Ingels Jr. N.B., "Active stiffening of mitral valve leaflets in the beating heart". *Am J Physiol Heart Circ Physiol*, 2009; 296: H1766-73.

[50] Iung B., Baron G., Butchart E.G., Delahaye F., Gohlke-Bärwolf C., Levang O.W., Tornos P., Vanoverschelde J.L., Vermeer F., Boersma E., Ravaud P., Vahanian A., "A Prospective Survey of Patients with Valvular Heart Disease in Europe: The Euro Heart Survey on Valvular Heart Disease". *Eur Heart J Cardiovasc Imag*, 2003; 24(13): 1231-43.

[51] Jimenez J.H., Soerensen D.D., He Z., He S., Yoganathan A.P., "Effects of a Saddle Shaped Annulus on Mitral Valve Function and Chordal Force Distribution: An *In Vitro* Study". *Ann Biomed Eng*, 2003; 31: 1171-81.

[52] Jimenez J.H., Soerensen D.D., He Z., Ritchie J., Yoganathan A.P., "Effects of Papillary Muscle Position on Chordal Force Distribution: An *in-vitro* Study". *J Heart Valve Dis*, 2005; 14: 295-302.

[53] Kaji S., Nasu M., Yamamuro A., Tanabe K., Nagai K., Tani T., Tamita K., Shiratori K., Kinoshita M., Senda M., Okada Y., Morioka S., "Annular Geometry in Patients With Chronic Ischemic Mitral Regurgitation: Three-Dimensional Magnetic Resonance Imaging Study". *Circ*, 2005; 112(suppl I): I-409-14.

[54] Kaplan S.R., Bashein G., Sheehan F.H., Legget M.E., Munt B., Li X.N., Sivarajan M., Bolson E.L., Zeppa M., Martin R.W., "Three-Dimensional Echocardiographic Assessment of Annular Shape Changes in the Normal and Regurgitant Mitral Valve". *Am Heart J*, 2000; 139: 378-87.

[55] Komoda T., Hetzer R., Uyama C., Siniawski H., Mæta H., Rosendahl U.P., Ozaki K., "Mitral Annular Function Assessed by 3D Imaging for Mitral Valve Surgery". *J Heart Valve Dis*, 1994; 3: 483-90.

[56] Kunzelman K., Cochran R.P., Verrier E.D., Eberhart R.C., "Anatomic Basis for Mitral Valve Modelling". *J Heart Valve Dis*, 1994; 3(5): 491-96.

[57] Kunzelman K.S., Cochran R.P., Chuong C., Ring W.S., Verrier E.D., Eberhart R.D., "Finite element analysis of the mitral valve". *J Heart Valve Dis*, 1993; 2(3): 326-40.

[58] Kwan J., Jeon M.J., Kim D.H., Park K.S., Lee W.H., "Does the Mitral Annulus Shrink or Enlarge During Systole? A Real-Time 3D Echocardiography Study". *J Korean Med Sci*, 2009; 24: 203-08.

[59] Lam H.C., Ranganathan N., Wigle E.D., Silver M.D., "Morphology of the Human Mitral Valve I. Chordæ Tendineæ: A New Classification". *Circ*, 1970; 41: 449-58.

[60] Lang R.M., Mor-Avi V., Dent J.M., "Three-Dimensional Echocardiography: Is It Ready for Everyday Clinical Use?". *Jacc: Cardiovascular Imaging*, 2009; 2(1): 114-17.

[61] Lang R.M., Tsang W., Weinert L., Mor-Avi V., Chandra S., "Valvular Heart Disease. The Value of 3-Dimensional Echocardiography". *J Am Coll Cardiol*, 2011; 58(19): 1933-44.

[62] Lau K.D., "Numerical Simulation of Mitral Valve Function". PhD thesis, University College of London, 2012.

[63] Levine R.A., Handschumacher M.D., Sanfilippo A.J., Hagege A.A., Harrigan P., Marshall J.E., Weyman A.E., "Three-Dimensional Echocardiography Reconstruction of the Mitral Valve, With Implications for the Diagnosis of Mitral Valve Prolapse". *Circ*, 1989; 80(3): 589-98.

[64] Liao J., Vesely I., "A Structural Basis for the Size-related Mechanical Properties of Mitral Valve Chordæ Tendineæ". *J Biomech*, 2003; 36: 1125-33.

[65] Lim K.H., Yeo J.H., Duran C.M.G., "Three-Dimensional Asymmetrical Modeling of the Mitral Valve: A Finite Element Study with Dynamic Boundaries". *J Heart Valve Dis*, 2005; 14(3): 386-92.

[66] Lim K.O., Boughner D.R., "Morphology and Relationship to Extensibility Curves of Human Mitral Valve Chordæ Tendineæ". *Circ Res*, 1976; 39(4): 580-85.

[67] Ling L.H., Enriquez-Sarano M., Seward J.B., Orszulak T.A., Schaff H.V., Bailey K.R., Tajik A.J., Frye R.L., "Early Surgery in Patients With Mitral Regurgitation Due To Flail Leaflets. A Long-term Outcome Study". *Circ*, 1997; 96: 1819-25.

[68] Lomholt M., Nielsen S.L., Hansen S.B., Andersen N.T., Hasenkam J.M., "Differential Tension Between Secondary and Primary Mitral Chordæ in an Acute *In-vivo* Porcine Model". *J Heart Valve Dis*, 2002; 11: 337-45.

[69] Macnab A., Jenkins N.P., Bridgewater B.J.M., Hooper T.L., Greenhalgh D.L., Patrick M.R., Ray S.G., "Three-Dimensional Echocardiography is Superior to Multiplane Transesophageal Echo in the Assessment of Regurgitant Mitral Valve Morphology". *Eur J Echocardiography*, 2004; 5: 212-22.

[70] Maisano F., Redaelli A., Soncini M., Votta E., Arcobasso L., Alfieri O., "An Annular Prosthesis for the Treatment of Functional Mitral Regurgitation: Finite Element Model Analysis of a Dog Bone-Shaped Ring Prosthesis". *Ann Thorac Surg*, 2005; 79: 1268-75.

[71] Mak G.J., Blanke P., Ong K., Naoum C., Thompson C.R., Webb J.G., Moss R., Boone R., Ye J., Cheung A., Munt B., Leipsic J., Grewal J., "Three-Dimensional Echocardiography Compared With Computed Tomography to Determine Mitral Annulus Size Before Transcatheter Mitral Valve Implantation". *Circ Cardiovasc Imaging*, 2016; 9(6): e004176.

[72] Mansi T.,Voigt I., Georgescu B., Zheng X., Mengue E.A., Hackl M., Ionasec R.I., Noack T., Seeburger J., Comaniciu D., "An Integrated Framework for Finite-Element Modeling of Mitral Valve Biomechanics from Medical Images: Application to Mitral Clip Intervention Planning". *Med Image Anal*, 2012; 16(7):1330-46.

[73] May-Newman K., Yin F.C.P., "A Constitutive Law for Mitral Valve Tissue". *J Biomech Eng*, 1998; 120: 38-47.

[74] Mazzoletti G., "Modellazione delle Proprietà Contrattili del Lembo Mitralico Anteriore durante la Sistole Ventricolare: Sviluppo di un Approccio Innovativo e Identificazione dei Parametri Costitutivi sulla base di Dati *In Vivo*". Thesis, Politecnico of Milano, 2012-13.

[75] Miller D.C., “Ischemic Mitral Regurgitation Redux – To Repair or to Replace?”. *J Thorac Cardiovasc Surg*, 2001; 122(6): 1059-62.

[76] Millington-Sanders C., Meir A., Lawrence L., Stolinski C., “Structure of Chordæ Tendineæ in the Left Ventricle Human Heart”. *J Anat*, 1998; 192: 573-81.

[77] Muresian H., “The Clinical Anatomy of the Mitral Valve”. Clinical Anatomy, 2009; 22(1): 85-98.

[78] Muresian H., Diena M., Cerin G., Filipoiu F., “The Mitral Valve: New Insights into the Clinical Anatomy”. *Mædica*, 2006; 1(4): 80-7.

[79] Netter F.H., “Atlas of Human Anatomy”, 6th Ed. *Elsevier*, 2014.

[80] Newman Dorland W.A., “Dorland’s Illustrated Medical Dictionary”, 32nd Ed. *Elsevier/Saunders,* 2012; p.1412.

[81] Nielsen S.L., Timek T.A., Green G.R., Dagum P., Daughters G.T., Hasenkam J.M., Bolger A.F., Ingels N.B., Miller D.C., “Influence of Anterior Mitral Leaflet Second-Order Chordæ Tendineæ on Left Ventricular Systolic Function”. *Circ*, 2003; 108: 486-91.

[82] Nkomo V.T., Gardin J.M., Skelton T.N., Gottdiener J.S., Scott C.G., Enriquez-Sarano M., “Burden of Valvular Heart Diseases: A Population-Based Study”. *Lancet*, 2006; 368(9540): 1005-11.

[83] O’Gara P., Sugeng L., Lang R., Sarano M., Hung J., Raman S., Fischer G., Carabello B., Adams D., Vannan M., “The Role of Imaging in Chronic Degenerative Mitral Regurgitation”. *JACC Cardiovasc Imaging*, 2008; 1(2): 221-37.

[84] Oertel H., Krittian S., “Modelling the Human Cardiac fluid mechanics”, 4th Ed. *KIT Scientific Publishing*, 2012; Ch.2.

[85] Ormiston J.A., Shah P.M., Tei C., Wong M., “Size and Motion of the Mitral Valve Annulus in Man. I. A Two-Dimensional Echocardiographic Method and Findings in Normal Subjects”. *Circ*, 1981; 64(1): 113-20.

[86] Otsuji Y., Handschumacher M.D., Liel-Cohen N., Tanabe H., Jiang L., Schwammenthal E., Guerrero J.L., Nicholls L.A., Vlahakes G.J., Levine R.A., “Mechanism of Ischemic Mitral Regurgitation With Segmental Left Ventricular Dysfunction: Three-Dimensional Echocardiographic Studies in Models of Acute and Chronic Progressive Regurgitation”. *J Am Coll Cardiol*, 2001; 37(2): 641-48.

[87] Pepi M., Tamborini G., Maltafliati A., Galli C.A., Sisillo E., Salvi L., Naliato M., Porqueddu M., Parolari A., Zanobini M., Alamanni F., “Head-to-Head Comparison of Two- and Three-Dimensional Transthoracic and Transesophageal

Echocardiography in the Localization of Mitral Valve Prolapse". *J Am Coll Cardiol*, 2006; 48(12): 2524-30.

[88] Perloff J.K., Roberts W.C., "The Mitral Apparatus: Functional Anatomy of Mitral Regurgitation". *Circ*, 1972; 46(2): 227-39.

[89] Piazza N., de Jaegere P., Schultz C., Becker A.E., Serruys P.W., Anderson R.H., "Anatomy of the Aortic Valvar Complex and its Implications for Transcatheter Implantation of the Aortic Valve". *Circ: Cardiovasc Interventions*, 2008; 1(1): 74-81.

[90] Pouch A.M., Xu C., Yushkevich P.A., Jassar A.S., Vergnat M., Gorman III J.H., Gorman R.C., Sehgal C.M., Jackson B.M., "Semi-Automated Mitral Valve Morphometry and Computational Stress Analysis Using 3D Ultrasound". *J Biomech*, 2012; 45(5): 903-7.

[91] Prot V., Skallerud B., Holzapel G.A., "Transversely Isotropic Membrane Shells With Application to Mitral Valve Mechanics. Constitutive Modelling and Finite Element Implementation". Int J Numer Meth Eng, 2007; 71: 987-1008.

[92] Rabbah J.P., Saikrishnan N., Yoganathan A.P., "A Novel Left Heart Simulator for the Multy-modality Characterization of Native Mitral Valve Geometry and Fluid Mechanics". *Ann Biomed Eng*, 2013; 41(2): 305-15.

[93] Rabbah J.P.M., Saikrishnan N., Siefert A.W., Santhanakrishnan A, Yoganathan A.P., "Mechanics of Healthy and Functionally Diseased Mitral Valves: A Critical Review". *J Biomech Eng*, 2013; 135(2): 021009-1-16.

[94] Ragusa G., "Studio di Fattibilità per un Modello *in vitro* di Valvola Mitrale Insufficiente". Thesis, Politecnico of Milano, 2012-13.

[95] Ranganathan N., Lam J.H.C., Wigle E.D., Silver M.D., "Morphology of the Human Mitral Valve: II. The Valve Leaflets". *Circ*, 1970; 41: 459-67.

[96] Ritchie J., Warnock J.N., Yoganathan A.P., "Structural Characterization of tha Chordæ Tendineæ in Native Porcine Mitral Valves". *Ann Thorac Surg*, 2005; 80: 189-97.

[97] Rusted I.E., Scheifley C.H., Edwards J.E., "Studies of the Mitral Valve. I. Anatomic Features of the Normal Mitral Valve and Associated Structures". *Circ*, 1952; 6(6): 825-31.

[98] Ryan L.P., Jackson B.M., Enomoto Y., Parish L., Plappert T.J., St. John-Sutton M.G., Gorman R.C., Gorman J.H., "Description of Regional Mitral Annular

Nonplanarity in Healthy Human Subjects: A Novel Methodology". *J Thorac Cardiovasc Surg*, 2007; 134: 644-48.

[99] Ryan L.P., Salgo I.S., Gorman R.C., Gorman J.H., "The Emerging Role of Three-Dimensional Echocardiography in Mitral Valve Repair". *Semin Thorac Cardiovasc Surg*, 2006; 18: 126-34.

[100] Sakai T., Okita Y., Ueda Y., Tahata T., Ogino H., Matsuyama K., Miki S., "Distance Between Mitral Annulus and Papillary Muscles: Anatomic Study in Normal Human Hearts". *J Thorac Cardiovasc Surg*, 1999; 118(4): 636-41.

[101] Saladin K., "Anatomy Physiology. The Unit of Form and Function", 4th Ed. *McGraw-Hill Science/Engineering/Math*, 2006.

[102] Salgo I.S., Gorman J.H., Gorman R.C., Jackson B.M., Bowen F.W., Plappert T., St. John-Sutton M.G., Edmunds L.H., "Effect of Annular Shape on Leaflet Curvature in Reducing Mitral Leaflet Stress". *Circ*, 2002; 106: 711-17.

[103] Scampardonis G., Yang S.S., Maranhao V., Golberg H., Gooch A.S., "Left Ventricular Abnormalities in Prolapsed Mitral Leaflet Syndrome. Review of eighty-seven Cases". *Circ*, 1973; 48: 287-97.

[104] Silbiger J.J., "Anatomy, Mechanics, and Pathophysiology of the Mitral Annulus". *Am Heart J* 2012; 164:163-76.

[105] Silverthorn D.U., Passatore M., Roatta S., Sacchi V.F., "Human Physiology: an Integrated Approach". *Pearson/Benjamin Cummings*, 2010.

[106] Šmíd M., Ferda J., Baxa J., Čech J., Hájek T., Kreuzberg B., Rokyta R., "Aortic Annulus and Ascending Aorta: Comparison of Preoperative and Perioperative Measurement in Patients with Aortic Stenosis". *Eur J Rad*, 2010; 72: 152-55.

[107] Solis J., Sitges M., Levine R.A., Hung J., "Three-Dimensional Echocardiography. New Possibilities in Mitral Valve Assessment". *Rev Esp Cardiol*, 2009; 62(2): 188-98.

[108] Squeri A., Censi S., Reverberi C., Gaibazzi N., Baldelli M., Binno S.M., Properzi E., Bosi S., "Three-Dimensional Echocardiography in Various Types of Heart Disease: A Comparison Study of Magnetic Resonance Imaging and 64-Slice Computed Tomography in a Real-World Population". *J Echocardiogr*, 2016; doi: 10.1007/s12574-016-0315-3.

[109] Stevanella M., Maffesanti F., Conti C.A., Votta E., Arnoldi A., Lombardi M., Parodi O., Caiani E.G., Redaelli A., "Mitral Valve Patient-Specific Finite Element Modeling

from Cardiac MRI: Application to an Annuloplasty Procedure". *Cardiovasc Eng Technol*, 2011; 2(2): 66-76.

[110] Stevanella M., Votta E., Redaelli A., "Mitral Valve Finite Element Modeling: Implications of Tissues' Nonlinear Response and Annular Motion". *J Biomech Eng-*T ASME, 2009; 131: 121010-1-9.

[111] Sturla F., "An Image-Based Framework for the Biomechanical Analysis of Mitral Valve Prolapse Repair". PhD thesis, University of Verona, XXVII Cycle.

[112] Sugeng L., Shernan S.K., Salgo I.S., Weinert L., Shook D., Raman J., Jeevanandam V., DuPont F., Settlemier S., Savord B., Fox J., Mor-Avi V., Lang R.M., "Live 3-Dimensional Transesophageal Echocardiography: Initial Experience Using the Fully-Sampled Matrix Array Probe". *J Am Coll Cardiol*, 2008; 52(6): 446-49.

[113] Sutton J.P. III, Ho S.Y., Anderson R.H., "The Forgotten Interleaflet Triangles: A Review of the Surgical Anatomy of the Aortic Valve". *The Annals of Thorac Surg*, 1995; 59(2): 419-27.

[114] Thubrikar M.J., Labrosse M.R., Zehr K.J., Robicsek F., Gong G.G., Fowler B.L., "Aortic Root Dilatation may alter the dimensions of the Valve Leaflet". *Eur J Cardio-Thorac Surg*, 2005; 28: 850-56.

[115] Timek T.A., Green G.R., Tibayan F.A., Lai D.T., Rodriguez F., Liang D., Daughters G.T., Ingels N.B., Miller D.C., "Aorto-Mitral Annular Dynamics". *Ann Thorac Surg*, 2003; 76(6): 1944-50.

[116] Timek T.A., Miller D.C., "Experimental and Clinical Assessment of Mitral Annular Area and Dynamics: What Are We Actually Measuring?". *Ann Thorac Surg*, 2001; 72: 966-74.

[117] Titus J.L., "Surgery for Acquired Mitral Valve Disease. Anatomy and Pathology of the Mitral Valve". Ellis F.H. Philadelphia, W.B Saunders Company, 1967; pp.53-5.

[118] Ton-Nu T.T., "Geometric Determinants of Functional Tricuspid Regurgitation: Insights From 3-Dimensional Echocardiography". *Circ*, 2006; 114(2): 143-49.

[119] Tortora G.J., Nielsen M.T., "Principles of Human Anatomy", 11th Ed. *John Wiley & Sons*, 2009; pp.84–5.

[120] Veronesi F., Corsi C., Sugeng L., Mor-Avi V., Caiani E.G., Weinert L., Lamberti C., Lang R.M., "A Study of Functional Anatomy of Aortic-Mitral Valve Coupling Using 3D Matrix Transesophageal Echocardiography". *Circ Cardiovasc Imaging*, 2009; 2: 24-31.

[121] Votta E., Caiani E., Veronesi F., Soncini M., Montevecchi F.M., Redaelli A., "Mitral Valve Finite-Element Modelling from Ultrasound Data: A Pilot Study for a New Approach to Understand Mitral Function and Clinical Scenarios". *Phil Trans R Soc A*, 2008; 366: 3411-34.

[122] Votta E., Le T.B., Stevanella M., Fusini L., Caiani E.G., Redaelli A., Sotiropoulos F., "Toward Patient-Specific Simulations of Cardiac Valves: State-of-the-Art and Future Directions". *J Biomech*, 2013; 46(2): 217-28.

[123] Votta E., Maisano F., Bolling S.F., Alfieri O., Montevecchi F.M., Redaelli A., "The Geoform Disease-Specific Annuloplasty System: A Finite Element Study". *Ann Thorac Surg*, 2007; 84(1): 92-102.

[124] Votta E., Maisano F., Soncini M., Redaelli A., Montevecchi F.M., Alfieri O., "3-D Computational Analysis of the Stress Distribution on the Leaflets after Edge-to-Edge Repair of Mitral Regurgitation". *J Heart Valve Dis*, 2002; 11(6): 810-22.

[125] Wang Q., Sun W., "Finite Element Modeling of Mitral Valve Dynamic Deformation Using Patient-Specific Multi-Slices Computed Tomography Scans". *Ann Biomed Eng*, 2013; 41(1): 142-53.

[126] Wang Q., Sun W., "Finite Element Modeling of Mitral Valve Dynamic Deformation Using Patient-Specific Multi-Slices Computed Tomography Scans". *Ann Biomech Eng*, 2012; 41(1): 142-53.

[127] Watton P.N., Luo X.Y., Yin M., Bernacca G.M., Wheatley D.J., "Effect of Ventricle Motion on the Dynamic Behaviour of Chorded Mitral Valves". *J Fluids and Structures*, 2008; 24: 58-74.

[128] Wenk J.F., Zhang Z., Cheng G., Malhotra D., Acevedo-Bolton G., Burger M., Suzuki T., Saloner D.A., Wallace A.W., Guccione J.M., Ratcliffe M.B., "First Finite Element Model of the Left Ventricle With Mitral Valve: Insights Into Ischemic Mitral Regurgitation". *Ann Thorac Surg*, 2010; 89: 1546-54.

[129] Xu C., Brinster C.J., Jassar A.S., Vergnat M., Eperjesi T.J., Gorman R.C., Gorman III J.H, Jackson B.M., "A Novel Approch to *in vivo* Mitral Valve Stress Analysis". *Am J Physiol Heart Circ Physiol*, 2010; 299: H1790-94.

[130] Xu C., Jassar A.S., Nathan D.P., Eperjesi T.J., Brinster C.J., Levack M.M., Vergnat M., Gorman R.C., Gorman III J.H., Jackson B.M., "Augmented Mitral Valve Leaflet Area Decreases Leaflet Stress: A Finite Element Simulation". *Ann Thorac Surg*, 2012; 93(4): 1141-45.

[131] Yiu S.F., Enriquez-Sarano M., Tribouilloy C., Seward J.B., Tajik A.J., "Determinants of the Degree of Functional Mitral Regurgitation in Patients With Systolic Left Ventricular Dysfunction". *Circ*, 2000; 102: 1400-06.

[132] Yoganathan A.P., Lemmon J.D., Ellis J.T., "The Biomedical Engineering Handbook". 2nd Ed. *Bronzino J.D.*, 2000; Ch.29.

Web sites:

[133] http://laura-pc:2080/v6.12/books/gsa/default.htm?startat=book01.html#gsa – Abaqus 6.12, SIMULIA, Documentation

[134] http://radiologykey.com/mitral-regurgitation/ Lambert A.S., "Mitral Regurgitation", posted on Cardiovascular Imaging; Sept 1, 2016.

[135] http://www.grasshopper3d.com/

[136] http://www.it.rhino3d.com

[137] http://www.mitralvalverepair.org

[138] http://www.slideshare.net/madhusiva03/anatomy-of-mitral-valve-echo-evaluation Dr. Krishna K.V.S., "Anatomy of Mitral Valve: echocardiographic Evaluation", published in Health & Medicine; April 13, 2014.

[139] http://www.softpedia.com/get/Science-CAD/Grasshopper-for-Rhino.shtml

[140] http://www.vhlab.umn.edu/atlas/external-images/anterior/index.shtml External Imaging – Anterior | Atlas of Human Cardiac Anatomy [2014 Sept 7]

[141] https://vimeopro.com/rhino/grasshopper-getting-started-by-david-rutten

[142] tele.med.ru/book/cardiac_anesthesia/text/pe/pe008.htm

[143] WebDm, Anatomical Line Drawings visit at www.webdm.com

[144] www.echopedia.org images thumb f f1 MVtee.svg 235px-MVtee_svg

[145] www.uniroma2.it

Appendix A

Mitral Valve: our parametric models

First Model

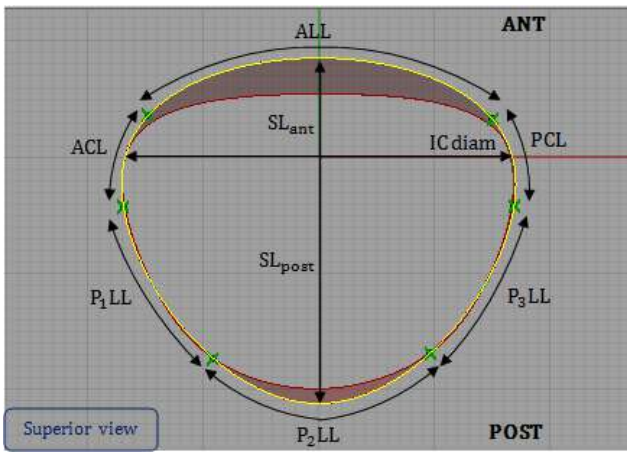

IC diam	Intercommissural diameter
SL_{ant}	Septolateral diameter, Anterior portion
SL_{post}	Septolateral diameter, Posterior portion
ACL	Anterior Commissural Length of annular attachment
ALL	Anterior Leaflet Length of attachment
PCL	Posterior Commissural Length of annular attachment
P_1LL	Post. Leaflet Length of attachment, ant. scallop
P_2LL	Post. Leaflet Length of attachment, central scallop
P_3LL	Post. Leaflet Length of attachment, post. scallop

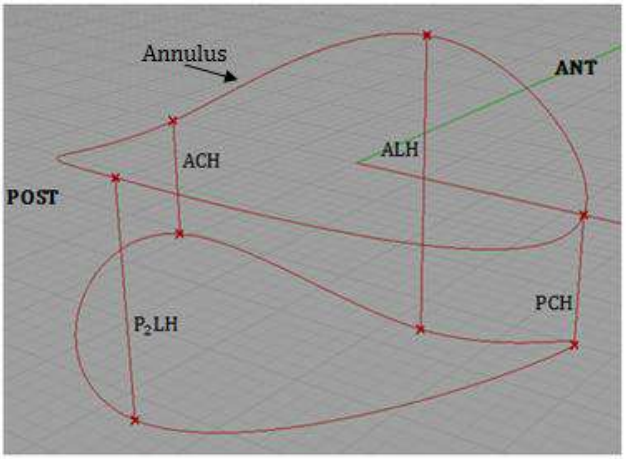

ACH	Anterolateral Commissure Height
ALH	Anterior Leaflet Height
PCH	Posteromedial Commissure Height
P_2LH	Posterior Leaflet Height, central scallop

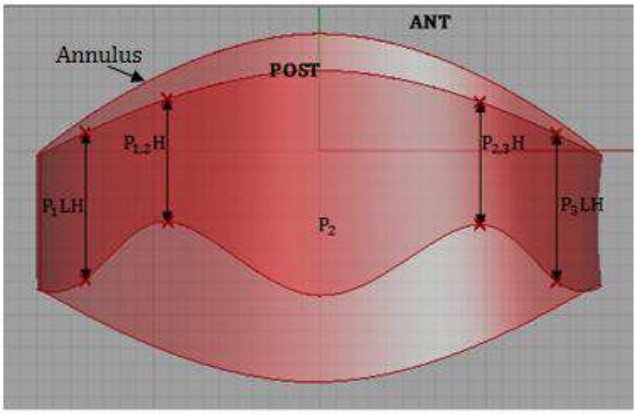

P_1LH	Posterior Leaflet Height, anterior scallop
$P_{1,2}H$	Leaflet Height between anterior and central scallops
$P_{2,3}H$	Leaflet Height between central and posterior scallops
P_3LH	Posterior Leaflet Height, posterior scallop

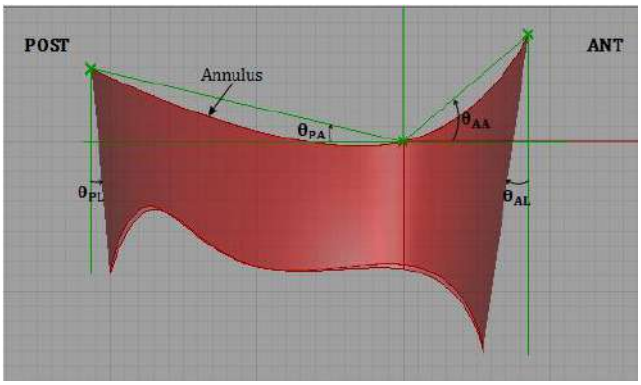

θ_{AA}	Rotation angle of the Anterior portion of the mitral Annulus (SL_{ant})
θ_{PA}	Rotation angle of the Posterior portion of the mitral Annulus (SL_{post})
θ_{AL}	Rotation angle of the Anterior Leaflet (ALH)
θ_{PL}	Rotation angle of the Posterior Leaflet (P_2LH)

Simplified representation of an atrial view and an excised mitral valve with parameters necessary to our first geometrical reconstruction.

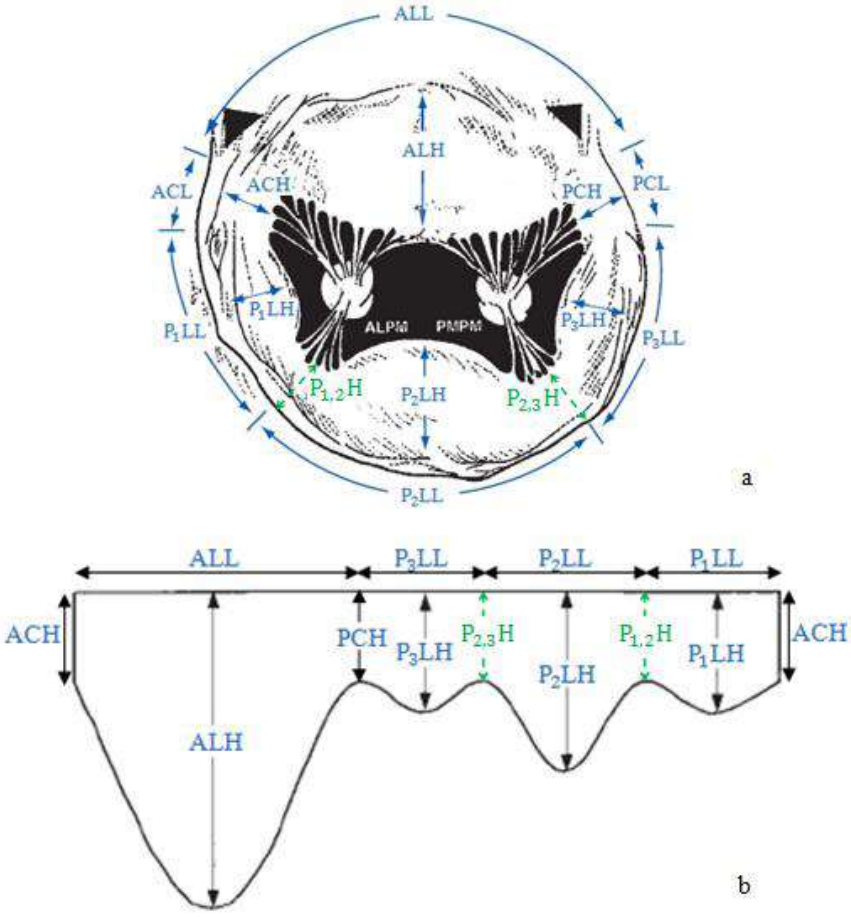

[Top: Sakai T., Okita Y., Ueda Y., Tahata T., Ogino H., Matsuyama K., Miki S., "Distance Between Mitral Annulus and Papillary Muscles: Anatomic Study in Normal Human Hearts". *J Thorac Cardiovasc Surg*, 1999; 118(4): 636-41.]

Model Parameters from Echocardiography

Measurements to be confirmed

Short-axis view (TTE)

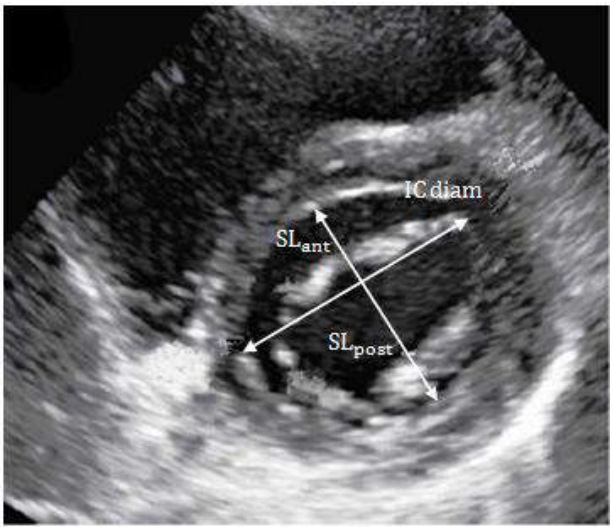

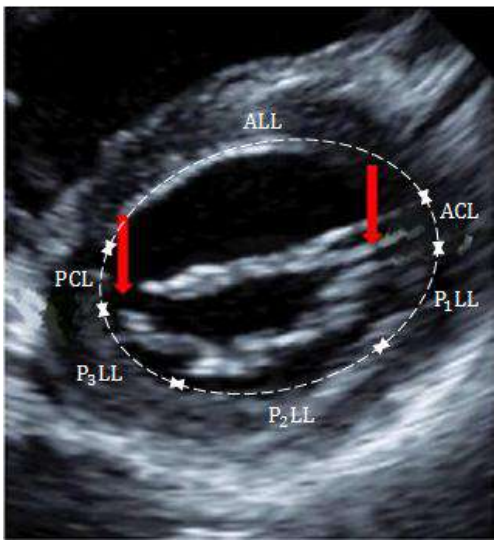

- Is it possible to measure the length of attachment for each leaflet scallop and commissure (red arrows)?

Parasternal long-axis view (TTE)

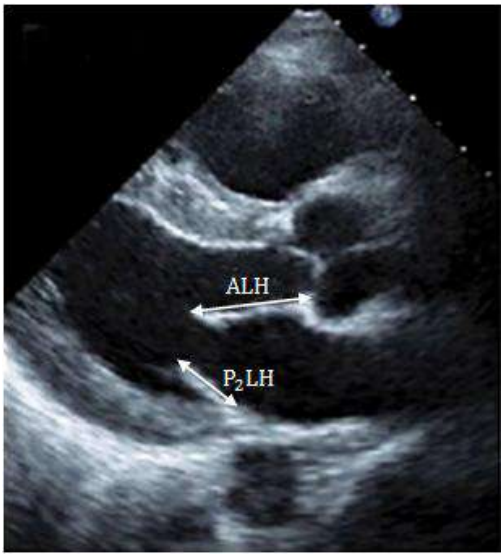

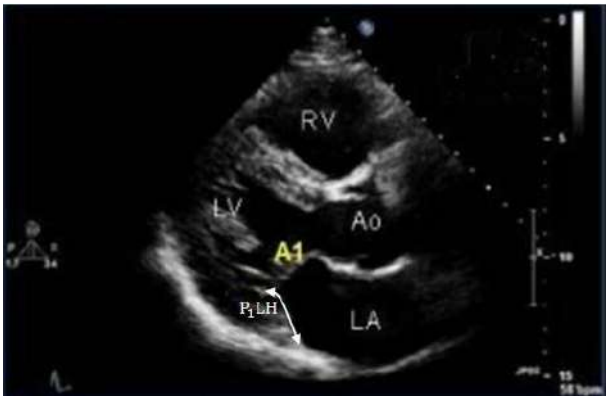

2-Chamber view

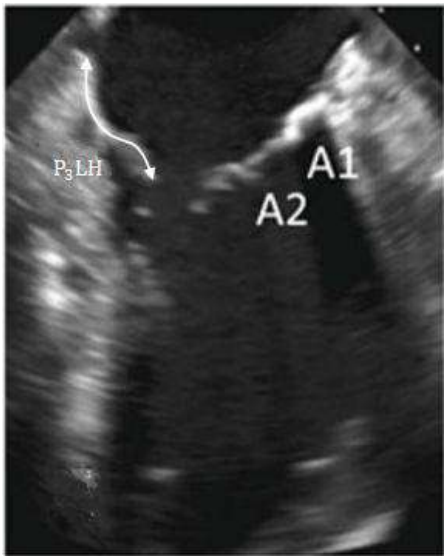

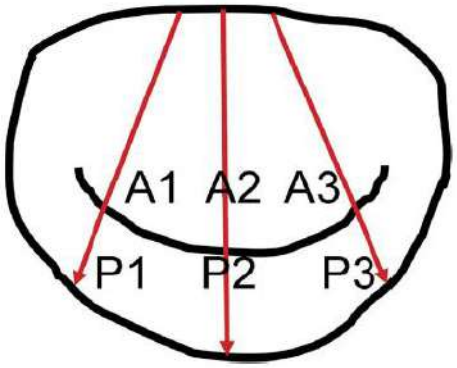

- Is it possible to measure <u>all maximum Posterior Leaflet Heights at the end-diastolic phase</u> (also from different views, if necessary)?
- Are these measurements reliable, or is it better to use three-dimensional echocardiography? <u>2DE could underestimate these lengths</u>?

- Can we precisely measure every scallop height (particularly P_1LH and P_3LH), for instance during systolic phase (fig. on the right), by adding the length of a leaflet to its coaptation length (see fig. below)?

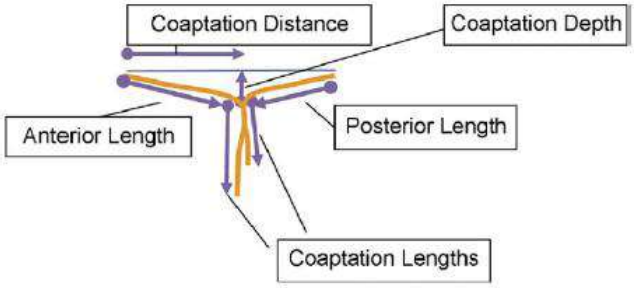

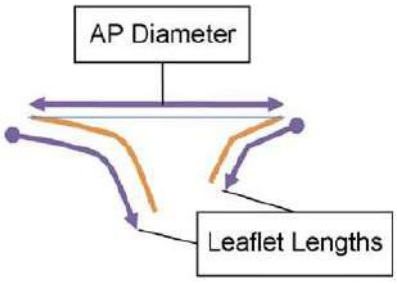

[Gogoladze G., S.L. Dellis, R. Donnino, G. Ribakove, D.G. Greenhouse, A. Galloway, E. Grossi. Analysis of the Mitral Coaptation Zone in Normal and Functional Regurgitant Valves. *Ann Thorac Surg*, 2010; 89:1158–62.]

<u>Hp</u>:

If systolic <u>Coaptation Distance</u> and <u>Depth</u> are known, we can approximate the length of the leaflet to a triangle hypotenuse and estimate it through the Pythagorean Theorem. Then we can add the <u>Coaptation Length</u> to the previous result to obtain the total <u>Leaflet Length</u> in systole.

If we know also the leaflets reduction rates between the systolic phase and the diastolic one,

- Can we calculate a reliable diastolic Leaflet Length value?

3D TEE (Surgical view)

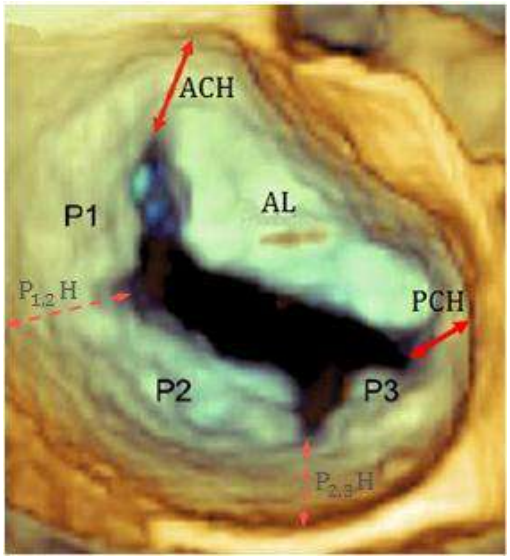

- Are these Commissural Heights measurements reliable? Is it possible to precisely obtain them by 2DE?
- From this view, is it possible to obtain also the heights of the leaflet portion between posterior scallops ($P_{1,2}H$, $P_{2,3}H$)?

Initial leaflets orientation

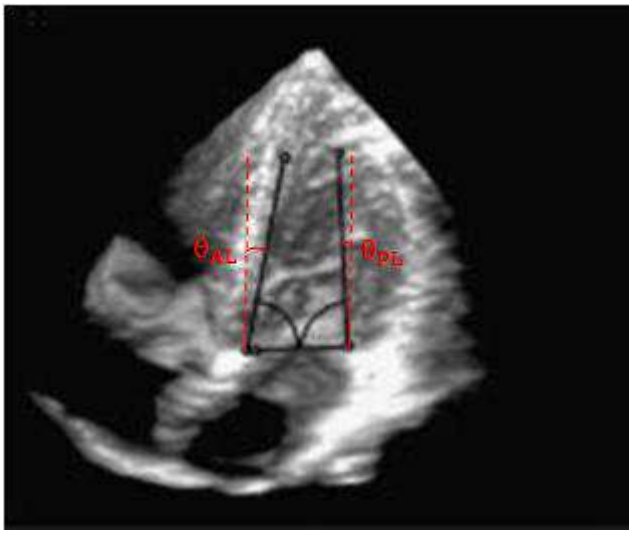

[Votta E., E. Caiani, F. Veronesi, M. Soncini, F.M. Montevecchi, A. Redaelli. Mitral Valve Finite-Element Modeling from Ultrasound Data: A Pilot Study for a New Approach to Understand Mitral Function and Clinical Scenarios. *Phil Trans R Soc A*, 2008; 366:3410-34.]

- Do θ_{AL} and θ_{PL} mainly correspond to the orientation of central portions of both mitral leaflets; is it possible to estimate also the other leaflet scallops tilt?
- How can we measure Height of the Mitral Annulus (rotation angles θ_{AA} and θ_{PA})?

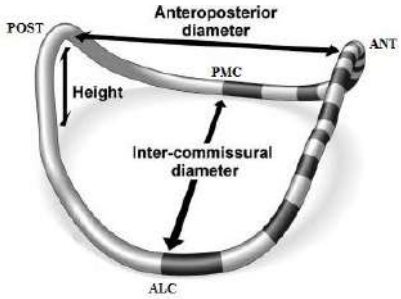

[Left: Stevanella M., E. Votta, A. Redaelli. Mitral Valve Finite Element Modeling: Implications of Tissues' Nonlinear Response and Annular Motion. J Biomech Eng, 2009; 131:121010-1-9.]
[Right: Grewal J., R. Suri; S. Mankad, A. Tanaka, D.W. Mahoney, H.V. Schaff, F.A. Miller, M. Enriquez-Sarano. Mitral Annular Dynamics in Myxomatous Valve Disease. New Insights With Real-Time 3-Dimensional Echocardiography. *Circulation*, 2010; 121:1423-31.]

- Do θ_{AA} and θ_{PA} really allow to estimate the annulus Height? Are they equivalent measurements? Which one can be obtained more easily by 2DE or is more reliable?

Second Model

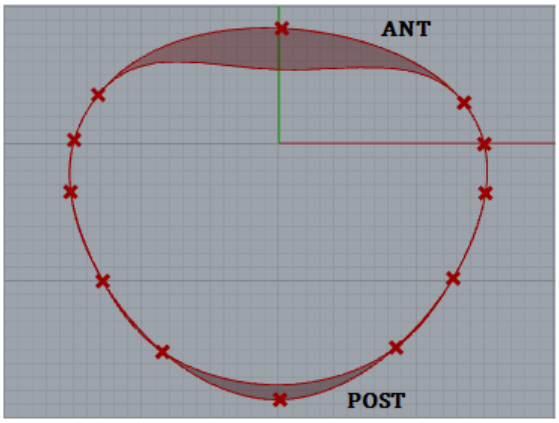

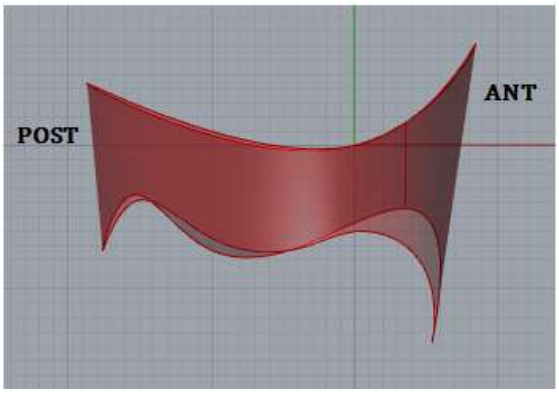

The Mitral Annulus profile has been computed like in the previous model, through two principal diameters: Intercommissural (IC) and Septolateral ones (SL_{ant} and SL_{post} portions).
The Annulus and central portions of mitral leaflets have the same rotation angles θ_{AA} and θ_{PA}, θ_{AL} and θ_{PL}, respectively.
The Annulus profile has been divided into six portions by using the measurements of leaflets and commissural lengths of attachment ACL, ALL, PCL, P_1LL, P_2LL, P_3LL.

- Is it possible to obtain all necessary measurements (i.e. IC and SL diameters, ACL, ALL, PCL, P_1LL, P_2LL and P_3LL) from a short axis view of 3D echocardiography of the mitral valve in diastolic phase?

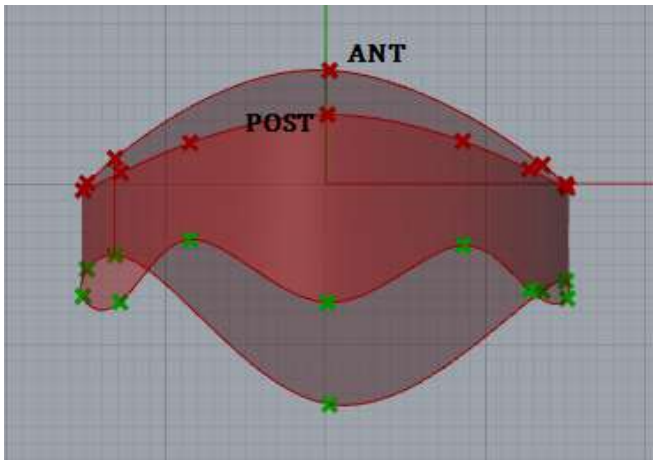

The profile of mitral leaflets free edges was generated, in accordance with data reported in literature [Kunzelman et al.], through a linear combination of sinusoids:

$$y = k + \sum_{n=1}^{12} a_n * \sin(n\omega x)$$

The curve obtained by this harmonic function interpolates the original data and expresses the annulus-to free edge distance as a function of the position on the annulus (x): it describes the profile of the excised valve (see green crosses in the fig. above).
This method avoids taking from echocardiography commissural and leaflets heights measurements.

[Kunzelman K.S., R.P. Cochran, E.D. Verrier, R.C. Eberhart. Anatomic Basis for Mitral Valve Modelling. *J Heart Valve Dis*, 1994; 3:491-496.]
[Votta E., F. Maisano, M. Soncini, A. Redaelli, F.M. Montevecchi, O. Alfieri. 3-D Computational Analysis of the Stress Distribution on the Leaflets after Edge-to-Edge Repair of Mitral Regurgitation. *J Heart Valve Dis*, 2002; 11:810-822]

- However, from 3D echo, could it be possible to measure the lengths of every leaflet scallops without under- or overestimating their real values?
- Can 3D echo take commissural dimensions or is it necessary to model them as points?

*Leaflets thickness has been always neglected.

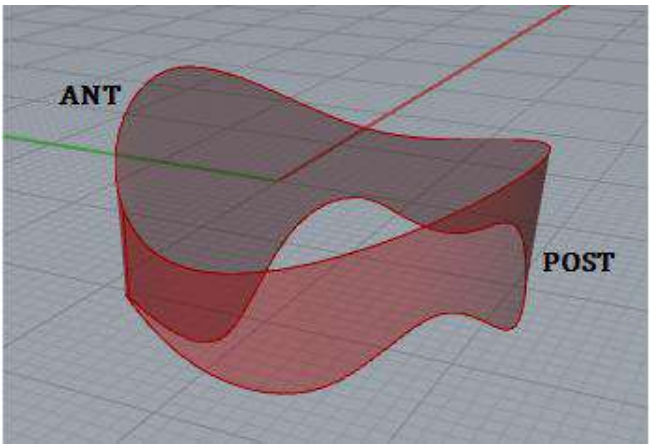

Other questions

- Are these models similar to the real Mitral Valve morphology? Which one is easier to realize only by echographically detectable data?
- Are used Literature data the nearest ones to real physiological values? As an alternative to not detectable data, is there any ratio among different parts size of the Mitral Valve to get the missing data?
- Which measurements are detectable by echocardiography, CT and CMRI?
- Which are the most useful echocardiographic views in clinical practice?
- Which different information is it possible to obtain by two- or three-dimensional, transthoracic or transesophageal echocardiography? Which is the most used method? And the most useful one?

- Is it possible to detect chordæ tendineæ and locate papillary muscles only by echocardiography? Which orders of cords can be identified? Which measurements are detectable (lengths, cross-sectional area, number, points of insertion on the papillary heads and on both leaflets portions) by echocardiography or through other methods? Which are the best views?

Literature Review

Measure	**Values** [mm]		**Reference**		**Syst.**	**Diast**	**Method**	**Sex**
IC diam	15.0-41.1		[4,5]				Autopsy, RT-3DE	F,M
SL_{ant}	10.4	22.0-36.6	[7]	[1,3]		X	3DE	
SL_{post}	21.1		[7]					
ACL	5.6-15.3		[2,6]				Autopsy	
ALL	27.2-36.8		[6]				Autopsy	
PCL	5.1-17.8		[2,6]				Autopsy	
P_1LL	10.5-17.7		[6]				Autopsy	
P_2LL	15.2-23.4		[6]				Autopsy	
P_3LL	10.3-16.9		[6]				Autopsy	
ALH	16.0-33.87		[3,5]				Autopsy,3D TEE	F,M
ACH	4.0-13.0		[5]				Autopsy(Formalin)	F,M
PCH	3.0-13.0		[5]				Autopsy(Formalin)	F,M
P_2LH	7.0-24.0		[5]				Autopsy(Formalin)	F
P_1LH	8.0-16.35		[3,6]				Autopsy,3D TEE	
$P_{1,2}$LH	NA						NA	
$P_{2,3}$LH	NA						NA	
P_3LH	8.6-13.6		[3]			X	3D TEE	
θ_{AA}	40.0°		[7]			X	NA	
θ_{PA}	13.0°		[7]			X	NA	
θ_{AL}	8.3°		[8]			X	RT-3D TTE	
θ_{PL}	5.3°		[8]			X	RT-3D TTE	

NA, Not Available

Appendix B

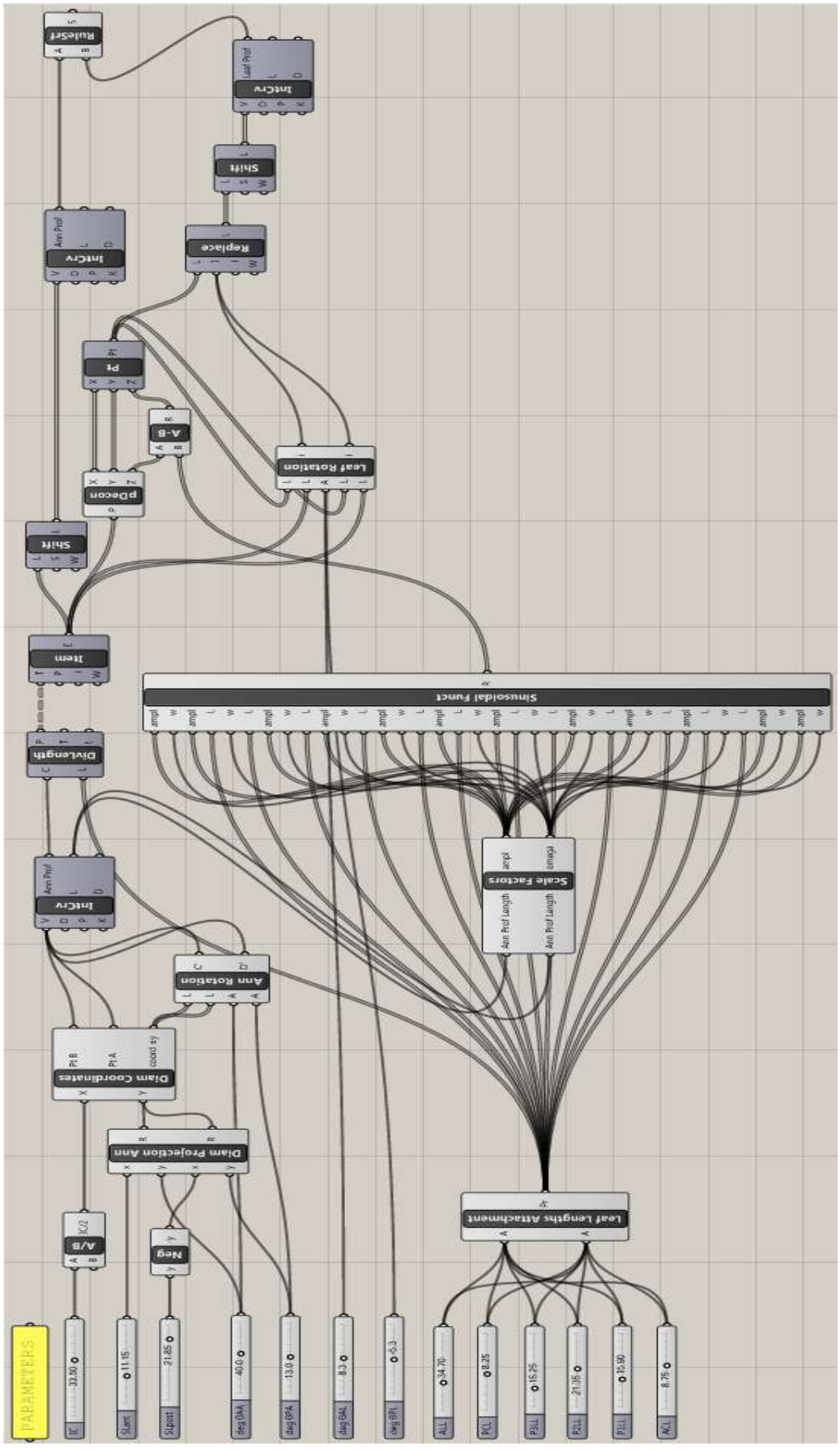
RulesFF
IntCrv
Shift
Replace
Pt
A-B
pDecon
Leaf Rotation
Item
Sinusoidal Funct
DivLength
Scale Factors
Ann Rotation
Diam Coordinates
Diam Projection Ann
Leaf Lengths Attachment
A/B
Neg
PARAMETERS

Appendix C

```
clear all
close all

a = [5.40814 4.2918 5.3063 3.06855 -0.09161 -0.5986 -0.30913 -1.15527
1.0269 0.25297 -0.64712 0.11715];
x = [109.5 120.6 93.2];

k = 6.0;
ntest = 3;

for j=1:ntest
    l = [0:0.01:x(j)];                    % annular circumferences lengths
    f_scale = x(j)/88;
    w = pi/x(j);                                % other scale factor (3)
    f = zeros(ntest,length(l));

    for i = 1:12
        f(j,:) = f(j,:) + k + f_scale*a(i)*sin(i*w*l);
    end

    color = ['r' 'b' 'm' 'k' 'g'];

    hold on
    plot(l,f(j,:), 'LineWidth',2, 'Color',color(j))
    xlabel('Frequency');
    ylabel('Amplitude');
    legend('Leaflets Profile 1','Leaflets Profile 2','Leaflets Profile
3');
    grid on

end
```

Ringraziamenti

Desidero ringraziare il Professor Morganti per la disponibilità e cortesia dimostratemi, per avermi lasciata libera di impostare il mio lavoro di tesi come meglio credevo, perché trovassi da sola lo stimolo a voler sempre migliorare. Grazie per il suo aiuto ma, sopratutto, per avermi sempre incoraggiata e sostenuta, professionalmente e umanamente, per essere stato capace di trasmettermi la sua passione per la ricerca e per aver alimentato in me questa curiosità.

Un grazie particolare anche al Professor Conti, per avermi guidata nell'ultima fase di lavoro e per essersi sempre reso disponibile.

Ringrazio, inoltre, la Dott.ssa Fabiana Gambarin della Clinica San Pio X di Milano e la Dott.ssa Giulia Magrini dell'IRCCS Policlinico San Matteo di Pavia per la preziosa collaborazione.

Il ringraziamento più grande va sicuramente ai miei genitori, e a mia sorella Elena, che mi hanno accompagnato in questo percorso con il loro sostegno e la loro fiducia in me anche, e soprattutto, nei momenti più difficili.

Grazie a Davide per avermi sempre incoraggiata, supportata e sopportata, per aver condiviso le mie preoccupazioni, le mie gioie e i miei sacrifici, e per essere sempre stato fiero di me, anche quando fallivo, per aver sempre creduto che ce l'avrei fatta e avermelo ricordato nei momenti più duri.

Un grazie alle mie coinquiline per i pianti e le risate, in particolare a Federica, che è stata per me come una sorella.

Ed, infine, un grazie agli amici e compagni di studi, per aver condiviso con me gioie e dolori, universitari e non, di questi ultimi anni.